Investigation of transversal cracking in cement bound reclaimed asphalt road base courses

Gianpaolo Baggio

TU Delft
Delft
University of
Technology

Challenge the future

Investigation of transversal cracking in cement bound reclaimed asphalt road base courses

Gianpaolo Baggio

in partial fulfilment of the requirements for the degree of

Master of Science

in Structural Engineering

at the Delft University of Technology,
to be defended publicly on Thursday 14th December 2017

Student number:	4440900	
Thesis committee:	Prof. dr. ir. S.M.J.G. Erkens	TU Delft
	Ir. L.J.M. Houben	TU Delft
	Dr. ir. drs. C.R. Braam	TU Delft
	Ing. J. Stigter	Boskalis
	Ir. D. Van der Ven	Kiwa KOAC
	Dr. ir. C.A.P.M. Van Gurp	Kiwa KOAC

An electronic version of this thesis is available at http://repository.tudelft.nl/.

TUDelft

ABSTRACT

This thesis is a study on the cracking behaviour of road bases constructed with cement bound reclaimed asphalt (also known in the Netherlands as AGRAC). It is decided to focus on this material because of the few researches available on the topic although the material being widely applied, at least in the Netherlands. The goal of adding cement to the recycled asphalt aggregate is primarily to increase the resistance to permanent deformation (rutting). But, as in all cement-bound materials, in the AGRAC base layer shrinkage cracks might occur which could reflect through the overlying asphalt layers. Because of this, during the last decades the cement content was reduced from the initial 4-5% down to 2-2.5% (by mass).

In order to study the cracking behaviour of AGRAC, in this research one grading and two cement contents (2% and 4% m/m) are considered. A series of tests is performed to evaluate the properties of the two AGRAC mixes at different values of curing time (up to 130 days) and 3 different temperatures (0, 15 and 30°C). The dependence on the curing time and temperature are considered because of the presence in the mix of cement and bitumen respectively. In particular the tests performed are: indirect tensile strength, modulus of elasticity, shrinkage, thermal deformation, Poisson's ratio and relaxation. The mechanical properties retrieved from these tests are used as input in a model which predicts the occurrence of cracks in an AGRAC base. If cracks occur, the model characterizes the crack pattern in terms of time of occurrence of the cracks, crack spacing and crack width. The calculations are done in two cases: non-weakened (plain) and weakened (with joints) base.

From the laboratory tests performed a dependence of the mechanical properties of AGRAC on the material temperature is clearly visible. Interesting results are also derived from the model, which shows the influence of the time of construction of the base (the worst scenario is observed for construction in August) and the difference in the cracking behaviour between the two AGRAC mixes (2 and 4% cement m/m). It is observed that the AGRAC mix with 4% cement leads to a higher risk of cracking compared to AGRAC 2%. In the worst scenario of base with AGRAC 4% constructed in August many crack series occur with a very close final crack spacing. The model shows how in this case even applying saw-cuts in the base is inefficient in terms of controlling the crack formation process.

PREFACE

This MSc thesis completes my Master's degree in Structural Engineering (Pavement Engineering specialization) at the Delft University of Technology. The research was conducted in collaboration with Boskalis and Kiwa-KOAC and involved many aspects related to design of the material, testing, analysis of the data and modelling. The tests were conducted in the TU laboratory.

I really enjoyed working on this research because of the many challenges involved. I hope this thesis will be useful in practice and possibly improved with knowledge from field data. This is the main goal of this work.

This thesis was a unique learning opportunity. Therefore, I would to thank all the persons who made it possible.

I would like to thank mr. Houben for trusting me with this project and for his constant guidance.

Furthermore, I would like to thank prof. Erkens for accepting to chair this thesis committee and for her precious advices.

Thanks to mr. Stigter and Boskalis for providing the material tested in this project and for the valuable collaboration especially during the designing phase of the material.

Thanks to mr. Van Gurp and mr. Van der Ven for helping me to define the thesis topic and for their supervision. Thanks to mr. Braam for his useful remarks on my work.

For the laboratory tests, I would like to thank Marco and Michele for their patience and willingness to help me with my tests.

A final big thanks to my family for their support.

Gianpaolo Baggio,
Delft, December 2017

CONTENTS

1

INTRODUCTION

This thesis is a study on the mechanical properties of the road base material "cement bound reclaimed asphalt", also known in the Netherlands as "AGRAC". The decision to perform a study on this particular base material is accounted for by the fact that few researches are at this moment available on the material although it is being widely applied, at least in the Netherlands. Within all possible relevant properties of AGRAC it is decided to focus on the cracking behaviour. Indeed, cement bound bases are susceptible to early cracking which can develop within the bound base and reflect through the above asphalt layers.

It is decided to study the cracking phenomenon of AGRAC using the approach presented in Report 7-08-216-5 "Model for transversal cracking (at joints) in plain concrete pavements", published in July 2008 by Ir. L.J.M. Houben [7]. This approach is chosen for the simplicity in which all factors influencing the cracking phenomenon are taken into account making the model a handy tool to estimate the influence of each of them. The goal of this thesis is then to extend this model (developed for plain concrete pavements) in order to account also for base layers constructed with AGRAC material. The model takes as input some mechanical properties of the AGRAC material retrieved through laboratory tests while as an output it shows whether cracks occur and, if so, characterizes the crack pattern (time of occurrence, crack width, crack spacing etc.). The major difference with report 7-08-216-5 is that the model created for AGRAC also takes into account the material temperature because of the presence of bitumen in the reclaimed asphalt.

In order to make the model a tool which can be used in construction, care is taken in order to test a material which is as close as possible to the one used in practice. For this reason the phase of designing the AGRAC recipe was conducted with a constant guidance from Boskalis NL, who also provided the reclaimed asphalt and sand materials. In particular two AGRAC mixes are tested: one mix with a cement percentage of 2% and one with 4% by mass.

It is important to note that from the results obtained in this research the trends more than the absolute values are of interest. The absolute values might not be reliable due not only to the limitations of the test programme but also to the cracking model used. Nevertheless, it would be interesting if a future research can validate or eventually adjust the parameters which in this research are assumed (e.g. friction of the AGRAC base with the surrounding layers) according to field data.

The thesis has the following structure: in **Chapter 2** the model structure is introduced and the test programme on the two AGRAC mixes is described. In **Chapter 3** the laboratory tests are described and the results presented. In **Chapter 4** a statistical analysis is performed on the results obtained in order to define the fitted curves which are used in the model. In **Chapter 5** the model is constructed and the results are shown for some particular combinations of parameters. In **Chapter 6** conclusions and recommendations are given.

2

DESCRIPTION OF TEST PROGRAMME

This chapter summarizes briefly the model developed with the purpose of justifying the test programme. The tests are then extensively discussed in Chapter 3 while the model is developed in Chapters 4 and 5.

2.1. THE MATERIAL

The material tested in this thesis is a base material composed of reclaimed asphalt, sand, cement and water. Such material is known in the Netherlands as AGRAC. Two different AGRAC mixes are considered: one with 2% and one with 4% cement m/m. With this regard, a small remark is given which will make the reading of this report easier: in the plots and tables presented, "red shade" colours (red, orange and yellow) are used for the AGRAC mix with 2% cement while "blue shade" colours (blue, violet and cyan) are used for the AGRAC mix with 4% cement. Furthermore, for simplicity the two mixes will be referred only as AGRAC 2% and AGRAC 4%.

2.2. THE MODEL
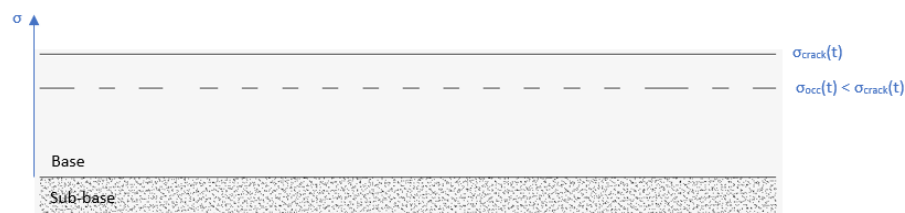
Figure 2.1: Model of the base before the occurrence of cracks
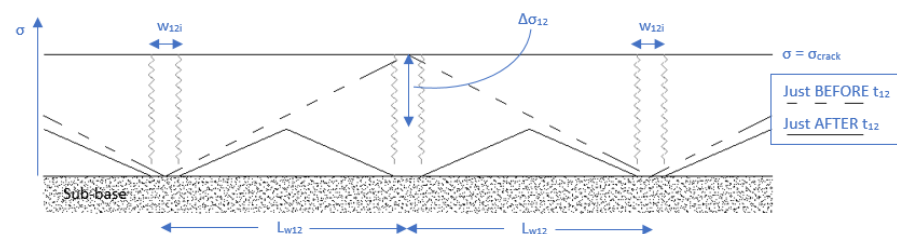
Figure 2.2: Example of stress distribution in the base as the first series of cracks occurs at time t_{12}

The AGRAC base is assumed to be a uniform layer of constant thickness placed on a sub-base layer (Figure 2.1) and fully restrained in the longitudinal direction. As the base starts cracking, the crack formation is governed by friction forces in the interface between the base and the sub-base layers (Figure 2.2).

The model is basically a comparison between the occurring stresses in the AGRAC base $\sigma_{occ}(t, T(t))$ which arise due to shrinkage and thermal deformation and the tensile strength $\sigma_{crack}(t, T(t))$, where t is the curing time and T the temperature of the AGRAC material. From this comparison we can determine whether and when cracks occur in the base ($\sigma_{occ} > \sigma_{crack}$) and characterise the crack pattern in terms of crack width and spacing. An example is given in Figure 2.4 where the cracks occur at around 90 days after construction.
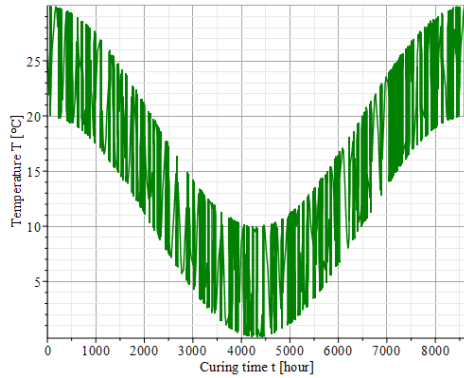
Figure 2.3: Temperature model for a base constructed on August 1st at 10.00
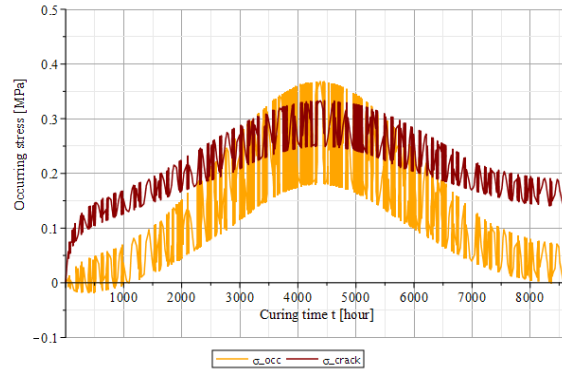
Figure 2.4: σ_{occ} and σ_{crack} for a base constructed with AGRAC 2% on August 1st at 10.00

On the two functions just introduced, the following observations are important:

- Both the occurring stresses and the tensile strength of AGRAC are considered to be dependent on the curing time (time from construction) t and the material temperature T, because of the presence of cement and bitumen respectively.

- The temperature of the base is modelled in this research as dependent on the time of construction (day and hour) in the year and the curing time, $T = T(t_{0_{day}}, t_{0_{hour}}, t)$. Therefore, by fixing the time of construction the temperature of the base can be written as $T(t)$. An example is given in Figure 2.3.

In the next sections the two stress functions introduced are described in detail. All equations presented in this chapter are valid for both AGRAC mixes (2 and 4% cement m/m).

2.3. TENSILE STRENGTH

The determination of the tensile strength function $\sigma_{crack}(t, T(t))$ consists of the following steps:

1 LABORATORY TEST:

The tensile strength is determined through Indirect Tensile Test (ITT) on AGRAC cylindrical specimens of dimensions ⌀=150 mm and h=100 mm. The samples are tested at different curing times (from 3 to 130 days) and different testing temperatures: 0, 15 and 30°C (Figure 2.5). These three testing temperatures are chosen because they represent the average and the two extreme temperatures that the base layer can experience according to the temperature model adopted. The curing temperature is 15°C for all the samples. Of course, in reality a base experiences temperature changes during its curing time. These temperature changes are not considered in this project because of the difficulty in reproducing in the lab a temperature-dependent curing, also taking into consideration that the curing

temperatures depend on the time of construction in the year. Furthermore this would introduce a variability in the samples which is difficult to control.

2 Through a statistical analysis the ITS values at each testing temperature are fitted with a curve (Figure 2.5). The three fitted curves are called $\sigma_{crack}(t,0)$, $\sigma_{crack}(t,15)$ and $\sigma_{crack}(t,30)$.

3 Starting from the three fitted curves defined the strength is also calculated for any other temperature in the range 0-30°C. At this point it is possible to obtain the development of the strength for a particular time of construction of the base (Figure 2.6). This function $\sigma_{crack}(t,T(t))$ only depends on the curing time t.
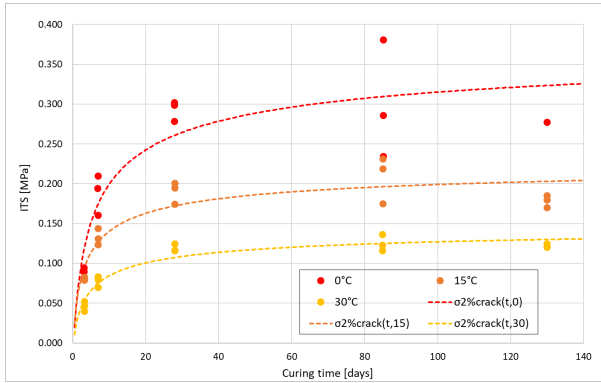
Figure 2.5: Values of ITS for AGRAC 2% obtained for different curing times at 0, 15 and 30°C and fitted curves
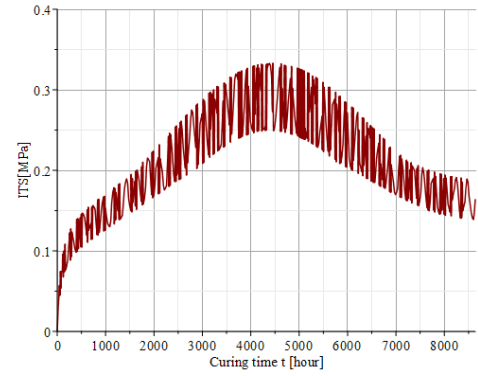
Figure 2.6: $\sigma_{crack}(t,T(t))$ for a base constructed with AGRAC 2% on August 1st at 10.00

2.4. Occurring stresses

The occurring stresses in the AGRAC base are given by Equation (2.1).

$$\sigma_{occ}(t,T(t)) = \sigma_{shr}(t,T(t)) + \sigma_{the}(t,T(t)) = r \cdot E(t,T(t)) \cdot [\epsilon_{shr}(t) + \epsilon_{the}(T(t))] \qquad \text{[MPa]} \qquad (2.1)$$

Where:

- $\boldsymbol{\sigma_{shr}(t,T(t))}$ [MPa] are the stresses arising in the base because of the shrinkage deformations.

- $\boldsymbol{\sigma_{the}(t,T(t))}$ [MPa] are the stresses arising in the base because of the thermal deformations.

- $\boldsymbol{r}$ [-] is a coefficient taking into account the relaxation of the material.

- $\boldsymbol{E(t,T(t))}$ [MPa] is the modulus of elasticity of the AGRAC material.

- $\boldsymbol{\epsilon_{shr}(t)}$ [-] is the strain due to shrinkage deformation.

- $\boldsymbol{\epsilon_{the}(T(t))}$ [-] is the strain due to thermal deformation.

An example of the thermal and shrinkage stresses and their sum (occurring stresses) is given in Figures 2.7, 2.8 and 2.9. All components of Equation (2.1) are now analysed separately.
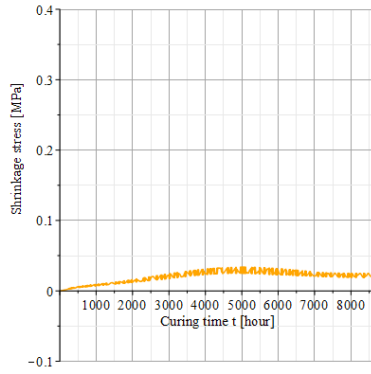
Figure 2.7: σ_{shr} for a base constructed with AGRAC 2% on August 1st at 10.00
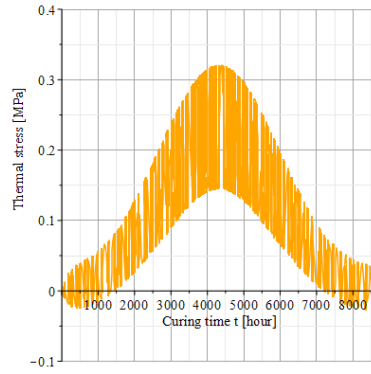
Figure 2.8: σ_{the} for a base constructed with AGRAC 2% on August 1st at 10.00
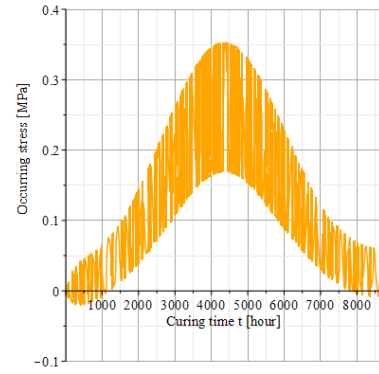
Figure 2.9: σ_{occ} for a base constructed with AGRAC 2% on August 1st at 10.00

2.4.1. RELAXATION COEFFICIENT

r is a constant coefficient which takes into account the relaxation of the material.

LABORATORY TEST:

It is decided to evaluate the relaxation in the Indirect Tensile Test set-up. The test set-up and the dimensions of the specimens tested are the same as the ones used for the determination of the Indirect Tensile Strength (ITS). It is believed that this will allow a reliable evaluation of the relaxation property of AGRAC. The relaxation behaviour depends on many parameters: temperature, curing time, applied strain etc. For this reason it is decided to reduce the parameters by considering only one testing temperature (15°C, average temperature for the model considered) and a few curing times.

2.4.2. MODULUS OF ELASTICITY

The modulus of elasticity is evaluated with Equation (2.2) [5] [4].

$$E(t, T) = (0.9988 \cdot v + 0.2714) \cdot \frac{S_h(t, T)}{h} \qquad \text{[MPa]} \qquad (2.2)$$

Where:

- $\boldsymbol{v}$ [-] is the Poisson's ratio.

- $\boldsymbol{S_h(t, T)}$ [N/mm] is the slope of the regression line in the plot "force - horizontal displacement" from the monotonic ITT test (section 2.3).

- **h** [mm] is the height of the specimen considered.

As a consequence, for each specimen tested in ITT one value of E is calculated. The modelling of the modulus of elasticity data is similar to what explained for the ITS in section 2.3. First the data are fitted with a curve for each testing temperature: $E(t, 0)$, $E(t, 15)$ and $E(t, 30)$ (Figure 2.10). Then, the modulus at all temperatures in the range 0-30°C is determined in order to obtain the function $E(t, T(t))$ (Figure 2.11) only dependent on the curing time (once the time of construction is chosen).
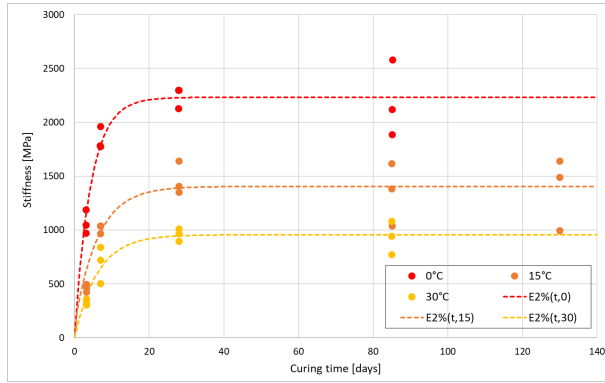
Figure 2.10: Values of E for AGRAC 2% obtained for different curing times at 0, 15 and 30°C and fitted curves
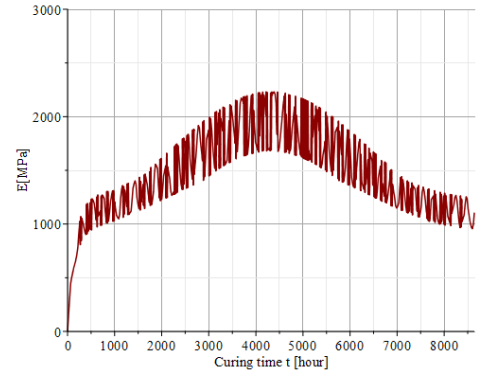
Figure 2.11: $E(t, T(t))$ for a base constructed with AGRAC 2% on August 1st at 10.00

2.4.3. POISSON'S RATIO

The Poisson's ratio is measured in this project with the purpose of determining the modulus of elasticity through Equation (2.2).

LABORATORY TEST:
The Poisson's ratio is evaluated on specimens of dimensions ⌀=100 mm and h=200 mm. A cyclic load is applied on top of the specimen while the radial and the axial deformation are measured. The ratio between the two deformations gives the Poisson's ratio value. The test is performed at different temperatures and loads.

2.4.4. SHRINKAGE STRAIN

The shrinkage strain $\epsilon_{shr}(t)$ is considered to be a function of the curing time only. The steps used to model this property are the following:

1 LABORATORY TEST:
The shrinkage of the AGRAC material is determined on specimens of dimensions ⌀=100 mm and h=200 mm by placing them in a curing room at standard conditions (20°C, 55%RH) and measuring the variation of their height in time through a dial gauge. It is therefore assumed that the shrinkage behaviour of the material is the same, independent on the temperature.

2 The measured strain is then adapted to the pavement situation through adjustments which take into account the relative humidity and the dimensions of the base.

2.4.5. THERMAL STRAIN

The thermal strain $\epsilon_{the}(T(t))$ is given by Equation (2.3).

$$\epsilon_{the}(T(t)) = \alpha \cdot \Delta(T(t)) \qquad [\text{-}] \qquad (2.3)$$

Where:

- α [m/m/°C] is the coefficient of linear thermal expansion of the AGRAC material.

- $\Delta(T(t)) = T(t) - T_0$ [°C] is the difference between the temperature at the curing time t and the temperature at the time of construction T_0.

LABORATORY TEST:

The coefficient α is calculated on specimens of dimensions $\varnothing$=100 mm and h=200 mm by recording the change in the height as the temperature of the specimen is lowered from 30 to 0°C. The test is performed at different curing times but it is modelled as a constant value. It should be noted that the thermal coefficient is kept constant for any temperature change within the range 0-30°C. In reality the coefficient might change within this temperature range.

2.5. APPLICABILITY OF THE MODEL

As previously described in this chapter, some assumptions are considered in order to reduce the complexity that the determination of certain properties of the AGRAC material would have implied. Nevertheless, these assumptions are believed not to affect, in general terms, the trends identified from the model results. With this regard it should be noted that the trends rather than the absolute values are of interest in this research. The absolute values might not be reliable, not only because of the limitations of the test programme but also because of the cracking model used and its assumed parameters (e.g. friction coefficient).

The biggest limitation to the applicability of the model is the assumption on the temperature. Indeed, the temperature model of the AGRAC base used in this thesis is designed for the Netherlands and considers a temperature range between 0 and 30°C. As a consequence all the properties investigated through laboratory tests are determined in this temperature range. The applicability of the model for a slightly wider temperature range (of ~5°C) is probably still possible but of course the material properties have to be extrapolated from the measured values.

<div align="right">

3

</div>

<div align="right">

LABORATORY TESTS

</div>

3.1. MANUFACTURING OF THE SPECIMENS

In this section the process of manufacturing the specimens from the raw materials is described. In this process care is taken in order to ensure that the resulting material is as close as possible to the one used in practice.

3.1.1. THE MATERIALS

RECLAIMED ASPHALT

The reclaimed asphalt consists of milled old base-layers and was provided by Boskalis Nederland. Boskalis also provided data from two extraction tests on the material delivered (Appendix A, Tables A.1 and A.2) and from a sieving test performed on the RAP material before extraction (Table 3.1).

Sieve [mm]	Percentage passing [% on total RAP mass]	
	Sieving test 1/2	Sieving test 2/2
63	100.0	100.0
45	97.1	100.0
31.5	95.7	97.1
22.4	87.8	90.8
16	79.3	81.3
11.2	68.0	71.0
8.0	56.3	59.4
5.6	44.3	46.2
4	34.2	36.1
2.0	21.6	22.8
PAN	0.0	0.0

Table 3.1: Sieving tests performed on the RAP before extraction

The material was delivered already divided in the following batches [mm]: < 2, 2 to 4, 4 to 5.6, 5.6 to 8, 8 to 11.2, 11.2 to 16 and 16 to 22.4 (sizes >22.4 mm are not used in this project as explained further on in this chapter). On the batch < 2mm a sieving test was performed in the university lab. The results are shown in Table 3.2.

Sieving test on RAP < 2mm		
Sieve [mm]	Retained [% m/m]	Passing [% m/m]
2	0.00	100.00
1	29.26	70.74
0.063	70.56	0.18
PAN	0.18	0.00
tot:	100.00	

Table 3.2: Sieving test performed on the RAP fraction <2mm

SAND

A river sand was provided by Boskalis. A sieving test was performed in the university lab on the sand after being oven dried (Table 3.3).

Sieving test on sand		
Sieve [mm]	Retained [% m/m]	Passing [% m/m]
2	0.00	100.00
1	12.87	87.13
0.063	86.21	0.93
PAN	0.93	0.00
tot:	100.00	

Table 3.3: Sieving test performed on the river sand

CEMENT

A cement CEM I (Portland cement) with strength class 42.5 is used. Two percentages of cement on the total mass of the dry aggregates (RAP + sand) are used: 2% m/m and 4% m/m.

3.1.2. GRADING CURVES

The **grading envelope** for the RAP (before extraction) + sand is prescribed in RAW - Table 80.2.1 [1] and given in Table 3.4:

	Percentages [% m/m]			
	Retained (cum.)		Passing	
Sieve	Min.	Max.	Upper limit	Lower limit
63 mm	-	0	100	100
45 mm	0	10	100	90
16 mm	10	40	90	60
4 mm	40	65	60	35
2 mm	50	75	50	25
0.063 mm	92	100	8	0

Table 3.4: Grading envelope for the RAP + sand material

In practice the milled RAP is normally used "as it is" by adding a quantity of sand which allows the grading curve to fit within the envelope prescribed by the Dutch standard. The same procedure is used in this project. The "design curve" (the grading curve used in this project) is constructed as follows:

First the **RAP before extraction** grading curve is calculated as the average of the two sieving tests performed by Boskalis on the RAP before extraction (Table 3.1). Second, the **design curve (max 63 mm)** is constructed

by adding, to the mix graded according to the "RAP before extraction" curve, a percentage of sand (16.7% on the total aggregates mass) which allows the curve to fit within the envelope. Retained and passing percentages for these two curves are given in Table A.3.

Finally, the **design curve** (the curve used in this project) is obtained from the "design curve (max 63 mm)" by limiting the maximum size of the aggregate to 22.4 mm instead of 63 mm. This is due to the dimensions of the cylindric samples to be tested in ITT which have dimensions of 150 mm for the diameter and 100 mm for the height. The design curve is constructed as follows: retained percentages for sieves equal or greater to 22.4 mm are set to 0% while the other retained percentages are adapted in a way that the sum of the retained percentages gives 100%.

The grading curves described above are plotted in Figure 3.1. Additionally, the retained and passing percentages for the "design curve" are given in Table 3.5.
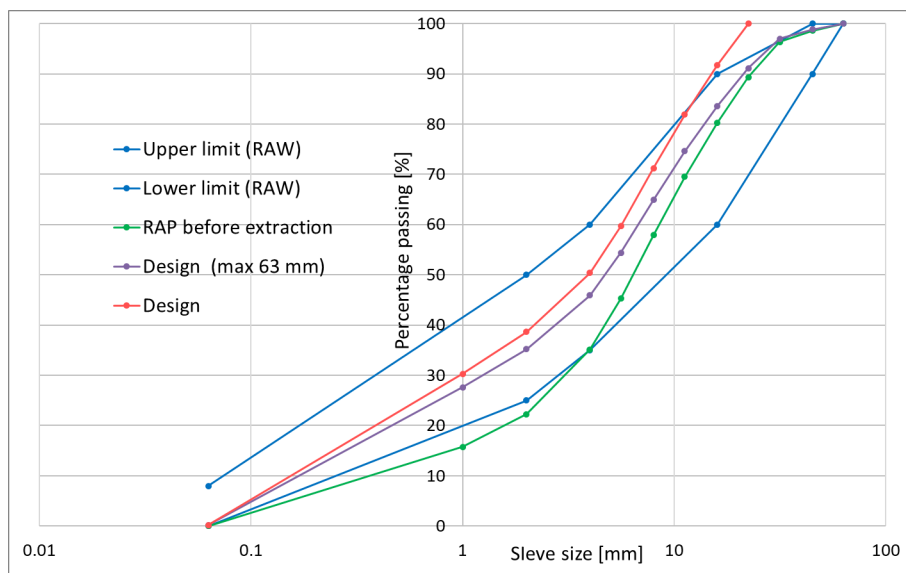
Figure 3.1: Design grading curve

	Percentages [% m/m]	
Sieve	Retained (on single sieve)	Passing
22.4	0.0	100.0
16	8.3	91.7
11.2	9.9	81.9
8	10.6	71.2
5.6	11.5	59.7
4	9.3	50.4
2	11.8	38.6
1	8.3	30.3
0.063	30.1	0.2
PAN	0.2	0.0
tot:	100.0	

Table 3.5: Retained and passing percentages for the "design curve"

3.1.3. Proctor test

It is common practice to use the Single Point Proctor test for determining the optimum water content and the Proctor density of the AGRAC base material. Nevertheless, the Standard Proctor test is chosen for this project. Indeed, the Standard Proctor test nicely gives the variation of density with respect to the water content. The mix graded according to the Design grading curve (Table 3.5) is tested through Standard Proctor test in order to determine the optimum water content and the Proctor density for the AGRAC mix with 2% cement. The AGRAC mix with 4% cement was not tested since from previous test performed on similar material it was found that the variation of the cement percentage has little effect both on the optimum water content and the Proctor density. Furthermore, it is decided to use the same water content and density for both mixes (2 and 4% cement) in order to introduce the least possible variations within the manufacturing of the specimens. The Standard Proctor test was performed in the soil lab at TU Delft. The test parameters were chosen from Table A.3 (Examples of alternatives for Proctor mould B) of NEN-EN 13286-2 [2] and are given in Table A.4.

The water contents considered and the respective calculated densities are given in Table 3.6. Two different water contents are given: "input w.c." is the water content added to the mix before determining the density through Proctor compaction while "oven w.c." is the water content measured from oven drying at 110°C a portion of the mix after the compaction procedure. Initially it was not clear whether the oven w.c. could be taken into consideration. Indeed, it was expected that some of the water would be involved in the hydration process and so wouldn't be released during the drying of the material in the oven. However, since no signs of cementation were observed in the samples placed in the oven, the oven w.c is considered a more precise measurement of the w.c. actually present in the mix. To be noted that for the 8.0 input w.c. some free water was noticed in the Proctor mould, meaning that this water content was too high. The dry densities from oven w.c. are plotted against the oven w.c. for the considered mix in Figure 3.2.

Cement 2% ($W_{cement}/W_{s(dry)}$ = 2%)				
Input w.c. ($W_w/W_{s(dry)}$) [%]	Oven w.c. ($W_w/W_{s(dry)}$) [%]	Bulk density ((W_s+W_w)/V) [kg/m³]	Dry density (W_s/V) from input w.c [kg/m³]	Dry density (W_s/V) from oven w.c [kg/m³]
5.0	4.8	1968.8	1875.1	1879.1
6.0	5.4	2019.2	1904.9	1915.1
7.0	6.6	2047.4	1913.5	1921.4
8.0	7.7	2066.6	1913.5	1918.2

Table 3.6: Water contents and dry densities from Proctor test on AGRAC mix with 2% cement

From the data showed in Figure 3.2 the optimum water content is chosen. In Table 3.7 the chosen optimum oven w.c., the correspondent dry density from oven w.c. and the bulk density are given. For the manufacturing of the samples the optimum oven w.c. is used while the target density is chosen as 102% of the Proctor density. Indeed, the requirement for the density in the road is 102% of the Proctor density (average of the production of one day) with an individual minimum of 98% [1]. The values of optimum water content and target density are listed in Table 3.8.

Optimum w.c. [%]	Dry density [kg/m³]	Bulk density [kg/m³]
6.5	1922	2047

Table 3.7: Optimum value of w.c. with correspondent dry and bulk densities
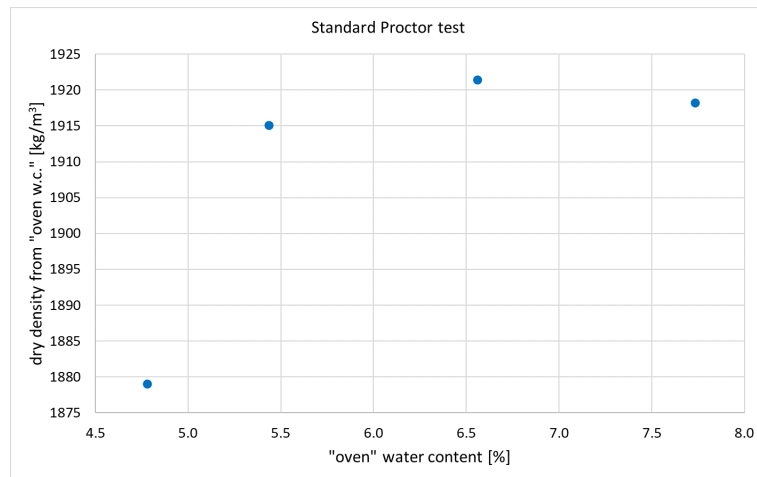
Figure 3.2: Water contents and dry densities from Proctor test on AGRAC mix with 2% cement

Optimum w.c. [%]	Target dry density [kg/m³]	Target bulk density [kg/m³]
6.5	1960	2090

Table 3.8: Target value of w.c. with correspondent dry and bulk densities

3.1.4. Specimen preparation (for ITT)

The samples to be tested in ITT set-up are cylindrical with the following dimensions: Ø=150mm, h=100mm. The preparation of these specimens consists of the three following phases:

Weighting of the components

Based on the results obtained from the Proctor compaction test, the target bulk density of the specimens is chosen as 2090 kg/m³. The total mass is composed by the three components: aggregates (RAP + sand), cement and water. The water mass is such that $W_{water}/W_{aggregates+cement} = 6.5\%$ while the mass of the cement is such that $W_{cement}/W_{aggregates} = 2\%$ or 4%. The remaining mass is composed by the aggregates (RAP + sand) whose fractions are present in the mix according to the design grading curve (Table 3.5). The aggregates before mixing are shown in Figure 3.3.

Figure 3.3: Aggregates before mixing and weighting phase

MIXING

Once the components are weighted, they are put into an automatic blender and mixed at the lowest speed for 2 minutes (Figures 3.4 and 3.5)

Figure 3.4: The components added to the blender

Figure 3.5: The mix blended with water and cement

COMPACTION

For the compaction of the specimens the Gyratory Compactor (SGC) is used. This is a rather innovative approach for cement treated materials which are usually compacted by means of impact or vibratory equipment [3]. The SGC is chosen for its compaction procedure which simulates the effect of the roller compactors in the field. Besides, this equipment allows the production of specimens with little variation in

the dimensions. The mould preparation procedure consists of the following phases: first the SGC mould is lubricated with water and a steel plate is placed in the bottom of the mould (Figure 3.6), then the blended mix is put in the mould with the top slightly pressed with a spoon (Figure 3.7) and another steel plate is added to the top (Figure 3.8).

Figure 3.6: SGC mould preparation - step 1/3

Figure 3.7: SGC mould preparation - step 2/3

Figure 3.8: SGC mould preparation - step 3/3

At this point the mould with the mix is placed in the SGC chamber and the compaction performed at the ambient temperature with a constant pressure of 600 kPa at speed of 30 rpm and angle 1.25°. The compaction process is automatically stopped when the desired height is reached. The number of gyrations required to compact the specimens are between 15 and 20. It is believed that the difference in the number of gyrations required is due to SGC set-up (lubrication of the mould, initial compression with the spoon, application of the load etc.) rather than to the material itself. A compaction curve is given as an example in Figure 3.9. The sample is at last extracted from the mould and placed on a tray (Figures 3.10 and 3.11).
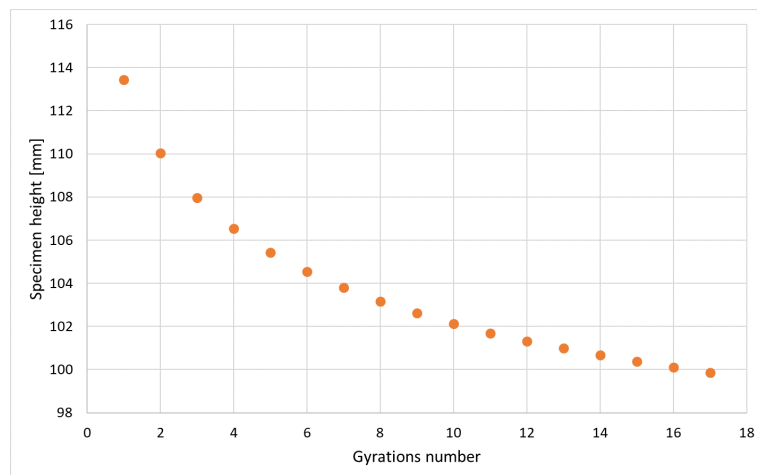
Figure 3.9: Example of SGC compaction curve

It is noted that, due to some spilling of water during compaction, the water content present in the samples after compaction was 5.7% instead of the 6.5% used in the mixing phase. As a consequence, the height was reduced from 100 to 98 mm in order to still reach the target density of 2090 kg/m^3. From mass measurements taken on the samples just after compacting it was observed that the target bulk density was reached.

Figure 3.10: Extraction from SGC mould

Figure 3.11: Samples on a tray before being placed in the curing room

3.1.5. SPECIMEN PREPARATION (FOR SHRINKAGE, THERMAL DEFORMATION AND POISSON'S RATIO)

The samples used for shrinkage, thermal deformation and Poisson's ratio measurements are cylindric with the following dimensions: Ø=100mm, h=200mm.

The weighting and mixing procedures are the same as the ones used for the ITT samples (3.1.4). The compaction procedure differs because of the different dimensions of the samples. Indeed, the height of the samples is the maximum allowed by the SGC mould with diameter of 100 mm, meaning that the mix cannot be compacted at once. Therefore, the samples are compacted in three layers, taking care that the density is about the same in each of them. After compacting the first layer the upper surface is made rough with a spoon in order to have a better bond with the second layer (Figures 3.12 and 3.13). The same is done between the second and the third layer. In the end the sample is extracted from the mould (Figure 3.14).

Figure 3.12: Compaction of the first third of the sample

Figure 3.13: The upper surface is scratched with a spoon

Figure 3.14: The sample is extracted from the mould

3.1.6. CURING

Once the samples are extracted from the SCG mould the two steel plates are removed and the samples are placed in a curing room at 15°C and 50% air humidity (Figure 3.15). For the samples described in 3.1.5 also the raw materials are placed in the curing room before manufacturing. This is done in order to reduce the

effect of temperature changes in the manufacturing process on the measurements (in particular on the shrinkage measurements). Indeed, shrinkage is significantly affected by the conditions before and after the setting [6].
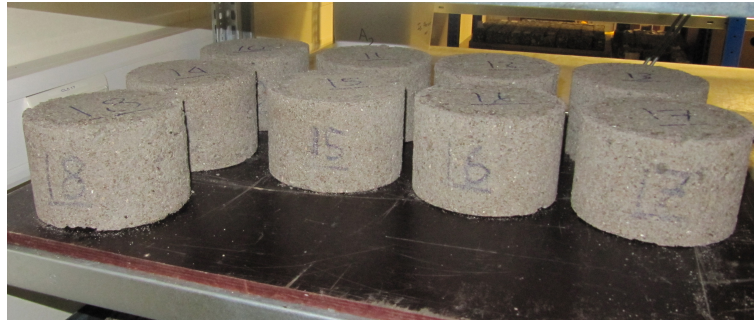
Figure 3.15: Samples in the curing room

3.2. INDIRECT TENSILE TEST - ITT

In this section the Indirect Tensile Test (ITT) is described. First the test set-up and parameters are introduced. Then the results are presented and discussed.

3.2.1. SAMPLES TESTED

The samples tested are manufactured according to 3.1.4. As previously mentioned, two AGRAC mixes are tested (one with 2% and one with 4% cement m/m) at different curing times and temperatures. Three samples are tested for each combination of parameters. An overview of the samples tested in ITT is given in Table 3.9.

Curing time	Temperature [°C]	Samples tested	
		Cement 2%	Cement 4%
3 days	0	3	3
	15	3	3
	30	3	3
7 days	0	3	3
	15	3	3
	30	3	3
28 days	0	3	3
	15	3	3
	30	3	3
90 days	0	3	3
	15	3	3
	30	3	3
130 days	0	3	3
	15	3	3
	30	3	3
Total num. of samples:		90	

Table 3.9: Overview of the samples tested in ITT set-up

3.2.2. TEST SET-UP

In the ITT chamber the temperature is set as the intended test temperature for each test. The samples are kept at the same temperature for around 3 hours prior to the test. This time interval was indeed found to be

sufficient to reach a uniform temperature in the material (section 3.4). The test is displacement controlled, being the vertical displacement applied by an actuator at the rate of 0.01mm/s. Such small deformation rate is chosen to simulate the deformations in the field due to shrinkage and thermal deformation which take place very slowly. The displacement is applied through a strip at the top of the specimen (the imposed deformation is double checked by two vertical transducers positioned between the loaded strip and the bottom plate). The actuator also measures the vertical force at each step of the applied deformation. Furthermore a frame allows the measurement of the radial deformation from two transducers positioned at the two sides of the cylindrical sample. Photos of the test set-up and of a cracked sample are given in Figure 3.16. A typical behaviour of force and displacements during the test is given in Figure 3.17 as a function of time.

Figure 3.16: ITT test set-up and photos of a cracked sample
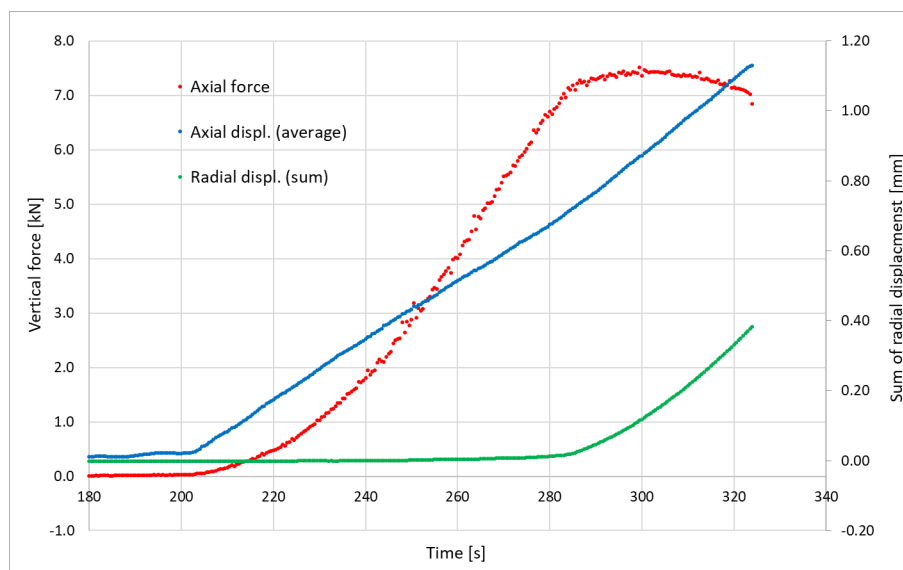
Figure 3.17: Results from ITT test for a sample with 4% cement tested at 0°C and 3 days curing time

3.2.3. INDIRECT TENSILE STRENGTH - ITS

DETERMINATION OF F_{crack}

In order to define the Indirect Tensile Strength (ITS) of the sample (at the given cement percentage, curing time and testing temperature) first the force F_{crack} at the time of occurrence of the crack (t_{crack}) has to be defined. It is noted that both the plot of the force and the plot of the radial displacement show a kink at the moment of cracking (Figure 3.17). Nevertheless t_{crack} cannot be determined precisely, especially at the high test temperatures, the material being more ductile. For this reason, it is decided to determine t_{crack} by plotting against testing time the derivative of the radial displacement (Figures 3.18 and 3.19). The derivative of the radial displacement is obtained by plotting against time the difference between the sum of the radial displacement at that time and the sum of the radial displacement at the instant just preceding. It is noted that this parameter is constant in the first part of the test and increases suddenly when the crack occurs. The resistance F_{crack} is determined as the force at t_{crack}.
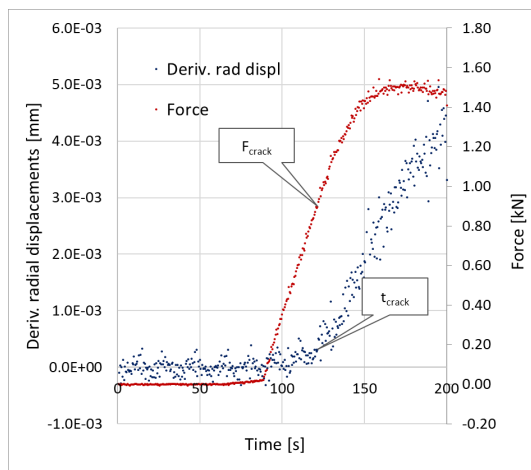
Figure 3.18: Force and derivative of radial displacement for a sample with 2% cement tested at 30°C and 3 days curing time
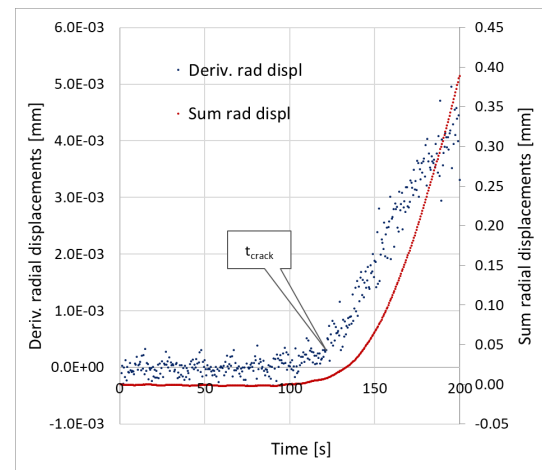
Figure 3.19: Sum of radial displacements and derivative of radial displacements for a sample 2% cement tested at 30°C and 3 days curing time

DETERMINATION OF σ_{crack}

Once F_{crack} is determined, the ITS σ_{crack} is calculated as prescribed by the European standard [9] through Equation (3.1).

$$\sigma_{\text{crack}} = \frac{2 \cdot F_{\text{crack}}}{\pi \cdot D \cdot h} \qquad [\text{MPa}] \qquad (3.1)$$

The diameter of the samples (D) is considered 150 mm for all the specimens. Instead, the height of the specimen (h) is calculated as the average of four height measurements taken on each specimen prior to testing.

The results for the ITS at different temperatures and curing times are presented separately for the two AGRAC mixes in Figures 3.20 and 3.21. Detailed information on the sample properties and the results obtained from the ITT test are given in Appendix B.
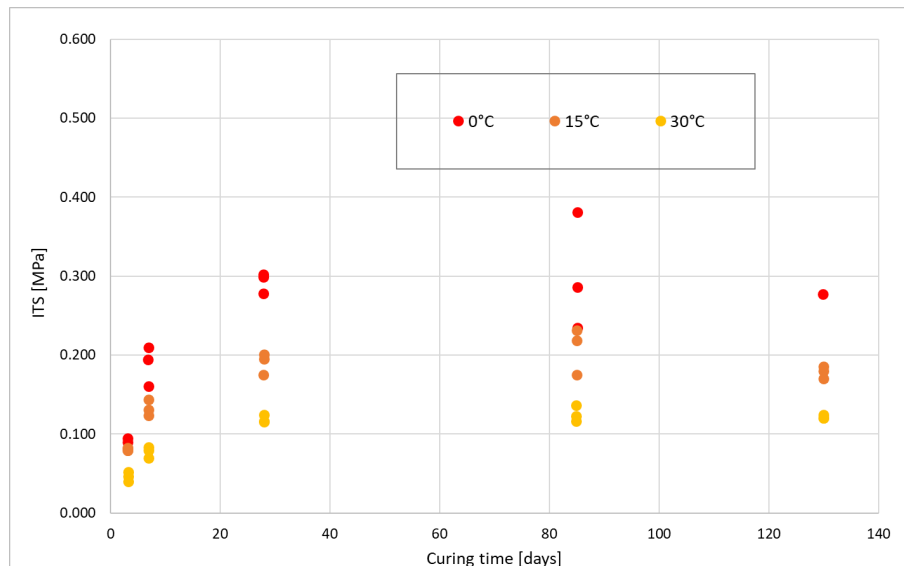
Figure 3.20: ITS results for the AGRAC mix with 2% cement
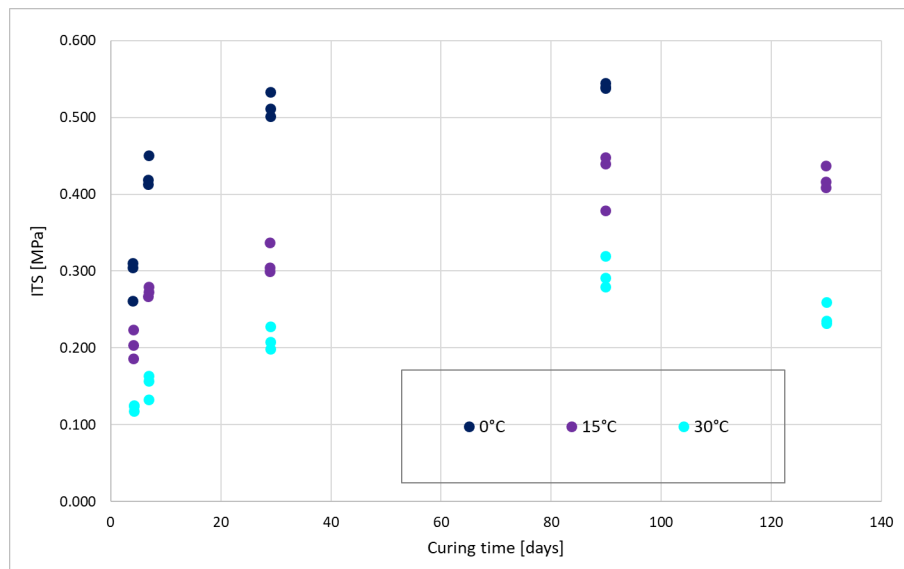
Figure 3.21: ITS results for the AGRAC mix with 4% cement

Discussion on the results

On the results obtained the following is observed:

- The results clearly show a dependence of the tensile strength of the AGRAC material on the testing temperature. This is believed to be caused by the presence of bitumen which weakens the interface bond between the aggregates and the cement-sand paste at high temperatures causing a decrease of the ITS values.

- The ITS values, as expected, increase with the curing time. An exception to this trend are the ITS values of AGRAC 4% tested at 30°C and 130 days curing time which are lower than the ones tested at 90 days. The decrease in the values is probably to attribute to some defect introduced in the specimens during the manufacturing process.

- The variability of the results for each combination of temperature and curing time is generally low. An exception are the values of AGRAC 2% tested at 0°C and 90 days curing time which show a higher variability. This is attributed to a malfunctioning of the Gyratory Compactor in the manufacturing phase.

- The ITS values range of the two AGRAC mixes tested is in line with the literature. In particular the value of Indirect Tensile Strength found by Grilli et al. on a similar mixture with 3% cement tested at 25°C after 7 days curing time is 0.21 MPa [10]. Furthermore, the ITS results of AGRAC 4% are comparable with the results obtained by Kolias on a mix only composed of reclaimed asphalt with 5% cement at the testing temperature of 20°C [11]. Indeed, the ITS values found by Kolias are 0.43 MPa at 7 days curing time and 0.71 MPa at 28 days. The influence of the cement percentage is also studied by Yuan et Al. [12] on a mix composed by reclaimed asphalt tested at 7 days curing time at 25°C. The results obtained were 0.12 MPa for a mix with 2% cement and 0.30 MPa for a mix with 4% cement.

3.3. SHRINKAGE

In this section first the shrinkage test set-up is described. Then, the results are presented.

3.3.1. TEST SET-UP

The samples used to measure the shrinkage are manufactured according to 3.1.5.

The specimens are placed in a room at constant temperature (20±1°C) and air humidity (55±1%). The variation of the specimen height is taken through a dial gauge positioned on top of the sample. The dial gauge is ensured stable by a steel bar which is connected magnetically to a steel plate positioned at the bottom of the sample (Figures 3.22 and 3.23). An overview of all the AGRAC samples tested in shrinkage set-up is given in Table 3.10.

Sample ID	Cement percentage	Measurements taken from [days after manufacturing]
S-1	2%	2.85
S-2	4%	2.83
S-3	2%	1.77
S-4	4%	1.73
S-5	2%	0.00
S-6	4%	0.00

Table 3.10: Overview of the samples tested in shrinkage set-up

Figure 3.22: Shrinkage test set-up

Figure 3.23: Dial gauge

3.3.2. THE RESULTS

By taking the deformation measurements at different curing times it is possible to calculate the increase of shrinkage strain as a function of curing time. First the results from the samples S-5 and S-6 are presented in Figure 3.24. It is noted that from 0 to 1.75 days the measurements show an alternative behaviour between shrinkage and swelling. This is attributed to small settlements of the fresh specimens and small temperature changes between the manufacturing and curing rooms. It is here assumed that the shrinkage starts at 1.75 days from manufacturing. As a consequence the two functions in Figure 3.24 are shifted upwards in a way that the shrinkage is 0 at 1.75 days curing time while the first part of the graph is not considered.
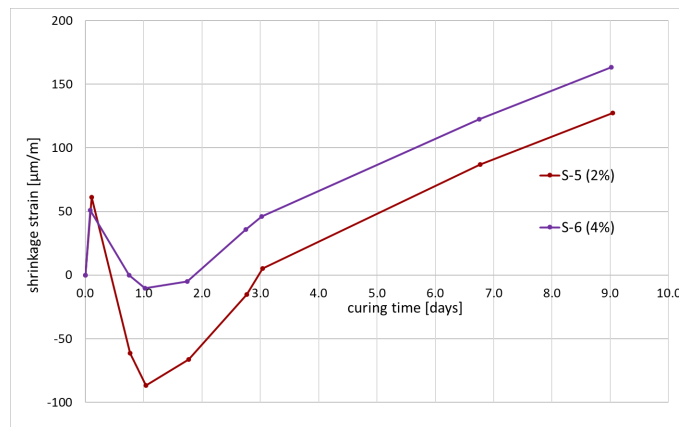
Figure 3.24: Shrinkage raw data of samples S-5 and S-6

The shifted curves obtained from S-5 and S-6 are given separately for the two AGRAC mixes in Figures 3.25 and 3.27 along with the results from the other samples tested (S-1 to S-4). In order to obtain a single shrinkage curve for each AGRAC mix the results in Figures 3.25 and 3.27 are modified as follows:

For each AGRAC mix the measurements of the samples tested starting from 3 days (samples S-1 and S-2) are added (at the correspondent curing time) to the measurements obtained from the other samples tested starting from around 1.75 days after manufacturing. The resulting adjusted shrinkage data are shown in Figures 3.26 and 3.28.
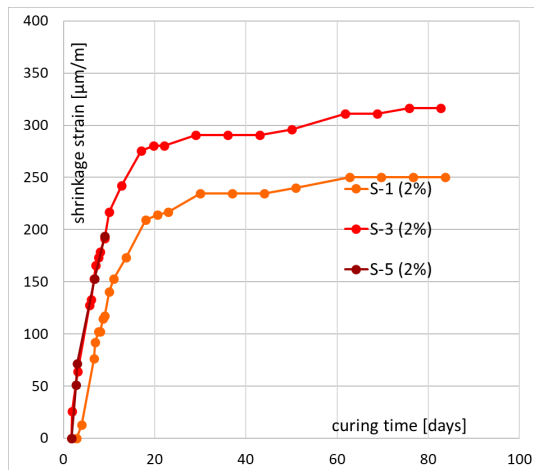
Figure 3.25: Shrinkage raw data for the AGRAC mix with 2% cement
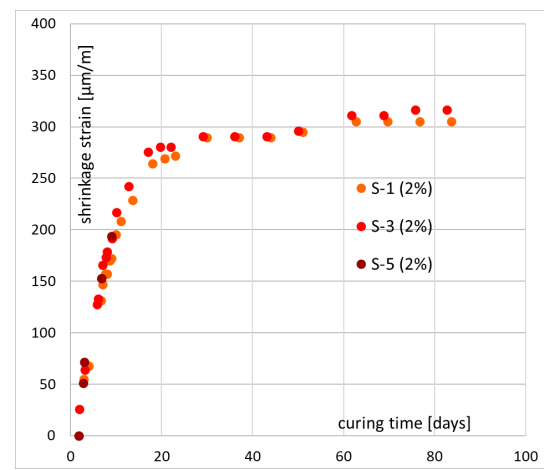
Figure 3.26: Adjusted shrinkage raw data for the AGRAC mix with 2% cement
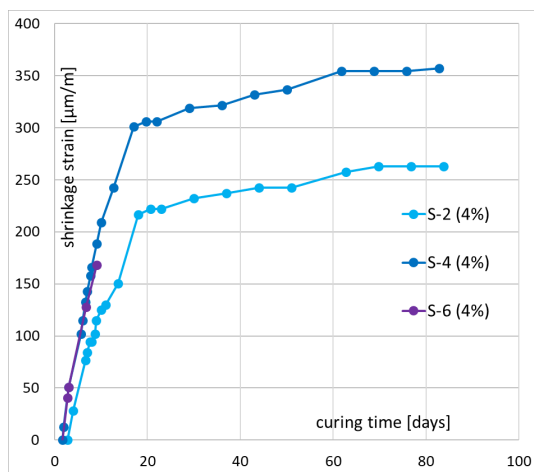
Figure 3.27: Shrinkage raw data for the AGRAC mix with 4% cement
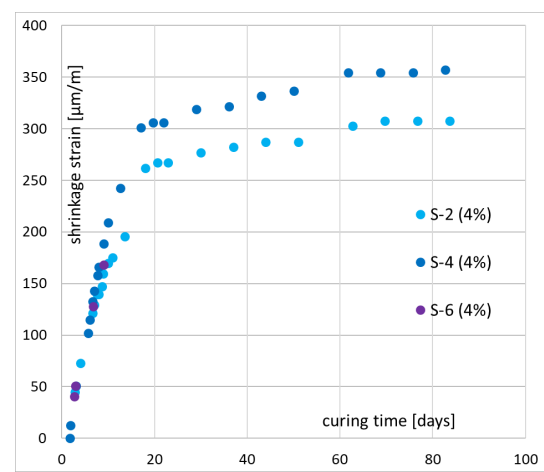
Figure 3.28: Adjusted shrinkage raw data for the AGRAC mix with 4% cement

DISCUSSION ON THE RESULTS

From the results obtained it is noted that:

- The results of AGRAC 4% show a higher variability than the mix with 2% cement. This is probably due to small changes introduced in the material during manufacturing.

- The results for AGRAC 4% are on average slightly higher than AGRAC 2% especially for high values of curing time. This was expected since the shrinkage normally increases with the percentage of cement present in the mix.

- The shrinkage results are comparable to the ones obtained by Saloua et al. [6] on mixes containing a varying percentage of RAP (up to 50% on the total aggregate mass) and treated with a cement percentage of 6% using a similar test set-up as done in this thesis.

3.4. THERMAL DEFORMATION

The thermal deformation test is performed with the aim of evaluating the coefficient of linear thermal expansion of the material. The samples used for this test are manufactured according to 3.1.5. The test is

performed as follows:

The sample to be tested is left at the ambient temperature (which is measured) for sufficient time to have a uniform temperature in the material. At this point the sample is placed in a testing chamber at 0°C and an aluminium plate (this also is at 0°C) is placed on the top surface. On the plate a transducer measures the vertical deformation in time. The sample is left in the testing chamber until the deformation does not show significant changes. To be noted that all the devices present in the testing chamber are at 0°C when the sample is introduced so that the only deformations measured are the ones of the sample. An overview of the test set-up is shown in Figures 3.29 and 3.30. An example of the vertical deformation with time is given in Figure 3.31. The coefficient of linear thermal expansion is then calculated by dividing the total measured strain by the difference between the ambient temperature ($T_{initial}$, around 25°C) and 0°C (T_{final}). The measured coefficients for the two AGRAC mixes at different curing times are given in Figure 3.32. All the results obtained are presented in Table C.1 (Appendix C) along with information on the sample properties.

Figure 3.29: Thermal deformation test set-up

Figure 3.30: Deatail of measuring device
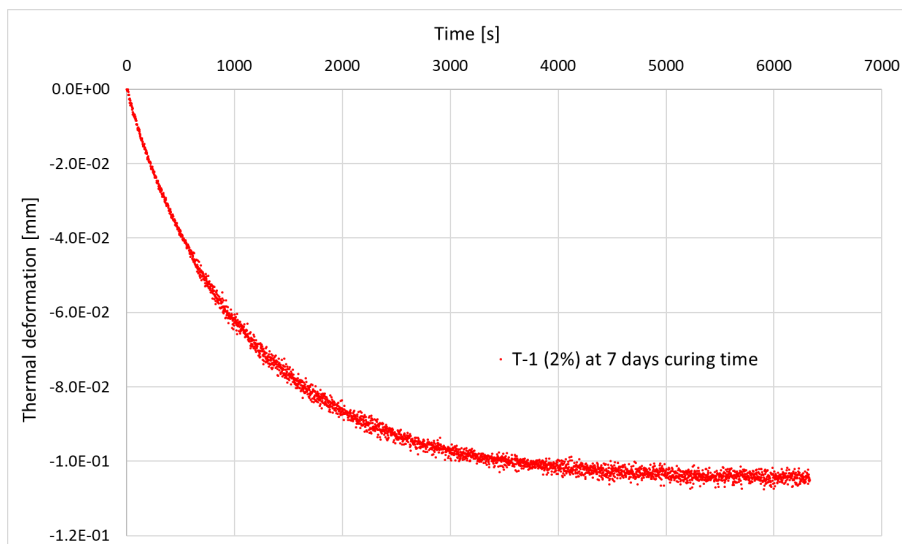
Figure 3.31: Thermal deformation plot for sample T-1 (AGRAC mix with 2% cement) at one week of curing time
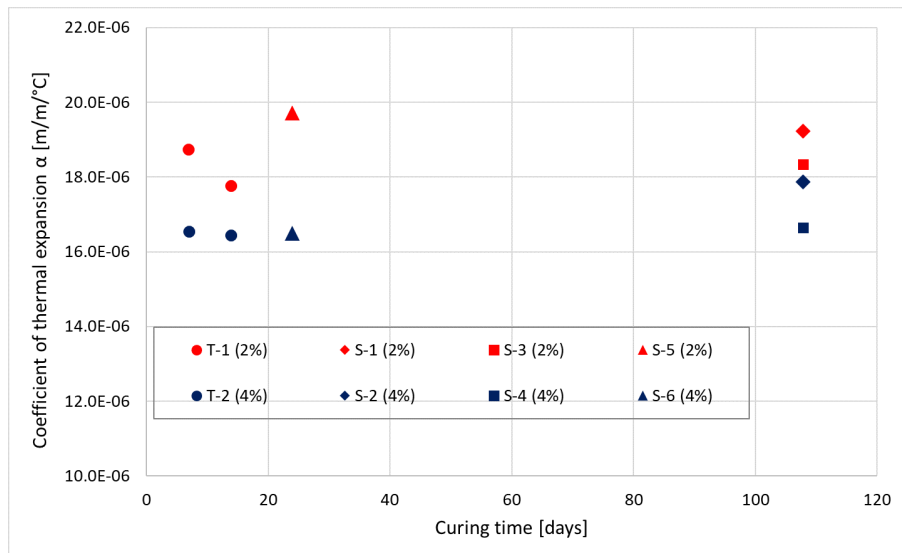
Figure 3.32: Thermal deformation resuts for the two AGRAC mixes

DISCUSSION ON THE RESULTS

Based on the results obtained from the thermal deformation test the following can be observed:

- According to the literature, the coefficient of thermal expansion (CTE) of concrete is in the range $[8 \div 15] \cdot 10^{-6}$ 1/°C while for asphalt it is in the range $[20 \div 30] \cdot 10^{-6}$ 1/°C. Therefore, the values obtained for the two AGRAC mixes are intermediate with respect to these two ranges. This is logical since AGRAC is composed by both materials.

- It seems that the curing time does not affect significantly the CTE results.

- For all the measurements the AGRAC samples with 2% cement show a higher CTE than the ones with 4% cement tested at the same curing time. This is attributed to the different water/cement ratio of the two AGRAC mixes (the AGRAC mix with 2% cement has double water/cement ratio compared with AGRAC 4%). Indeed, some research found the values of CTE to slightly increase with the increasing water/cement ratio [14].

- The other important factors influencing the CTE of concrete are the type of aggregates and the gradation of the mix [14]. It is not possible to evaluate the influence of these two factors in this project because only one type of reclaimed asphalt and one gradation curve is used for both mixes. Furthermore the reclaimed asphalt used might consist of different types of aggregates.

3.5. POISSON'S RATIO

The samples used for the determination of the Poisson's ratio are manufactured according to 3.1.5. The test is performed as follows:

The sample is placed at the intended temperature in the testing chamber (this also at the same temperature). Here a cyclic compressive load with frequency of 1 Hz is applied to the top of the specimen through a plate. As an output 4 dimensions are measured: three axial and one radial displacement. The three axial displacements are measured through LVDTs positioned along the lateral surface of the sample. The supports for the LVDTs are fixed with elastics at 1/6 of the specimen height from the top surface while three other small supports are

glued at 1/6 from the bottom (Figure 3.33). The radial displacement is recorded through a chain positioned around the cylinder (Figure 3.34).

Figure 3.33: Poisson's test set-up

Figure 3.34: Detail of the chain device

The amplitude of the deformation for each one of the 4 measurements is determined through a statistical analysis (non-linear least squares method) in which the data are fitted with a Fourier curve (Figures 3.35 and 3.36).
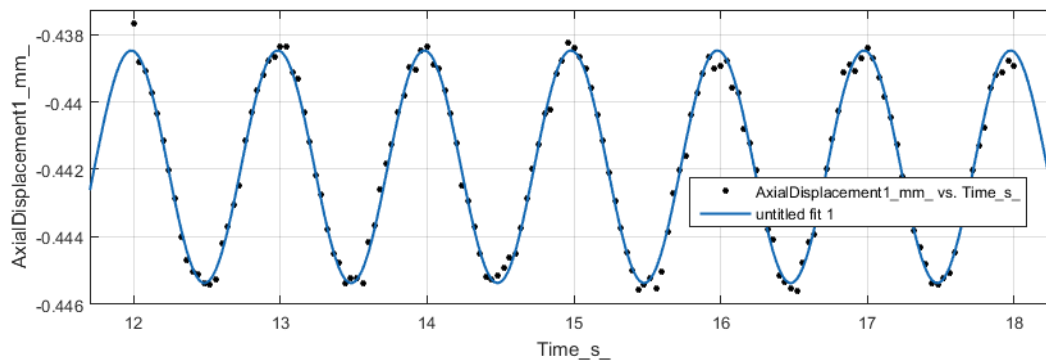
Figure 3.35: Example of axial displacement plotted against time and Fourier fitted curve

The axial strains are then obtained by dividing each axial deformation by the distance between the two supports (approximately 2/3 of the specimen height, 133 mm) and they are at last averaged to obtain the average axial strain amplitude (a_{ax}). The radial strain amplitude (a_{rad}) is obtained by dividing the radial deformation by the length of the sample circumference. The Poisson's ratio is then calculated as the ratio between the two amplitudes (Equation (3.2)). The Poisson's ratio results are given for two tested samples in Table 3.11. More detailed information on the obtained results are given in Table D.1 (Appendix D).

$$\nu = -\frac{a_{rad}}{a_{ax}} \qquad [\text{-}] \qquad (3.2)$$
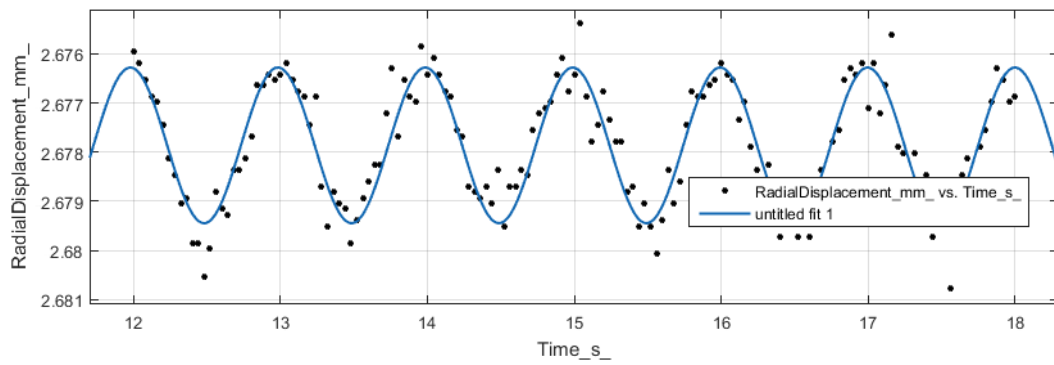
Figure 3.36: Example of radial displacement plotted against time and Fourier fitted curve

Sample ID	Cement	Curing time	Temperature	Load	Poisson's ratio
	%	days	°C	kN	-
S-3	2	104	25	1.5	**0.135**
S-3	2	104	15	1.5	**0.139**
S-3	2	104	15	3.0	**0.166**
S-4	4	104	15	3.0	**0.153**

Table 3.11: Poisson's ratio results

DISCUSSION ON THE RESULTS

Based on the results obtained from the Poisson's ratio test the following is noted:

- Changes due to temperature and applied load are observed (sample S-3). Nevertheless it is believed that the radial measurement is not accurate enough to determine the influence of these parameters on the Poisson's ratio. Indeed, the response of the radial chain is quite noisy (Figure 3.36). This is probably due to the rough surface of AGRAC which does not allow the chain to follow smoothly the deformations of the sample.

3.6. MODULUS OF ELASTICITY

The stiffness values are determined from the same data obtained from the ITT test (section 3.2).

From literature [5] it is found that the stiffness of a material can be derived from ITT monotonic test results through Equation (3.3).

$$E = (e\nu + f) \cdot \frac{S_h}{h} \qquad \text{[MPa]} \qquad (3.3)$$

Where:

- **e** and **f** [-] are parameters depending on the geometry of the sample. Here the values e=0.9988 and f=0.2714 are used [4].

- **ν** [-] is the Poisson's ratio, considered 0.15 for all curing times and temperatures (section 4.5).

- **S_h** [N/mm] is the slope of the regression line in the plot "Force - Horizontal displacement" from the monotonic ITT test.

- **h** [mm] is the height of the specimen, here considered as the average of four height measurements taken on the sample before testing.

DETERMINATION OF S_h

The regression line of the plot "Force - Horizontal displacement" (for a particular combination of AGRAC mix, temperature and curing time) is determined with the following criteria:

First the force F_{crack} for the chosen combination of parameters is considered (the values are determined in 3.2.3). Then the regression line is defined for the part of the graph between 20% and 80% of F_{crack}. The first part of the plot (0 to 20% of F_{crack}) is excluded because of the inaccurate measurements of the radial displacement for small values of the force. The last part of the plot (80 to 100% of F_{crack}) is excluded because of the change of slope that takes place as the normal force approaches F_{crack} which would cause a low R^2 value in the determination of S_h. An example of the determination of the regression line is given in Figure 3.37.
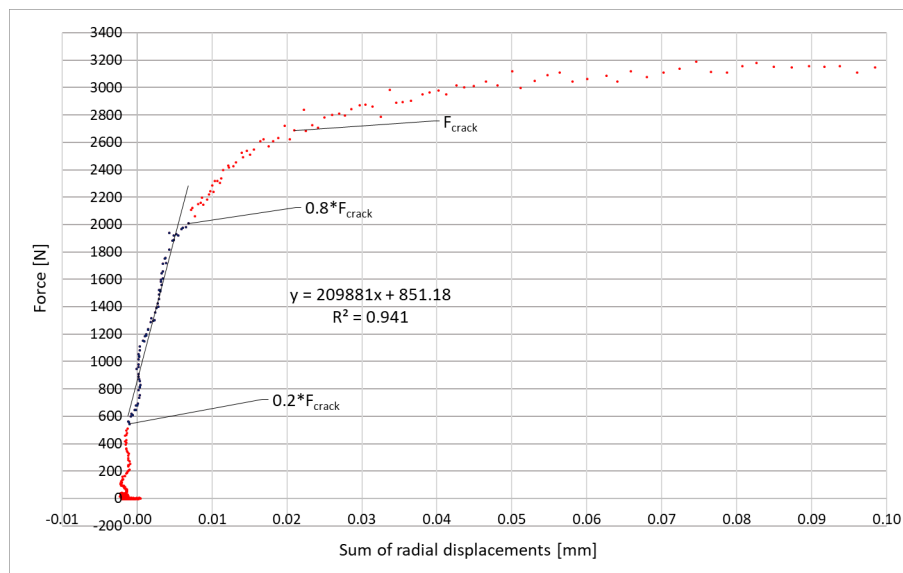
Figure 3.37: Plot of the vertical force against the horizontal displacement for a sample with 2% cement tested at 28 days curing time and 30°C

STIFFNESS RESULTS

By determining the regression line and its slope for all the samples it is possible to determine the stiffness E through Equation (3.3). The stiffness values can then be plotted against curing time for each one of the testing temperatures. These plots are given separately for the two AGRAC mixes in Figures 3.38 and 3.39. The stiffness values for the AGRAC mix with 4% cement at 28 days and some of the values for both mixes at 130 days curing time couldn't be derived because of an incorrect measurement of the horizontal displacement during the test. All the values are given in Appendix B along with the properties of each specimen.
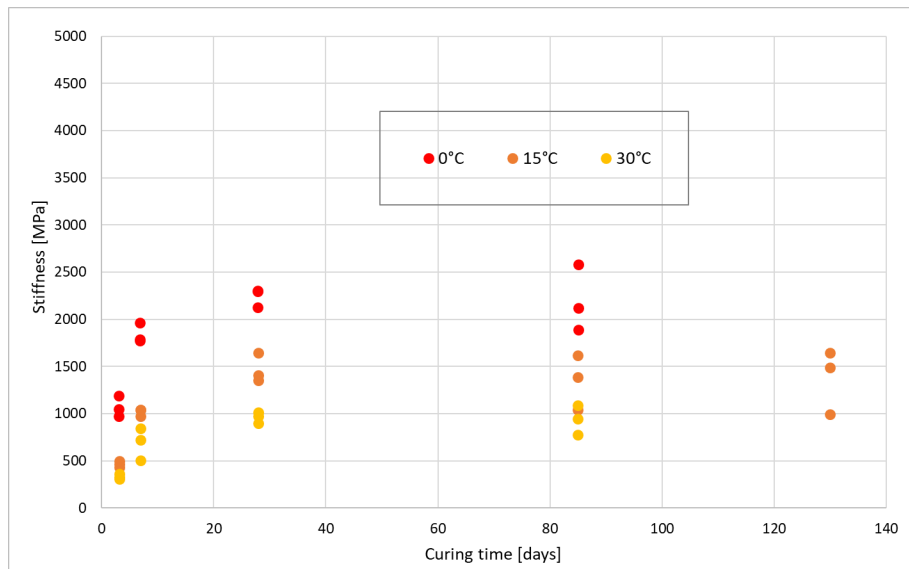
Figure 3.38: Plot of the stiffness for the AGRAC mix with 2% cement
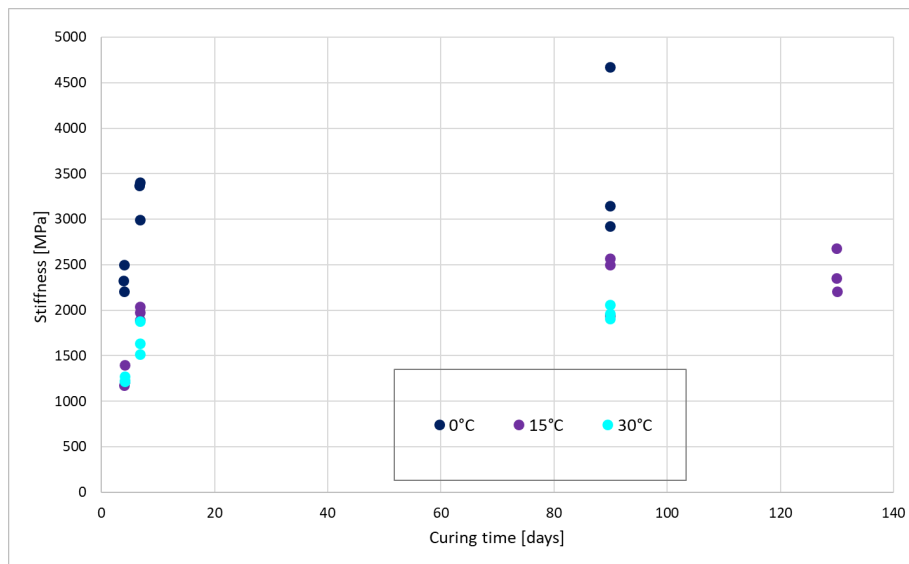
Figure 3.39: Plot of the stiffness for the AGRAC mix with 4% cement

DISCUSSION ON THE RESULTS

On the stiffness results the following is observed:

- As already found for the ITS, the stiffness values increase with an increase of the curing time and with a decrease of the temperature.

- The highest element of uncertainty in the determination of the stiffness values is the determination of S_h through the regression line. The method used for its determination (20 to 80% of F_{crack}) is considered reasonable for this particular case. Nevertheless, it is noted that the use of a different criterion might lead to a significant change in the E values, although the results would still show the same dependency with respect to curing time and temperature.

3.7. Relaxation

The evaluation of the relaxation properties of AGRAC is in a way the most challenging in this project for the following reasons:

- The amount of relaxation is expected to be dependent on many parameters e.g. temperature, amount of applied strain, curing time of the sample.

- From the relaxation results the decrease of the force due to relaxation has to be distinguished from the stiffness under development which will cause an increase of the force in time.

- The forces considered in the model are partly increasing with the curing time (due to shrinkage) and partly oscillatory (due to thermal deformation).

As a consequence only a few combinations of parameters can be tested. Therefore, the relaxation tests will only give an idea of the relaxation phenomenon in the material.

3.7.1. Test set-up

It is decided for the relaxation test to use the same set-up used for the ITT test (Figure 3.40, description of the set-up in 3.2.3). Indeed, the intention is to measure the relaxation in the same conditions in which the strength is measured. This will allow a more reliable comparison of the parameters in the model.

Figure 3.40: ITT test set-up

As mentioned before only a small combination of parameters are tested within the relaxation test. The test is controlled by the sum of the two radial displacements and it is performed as follows:

1. The specimen at 15°C is placed in the test set-up (this also at 15°C).

2. **Phase 1 (loading):** the sum of the radial displacements is increased linearly during 60 seconds until it reaches a defined value (around half of the displacement at which the crack occurs for the same curing time). As a consequence of course also the vertical force increases.

3. **Phase 2 (relaxation):** at this point the radial displacement is kept constant and the force necessary to keep constant that displacement is measured in time. The magnitude of the decrease of the force is the parameter which describes the relaxation of the material.

3.7.2. EXAMPLE

As an example the results obtained for an AGRAC sample with 4% cement are presented. The parameters of the tested sample are given in Table 3.12 where $F_{initial}$ is defined as the force at the end of the loading phase.

Sample ID	Cement percentage	Curing time at beginning of the test	Curing time at end of the test	Applied horizontal displacement	Initial force
	%	days	days	mm	kN
R-5	4%	1.98	5.75	0.0567	2.2820

Table 3.12: Sample R-5 relaxation parameters

The behaviour of the horizontal displacement is given for the first 10 minutes in Figure 3.41 (once the loading phase is finished, the behaviour of the horizontal displacement is the same until the end the test). The plot of the force is given in Figures 3.42, 3.43 and 3.44 for different time intervals. Also the behaviour of the stiffness for AGRAC mix with 4% cement at 15°C (determined in 3.6) is given in Figure 3.45 for the curing time interval corresponding to the duration of the relaxation test (from 1.98 to 5.75 days). From the figures the following is noticed:

- In Figures 3.41 and 3.42 the phases of loading and relaxation are clearly visible from the plots.

- Starting from around 10 minutes (from the starts of the test) the force starts oscillating around a fixed value (Figure 3.43). This oscillating behaviour is due to the radial transducers whose response becomes less accurate as the change in the force reduces.

- From Figure 3.43 we can notice that between the first and the second hour of the test the force oscillates around a constant value.

- Looking at the behaviour of the force during the 4 days (Figure 3.44) it can be seen that the force increases in time. This is due to the developing stiffness of the hardening material.

Therefore the problem is now to distinguish in the force plot the contribution of the relaxation from the contribution of the stiffness under development.
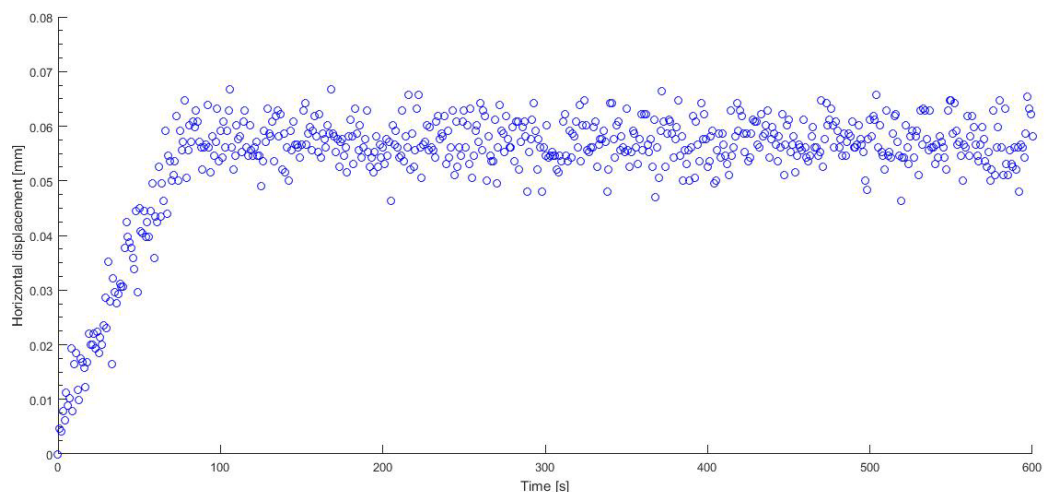
Figure 3.41: Relaxation of sample R-5: horizontal displacement (time up to 10 minutes)
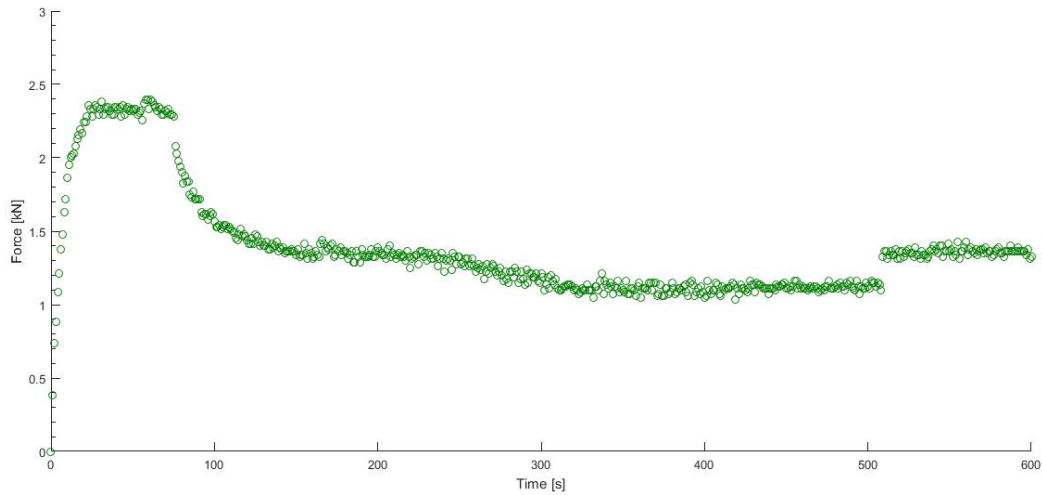
Figure 3.42: Relaxation of sample R-5: force (time up to 10 minutes)
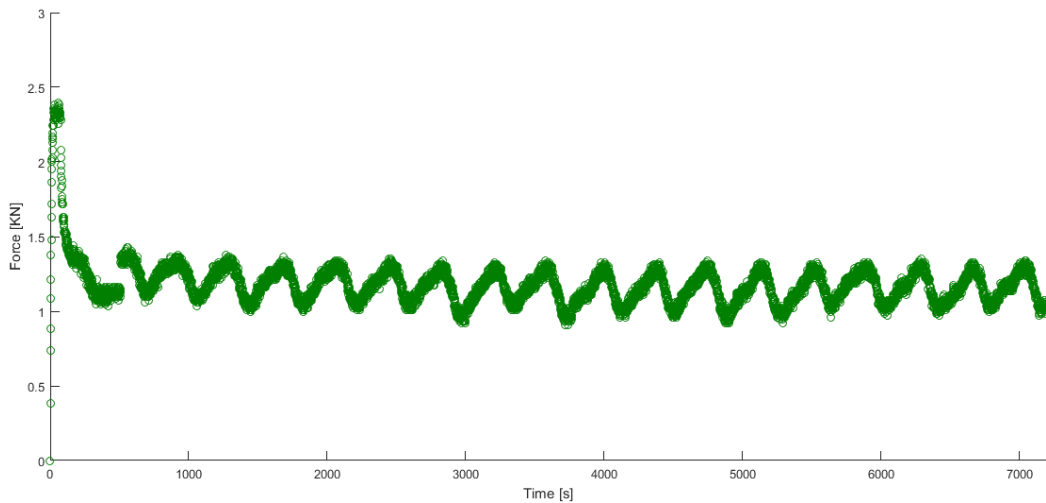
Figure 3.43: Relaxation of sample R-5: force (time up to 2 hours)

3.7.3. RELAXATION VS STIFFNESS

Looking at Figure 3.43 we can see that within 2 hours the force already reaches a stable value. If we can prove that the stiffness under development does not play a significant role in this time interval, this is enough to state that the relaxation phenomenon takes place within the first two hours of the test. Indeed, the relaxation rate decreases with time. Therefore, if this rate is already close to 0 within 2 hours of the test, then no more relaxation takes place in the remaining part of the test.

STEP 1: PROPORTIONALITY ASSUMPTION

In section 3.6 the modulus of elasticity E was calculated through Equation (3.4). Considering the Poisson's ratio (v) and the height of the specimen (h) as constant, the modulus E only depends on the slope of the regression line in the plot "Force - Horizontal displacement" S_h. In the relaxation test the horizontal displacement is kept constant. Therefore we can assume that the modulus of elasticity E during the relaxation test is proportional to the force F. This of course is an approximation because S_h was derived through a statistical analysis on the first part of the plot "Force - Horizontal displacement" and not just by taking the slope of the line connecting the origin of the graph with a given (displacement,force) coordinate.
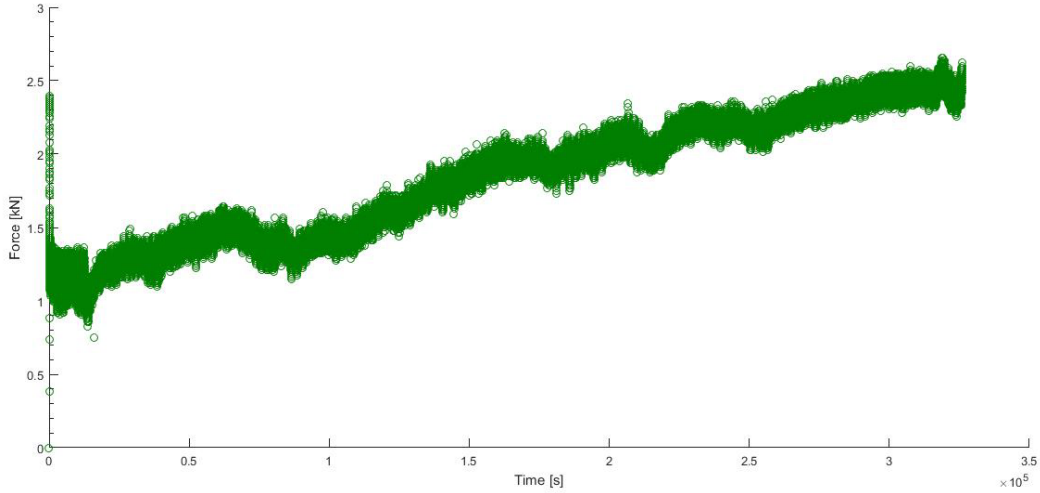
Figure 3.44: Relaxation of sample R-5: force (time until end of test)
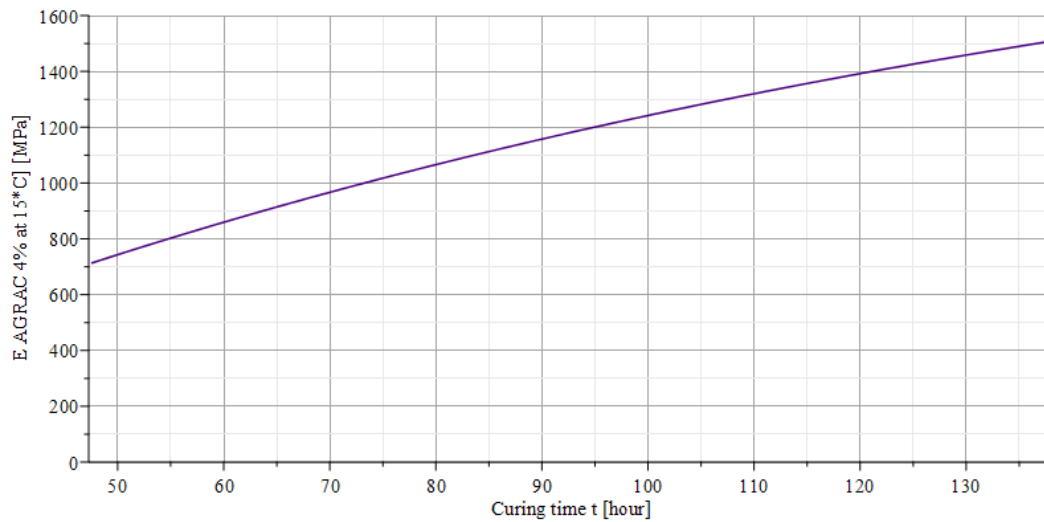
Figure 3.45: Stiffness of AGRAC 4% at 15°C from fitted curve (Equation (4.16))

The proportionality between E and F is expressed in Equation (3.5) (taking into account that in the example presented the AGRAC mix with 4% cement is used and that the test temperature is 15°C).

$$E = (ev + f) \cdot \frac{S_h}{h} \qquad \text{[MPa]} \tag{3.4}$$

$$\frac{E_{4\%}(1.98_{days}, 15)}{E_{4\%}(t, 15)} = \frac{F_{initial}}{F(t)} \qquad \text{[-]} \tag{3.5}$$

Let's now consider the first two hours of the test (Figure 3.43). It is noticed that from 1 hour from the start of the test until 2 hours the force oscillates around a value of around 1.145 kN (initial force at the end of the loading phase is 2.282 kN).

From the plot of the modulus of elasticity (Figure 3.45) of the same material for the same values of curing time it is derived that the modulus at 1.98 days and 1.98+2 hours curing time are $E_{4\%}(1.98, 15) = 715.75$ MPa and $E_{4\%}(1.98 + 2h, 15) = 738.62$. From the proportionality assumption we can calculate the increase of force after 2 hours of test due to the increasing stiffness (Equation (3.6)).

$$F(2_{hours}) = \frac{E_{4\%}(1.98 + 2h, 15)}{E_{4\%}(1.98, 15)} \cdot F_{initial} = \frac{738.62}{715.75} \cdot 1.145 = 1.181 \qquad \text{[kN]} \qquad (3.6)$$

From this equation it is known that the force in the first 2 hours of the test increases due to the developing stiffness by 0.037 kN. This value is equal to around 3% of the total decrease of the force in the first two hours of the test. Therefore, we can derive that in the first 2 hours of the test the stiffness under development can be neglected.

PROOF OF PROPORTIONALITY ASSUMPTION

The assumed proportionality between the modulus of elasticity and the force can be proven from the behaviour of the force in 4 days testing time. From Figures 3.44 and 3.45 we can write Equations (3.7) and (3.8).

$$\frac{E_{4\%}(5.75, 15)}{E_{4\%}(1.98, 15)} = \frac{1510}{714} = 2.115 \qquad \text{[-]} \qquad (3.7)$$

$$\frac{F(5.75_{days})}{F(1.98_{days})} = \frac{2.448}{1.145} = 2.138 \qquad \text{[-]} \qquad (3.8)$$

3.7.4. CALCULATION OF r

From what discussed in 3.7.3 it is decided to determine the percentage of the force left after relaxation through Equation (3.9).

$$r = \frac{F_{final}}{F_{initial}} \qquad \text{[\%]} \qquad (3.9)$$

Where:

- $F_{initial}$ [kN] is the force at the end of the loading phase.

- F_{final} [kN] is the force determined as the average of the force values between the first and the second hour of the test.

3.7.5. LIMITATIONS OF THE TEST PROCEDURE

As the stiffness of the AGRAC material increases the horizontal displacement corresponding to half of the strength is very small (a few μm). As a consequence the LVDT measurement of the radial displacement is not accurate enough and this leads to an inaccurate measurement of the force. As an example in Figures 3.46 and 3.47 is given the behaviour of the force in a relaxation test for an AGRAC sample with 4% cement tested at 3 weeks curing time. In this test the applied horizontal deformation was around 6 μm. From Figures 3.46 and 3.47 it is noticed that the force not only decreases but oscillates. This makes it more difficult to determine the amount of relaxation taking place in the material. As a conclusion we can state that in order to perform this test for high values of curing time a more accurate measuring device has to be used for the radial displacement (which is the controlled parameter in the test).
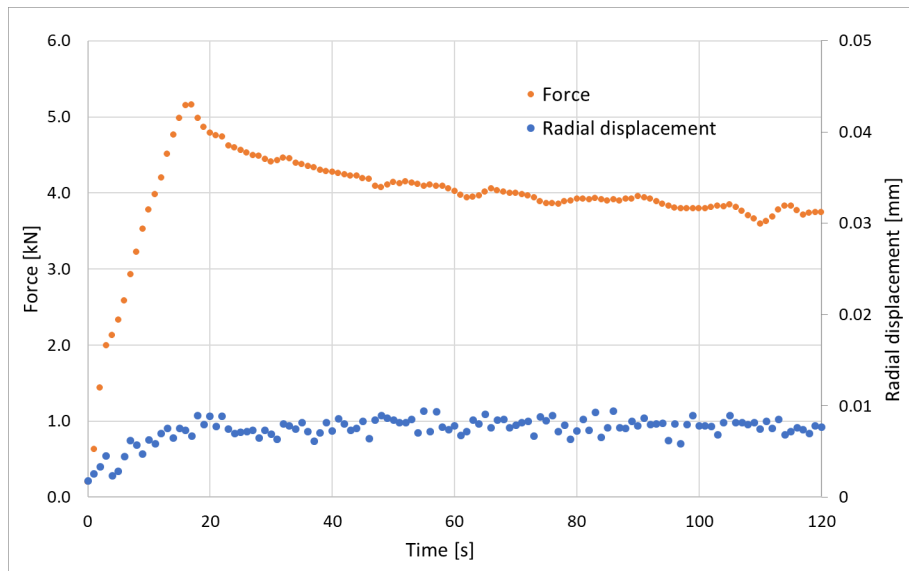
Figure 3.46: Sample R-6 (4% cement) tested at 3 weeks curing time (time up to 2 minutes)
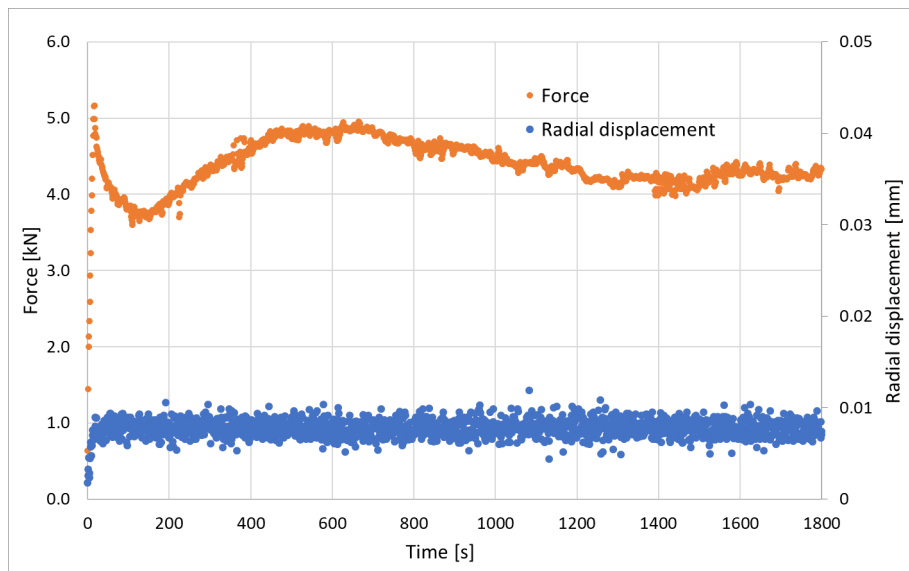
Figure 3.47: Sample R-6 (4% cement) tested at 3 weeks curing time (time up to 30 minutes)

3.7.6. THE RESULTS

The results obtained for the samples tested are given in Table 3.13. Additional information on the samples properties are given in Table E.1.

Sample ID	Cement percentage	Curing time at beginning of test	Applied horizontal displacement	Initial force	Final force	r
	%	days	mm	kN	kN	%
R-1	2%	8.08	0.0384	1.7830	0.5183	29.07
R-3	2%	1.96	0.0301	1.0338	0.3337	32.28
R-5	4%	1.98	0.0567	2.2820	1.1451	50.18

Table 3.13: Relaxation results

Discussion on the results

It is difficult, from the results obtained, to see the separate influences of the bitumen and cement on the relaxation results. What can be deduced from the results is that the relaxation is inversely proportional to the stiffness of the material. Indeed, the mix with 2% cement shows a higher relaxation than the mix with 4% cement.

4

STATISTICAL ANALYSIS OF THE RESULTS

In this chapter first the model for the temperature is described, then a statistical analysis is performed on the results presented in Chapter 3.

4.1. TEMPERATURE

The model for the temperature of the AGRAC base is the same as described in report 7-08-216-5 [7]. The year is considered 360 days long and each month consists of 30 days.
The "day average temperature" (temperature averaged on the 24 hours) is modelled as follows:

- The average value is 15°C and occurs on May 1st and November 1st.

- The amplitude is 10°C, thus the "day average temperature" is minimum 5°C (on February 1st) and maximum 25°C (on August 1st).

The "daily temperature" (temperature variation within 24 hours) is modelled as follows:

- During a day the temperature is equal to the "day average temperature" at 10:00 and 22:00.

- The amplitude of the "daily temperature" is 5°C, the minimum temperature occurs at 4:00 and the maximum at 16:00.

Therefore, the temperature T of the base from the time of construction is described by Equation (4.1).

$$T(t_{0_{day}}, t_{0_{hour}}, t) = 15 + 10 \cdot \sin\left[\left(\frac{t}{24} + t_{0_{day}}\right)\frac{\pi}{180}\right] + 5 \cdot \sin\left[\left(t - 10 + t_{0_{hour}}\right)\frac{\pi}{180}\right] \qquad [\text{°C}] \qquad (4.1)$$

Where:

- $t_{0_{day}}$ is the day of construction expressed as the number of days after May 1st.

- $t_{0_{hour}}$ is the hour of construction expressed as number from 0 to 24.

- t is the curing time in hours (time in hours after the time of construction).

It is noted that by fixing $t_{0_{day}}$ and $t_{0_{hour}}$ the temperature of the base is a function of curing time only. The function $T(t_{0_{day}}, t_{0_{hour}}, t)$ will be referred in the following sections simply as $T(t)$. As an example the temperature is plotted in the case of construction on August 1st at 10:00 ($t_{0_{day}} = 90$ and $t_{0_{hour}} = 10$) in

Figures 4.1 and 4.2.
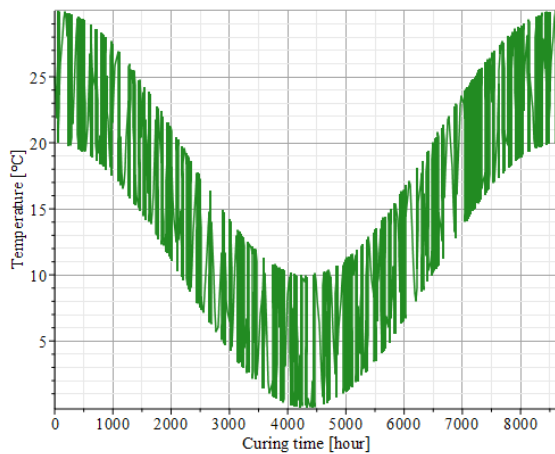
Figure 4.1: Temperture model for construction on August 1st at 10:00 (time up to 1 year)
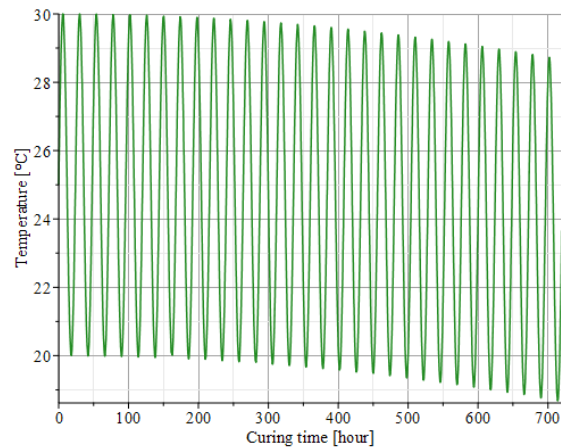
Figure 4.2: Temperature model for construction on August 1st at 10:00 (time up to 1 month)

4.2. INDIRECT TENSILE TEST - ITT

Taking as input the ITS results presented in 3.2.3, in this section the fitted curves are defined for the two AGRAC mixes at each testing temperature with a non-linear regression analysis (non-linear least squares method). Then, starting from these functions, the ITS values at all other temperatures in the range 0-30°C are determined. At last, using the definition of temperature given in section 4.1, the strength of the base is given as a function of curing time only.

4.2.1. FITTED CURVES

The equation used for fitting the ITS values (for each combination of AGRAC mix and temperature) is Equation (4.2), where t is the curing time (in hours) while a and b are the parameters to be determined. The equation is similar to the one suggested by Eurocode 2 to describe the development of the tensile strength of concrete in time [8]. To be noted that the equation implicitly assumes that the strength starts developing right after manufacturing ($t = 0$).

$$f(t) = a \cdot \exp\left(1 - \sqrt{\frac{b}{\frac{t}{24}}}\right) \qquad \text{[MPa, t in hours]} \qquad (4.2)$$

By running a statistical analysis (non-linear least squares method), the ITS data presented in 3.2.3 are fitted with the given equation. The parameters obtained from the analysis are given in Table 4.1. The fitted curves for AGRAC 2% ($\sigma_{2\%crack}(t,0)$, $\sigma_{2\%crack}(t,15)$ and $\sigma_{2\%crack}(t,30)$) and the ones for AGRAC 4% ($\sigma_{4\%crack}(t,0)$, $\sigma_{4\%crack}(t,15)$ and $\sigma_{4\%crack}(t,30)$) are presented separately in Figures 4.3 and 4.4.

	AGRAC 2% cement			AGRAC 4% cement		
	0°C	15°C	30°C	0°C	15°C	30°C
a	0.1433	0.0861	0.0565	0.2369	0.1778	0.1180
b	4.4910	2.6260	3.5650	1.7550	2.8880	3.8950
s*	0.0388	0.0199	0.0088	0.0250	0.0271	0.0236
R^{2}**	0.907	0.934	0.968	0.977	0.969	0.946

*Standard error of estimate   **R-squared: coefficient of determination

Table 4.1: Parameters for the fitted curves on the ITS results
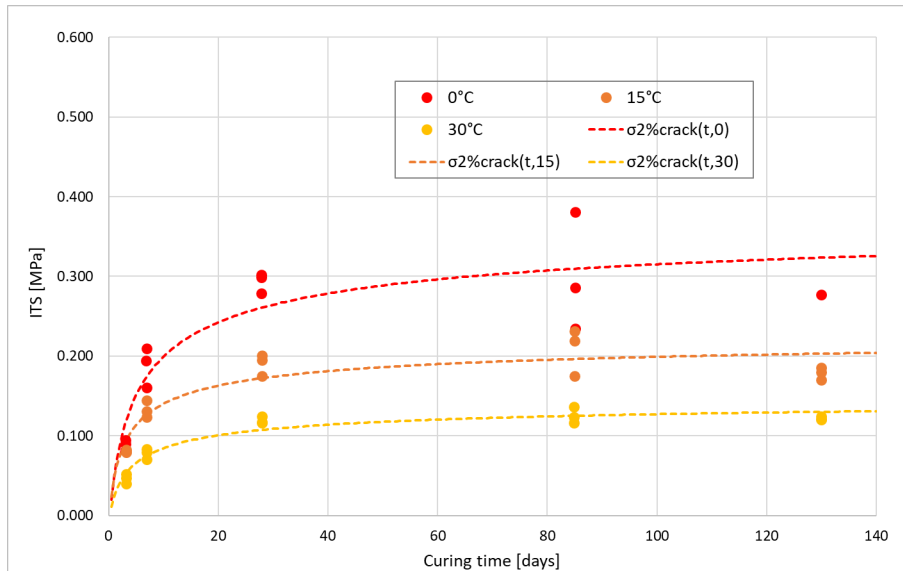
Figure 4.3: Fitted curves on the ITS results for the AGRAC mix with 2% cement
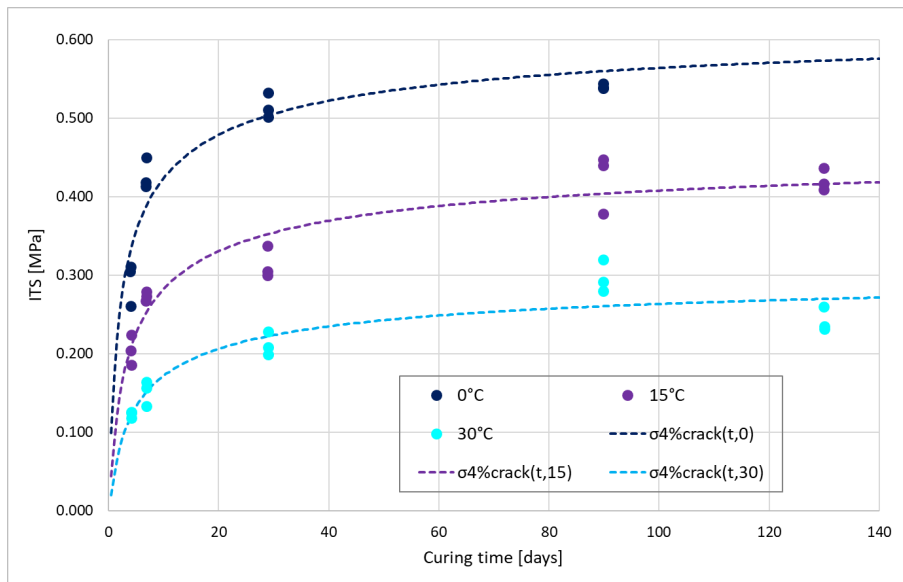
Figure 4.4: Fitted curves on the ITS results for the AGRAC mix with 4% cement

4.2.2. Strength function

The tensile strength has now to be defined as a function of curing time. This process is now described:

The first step consists of defining for every fixed curing time t^* the ITS values for all the temperatures in the range 0-30°C by considering a linear variation between and $\sigma_{crack}(t^*,0)$ and $\sigma_{crack}(t^*,15)$ and between $\sigma_{crack}(t^*,15)$ and $\sigma_{crack}(t^*,30)$ (Figures 4.5 and 4.6). As a consequence the value of $\sigma_{crack}(t^*,T^*)$ at a given curing time t^* and temperature T^* between 0°C and 30°C is described by Equation (4.3).
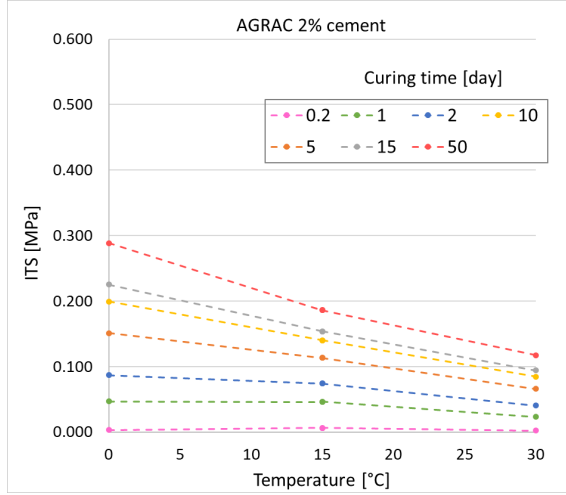
Figure 4.5: Linear variation of the ITS values with respect to the temperature at fixed curing times for the AGRAC mix with 2% cement. ITS values at 0, 15 and 30°C obtained from the fitted curves.
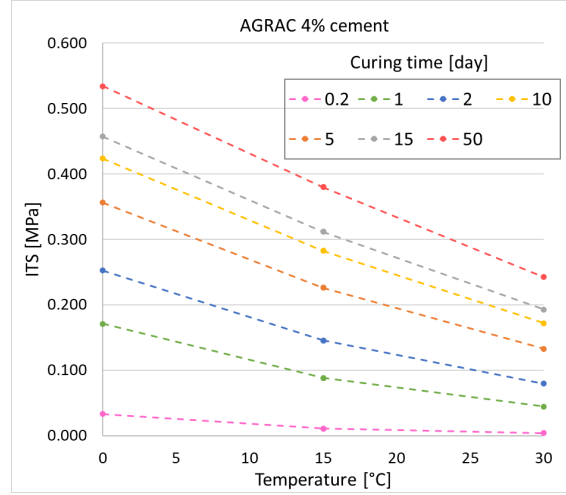
Figure 4.6: Linear variation of the ITS values with respect to the temperature at fixed curing times for the AGRAC mix with 4% cement. ITS values at 0, 15 and 30°C obtained from the fitted curves.

$$\sigma_{crack}(t^*,T^*) = \left(\sigma_{crack}(t^*,0) - \left[\sigma_{crack}(t^*,0) - \sigma_{crack}(t^*,15)\right] \cdot \frac{T^*}{15}\right) \cdot p_{0-15}(T^*)$$

$$+ \left(\sigma_{crack}(t^*,15) - \left[\sigma_{crack}(t^*,15) - \sigma_{crack}(t^*,30)\right] \cdot \frac{T^*-15}{15}\right) \cdot p_{15-30}(T^*) \qquad \text{[MPa, T* in °C]} \quad (4.3)$$

Where p_{0-15} and p_{15-30} are two piecewise functions defined as:

$$p_{0-15}(T^*) = \begin{cases} 1 & T^* \leq 15 \\ 0 & \text{otherwise} \end{cases} \qquad (4.4)$$

$$p_{15-30}(T^*) = \begin{cases} 1 & T^* > 15 \\ 0 & \text{otherwise} \end{cases} \qquad (4.5)$$

The dependence of the tensile strength on the curing time and temperature for the two mixes is also given in Appendix G in a format more convenient for practice usage.

The next step is to define the tensile strength of the AGRAC base as a function of curing time only. Indeed, by fixing the construction time in the year, the temperature of the AGRAC base $T(t_{0_{day}}, t_{0_{hour}}, t) = T(t)$ varies according to Equation (4.1). By replacing in Equation (4.3) T^* with $T(t)$ and t^* with t (curing time in hours from moment of construction) the resulting AGRAC base strength is given by Equation (4.6).

$$\sigma_{crack}(t,T(t)) = \left(\sigma_{crack}(t,0) - \left[\sigma_{crack}(t,0) - \sigma_{crack}(t,15)\right] \cdot \frac{T(t)}{15}\right) \cdot p_{0-15}(T(t))$$

$$+ \left(\sigma_{crack}(t,15) - \left[\sigma_{crack}(t,15) - \sigma_{crack}(t,30)\right] \cdot \frac{T(t)-15}{15}\right) \cdot p_{15-30}(T(t)) \qquad \text{[MPa, T in °C]} \quad (4.6)$$

It is again noted that by choosing an AGRAC mix (2 or 4% cement) the 3 ITS functions ($\sigma_{crack}(t,0)$, $\sigma_{crack}(t,15)$ and $\sigma_{crack}(t,30)$) are known. Furthermore, by fixing the moment of construction the temperature of the base $T(t)$ is also known. As a results the tensile strength of the base $\sigma_{crack}(t,T(t))$ only depends on the curing time t. As an example, the function $\sigma_{crack}(t,T(t))$ is plotted in Figures 4.7 and 4.8 for both AGRAC mixes for a base constructed on August 1st ($t_{0_{day}} = 90$) at 10:00 ($t_{0_{hour}} = 10$). In Figures 4.7 and 4.8 it is noted that the tensile strength reaches its peak when the temperature is lowest (on February 1st, 4320 hours from construction). The behaviour of the temperature throughout the year for the chosen time of construction is given in Figure 4.1.
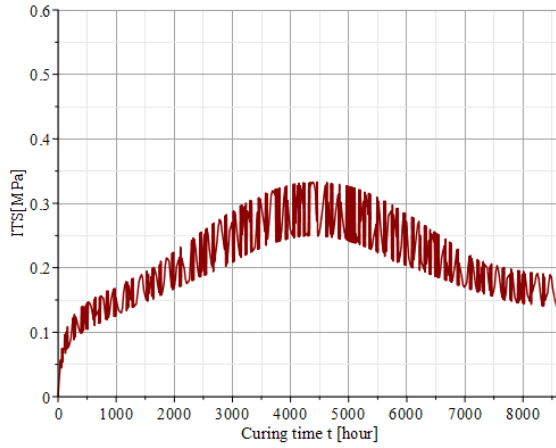
Figure 4.7: ITS function of AGRAC mix with 2% cement for a base constructed on August 1st at 10.00 (time up to 1 year)
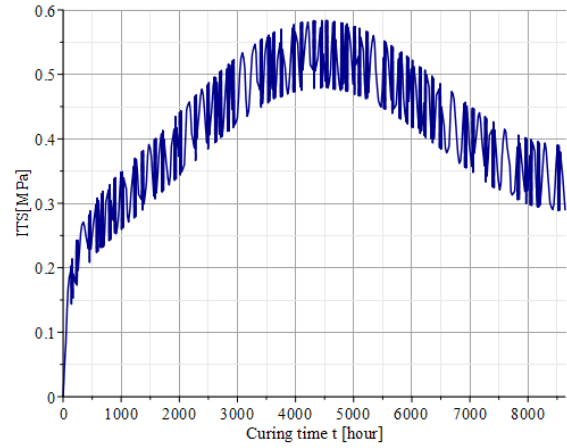
Figure 4.8: ITS function of AGRAC mix with 4% cement for a base constructed on August 1st at 10.00 (time up to 1 year)

4.3. SHRINKAGE

In this section first the shrinkage data presented in section 3.3 are fitted with an equation derived form the shrinkage model CEB90. Second, the fitted curves obtained for the specimens are adapted to the road base conditions through factors which take into account the relative humidity and the dimensions of the base.

4.3.1. THE MODEL CEB90

Many models are available which predict the development of shrinkage in concrete structures, however at the moment none of them was specifically developed for a material similar to AGRAC. Nevertheless, Saloua et Al. found that the shrinkage model CEB90 can predict the shrinkage strains in cement treated RAP mixes [6]. This observation was based on a series of shrinkage tests (test set-up was very similar to the one used in this research) on a cement treated material where the RAP used was up to 50% of the total aggregates mass and the cement content was 6% m/m. For this reason the model CEB90 is used in this project.

Shrinkage model CEB90 is valid for normal weight plain structural concrete having an average compressive strength (f_{cm28}) in the range of 20-90 MPa, moist cured at normal temperatures not longer than 14 days and exposed to a mean ambient relative humidity in the range of 40 to 100% at mean ambient temperatures (5 to 30°C) [13]. The total shrinkage strain $\epsilon_{sh}(t,t_s)$, which takes into account both the drying and the autogenous shrinkage, is given by Equation (4.7).

$$\epsilon_{sh}(t,t_s) = \epsilon_s \cdot \beta_{RH}(h) \cdot \beta_s(t - t_s) \qquad [-] \qquad (4.7)$$

- t [days] is the age of concrete and t_s [days] is the age of concrete at the beginning of drying.

- ϵ_s [-] is a factor depending on the type of cement and the strength of concrete at 28 days.

- $\beta_{RH}(h)$ [-] takes into account the relative humidity and it is given by $\beta_{RH}(h) = 1 - h^3$ where h is the relative humidity (as a decimal).

- $\beta_s(t - t_s)$ [-] is the coefficient describing the development of shrinkage with time of drying. It is given by Equation (4.8) [6] or Equation (4.9) [13] where $\left(\frac{A_c}{u}\right)$ [-] (in mm) is the ratio between the cross section and the perimeter in contact with the atmosphere and $\left(\frac{V}{S}\right)$ [-] (in mm) is the ratio between the volume and the surface in contact with the atmosphere.

$$\beta_s(t - t_s) = \left(\frac{(t - t_s)}{(t - t_s) + 0.14 \cdot \left(\frac{A_c}{u}\right)^2} \right)^{0.5} \qquad [-] \tag{4.8}$$

$$\beta_s(t - t_s) = \left(\frac{(t - t_s)}{(t - t_s) + 0.14 \cdot \left(\frac{V}{S}\right)^2} \right)^{0.5} \qquad [-] \tag{4.9}$$

4.3.2. Adjustment of model CEB90 to AGRAC results

At this point we try to fit the shrinkage results with Equation (4.7) through a non-linear regression analysis by considering $t_s = 1.75$ (section 3.3), $h = 0.55$ (moisture in curing room) and $\frac{V}{S} = 22.2$ (from samples geometry, bottom surface not considered in S). The analysis is then performed with the only unknown of ϵ_s (Equation (4.10)). The results for the AGRAC mix with 2% cement are given in Figure 4.9. As it can be seen from the picture, the analysis gives very poor results because the shape of the function (given by $\beta_s(t - t_s)$) does not fit the shape of the data.

$$\epsilon_{sh}(t, 1.75) = \epsilon_s \cdot (1 - 0.55^3) \cdot \left(\frac{(t - 1.75)}{(t - 1.75) + 0.14 \cdot 22.2^2} \right)^{0.5} \qquad \left[\frac{\mu m}{m}, \text{t in days} \right] \tag{4.10}$$
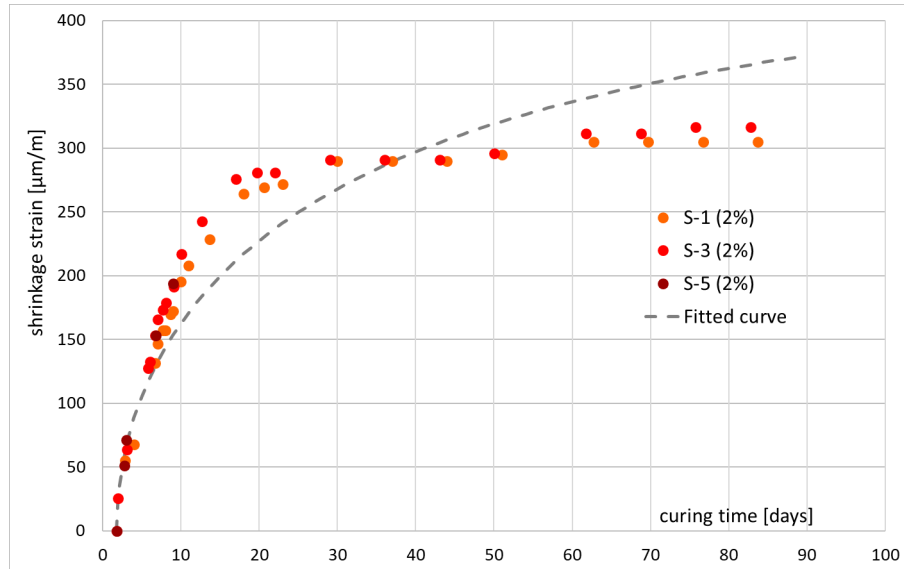
Figure 4.9: Fitted curve on the shrinkage results for the AGRAC mix with 2% cement, from the analysis $\epsilon_s = 596.5 \mu\text{m/m}$

It is decided to change the value 0.14 in Equation (4.10) with a free parameter to be calculated through the statistical analysis. It is found that the most suitable value is 0.045. This value is used for both AGRAC mixes.

Indeed, the differences due to the different strength of the materials are taken into account by ϵ_s. The functions used for fitting the results is then Equation (4.11). The analysis leads to $\epsilon_s = 440.8\ \mu$m/m for AGRAC 2% and $\epsilon_s = 448.7\ \mu$m/m for AGRAC 4% (Figures 4.10 and 4.11).

$$\epsilon_{sh}(t, 1.75) = \epsilon_s \cdot (1 - 0.55^3) \cdot \left(\frac{(t - 1.75)}{(t - 1.75) + 0.045 \cdot 22.2^2} \right)^{0.5} \qquad \left[\frac{\mu m}{m}, \text{t in days} \right] \qquad (4.11)$$
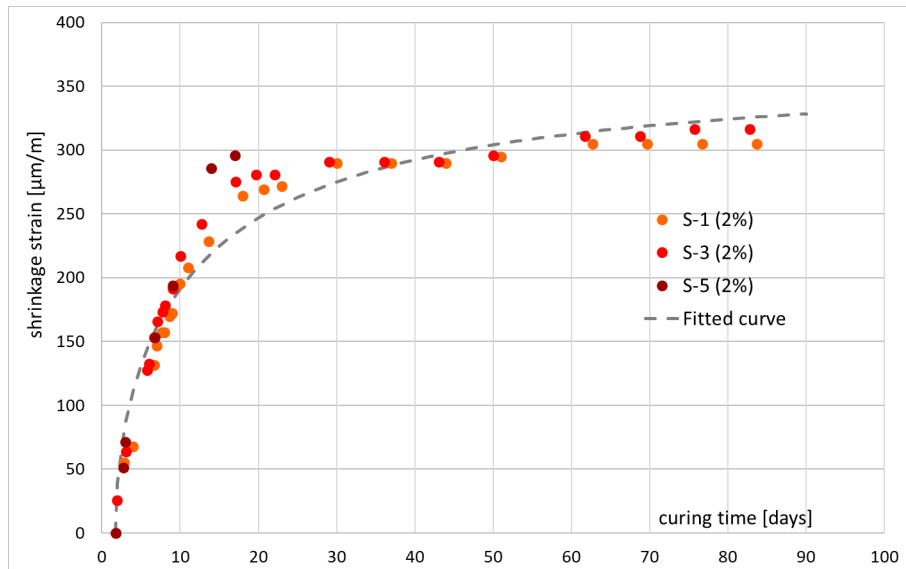
Figure 4.10: Fitted curve on the shrinkage results for the AGRAC mix with 2% cement, from the analysis $\epsilon_s = 440.8\ \mu$m/m
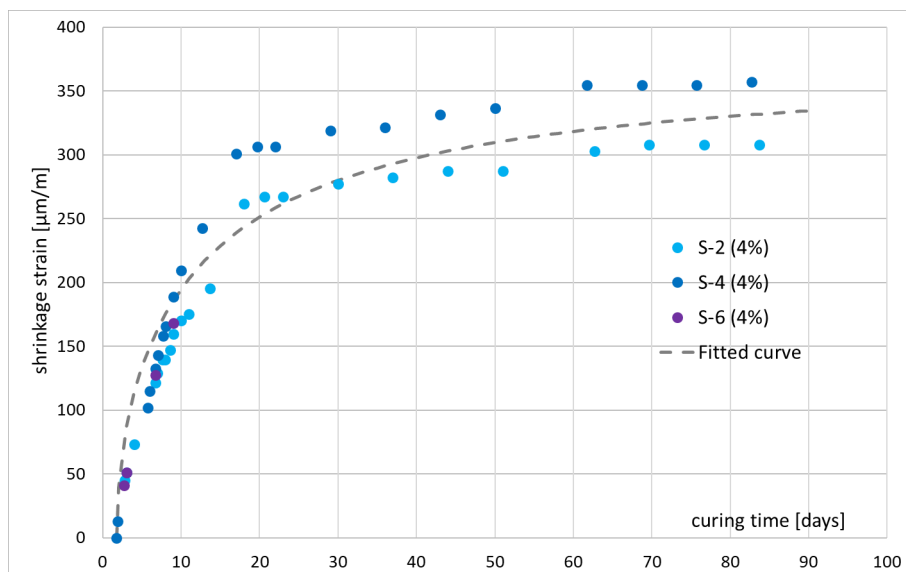
Figure 4.11: Fitted curve on the shrinkage results for the AGRAC mix with 4% cement, from the analysis $\epsilon_s = 448.7 \mu$m/m

4.3.3. FROM SAMPLES TO ROAD BASE

The shrinkage curves determined for the specimens have now to be adapted to the road base situation. This is done by taking into account the changes in humidity and geometry. In particular the following assumptions are made:

- The relative humidity at the place where the base is constructed is 80%. This leads to $\beta_{RH}(0.80) = 1 - 0.80^3$.

- Instead of $\frac{V}{S}$, for the base the ratio $\frac{A_c}{u}$ is used. Considering a base 10 m wide and 0.3 m deep the ratio is equal to $\frac{A_c}{u} = 283.0$. To be noted that in this calculation it is assumed that the upper surface and the two lateral edges of the base are exposed to the atmosphere (upper layer is not yet constructed).

By substituting this values in the fitted curves found for the specimens (leaving unchanged all the remaining parameters) the resulting equations for the shrinkage strain of road base are given by Equations (4.12) and (4.13) for the AGRAC mixes with 2 and 4% cement respectively.

$$\epsilon_{sh}(t,1.75) = 440.8 \cdot (1-0.80^3) \cdot \left(\frac{(t-1.75)}{(t-1.75)+0.045\cdot 283.0^2}\right)^{0.5} \qquad \left[\frac{\mu m}{m}, \text{t in days}\right] \qquad (4.12)$$

$$\epsilon_{sh}(t,1.75) = 448.7 \cdot (1-0.80^3) \cdot \left(\frac{(t-1.75)}{(t-1.75)+0.045\cdot 283.0^2}\right)^{0.5} \qquad \left[\frac{\mu m}{m}, \text{t in days}\right] \qquad (4.13)$$

The curves plotted for curing time up to 1 year are given in Figure 4.12. It can be noted that the two curves in Figure 4.12 don't show any significant difference and therefore in the model (developed in Chapter 5) a single curve will be considered for both AGRAC mixes. This curve is obtained by averaging the two values of ϵ_s of the two curves and it is given in Equation (4.14).
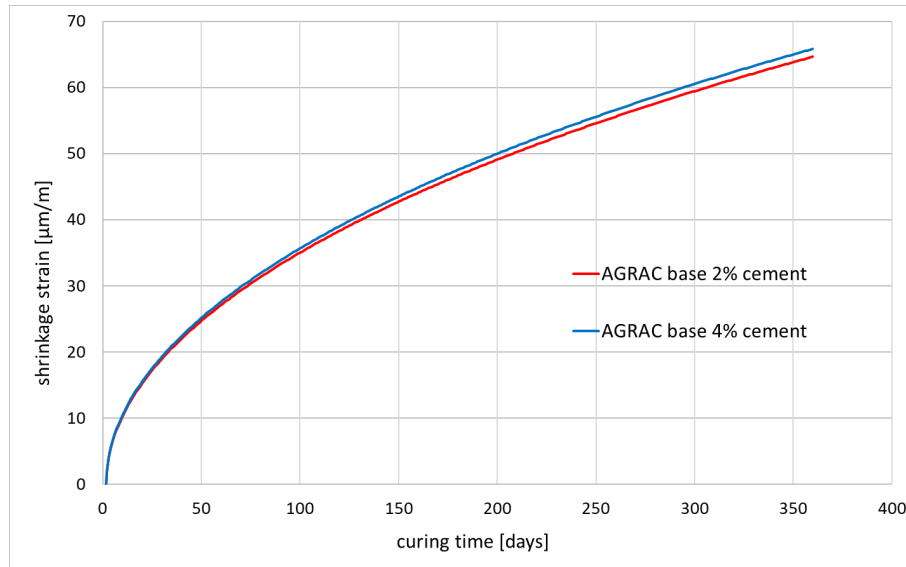
Figure 4.12: Prediction of the shrinkage of the AGRAC base for the two mixes

$$\epsilon_{shr}(t,1.75) = \frac{444.8}{10^6} \cdot (1-0.80^3) \cdot \left(\frac{\left(\frac{t}{24}-1.75\right)}{\left(\frac{t}{24}-1.75\right)+0.045\cdot 283.0^2}\right)^{0.5} \qquad [\text{strain, t in hours}] \qquad (4.14)$$

4.4. THERMAL DEFORMATION

The thermal coefficients are considered constant for each AGRAC mix and are determined as the average of the values presented in section 3.4. The two resulting thermal coefficients are given in Figure 4.13 and Equation (4.15).
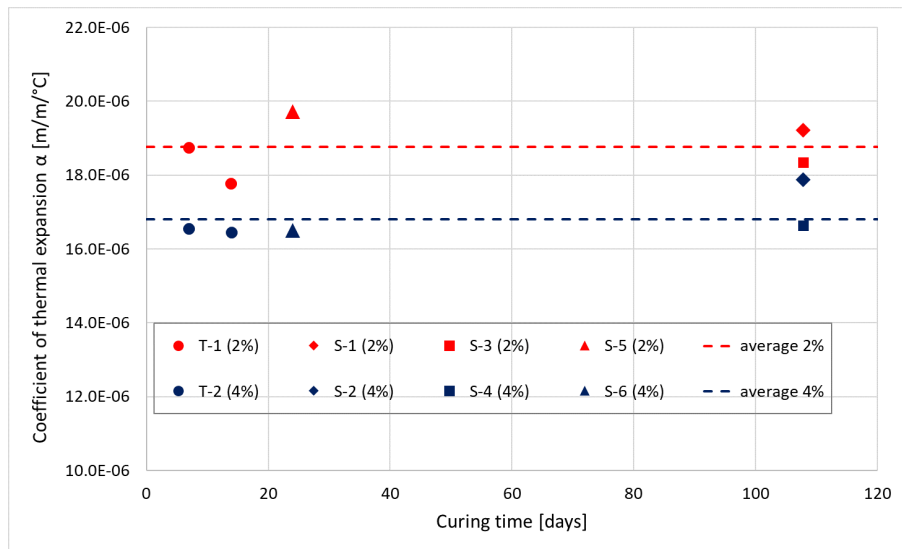
Figure 4.13: Thermal coefficients for the two AGRAC mixes

$$\alpha_{2\%} = 18.76 \cdot 10^{-6} \qquad \alpha_{4\%} = 16.80 \cdot 10^{-6} \qquad \text{[m/m/°C]} \qquad (4.15)$$

4.5. POISSON'S RATIO

Considering what discussed in section 3.5 it is decided to use a single constant value of Poisson's ratio for the two AGRAC mixes: $\nu = 0.15$.

4.6. MODULUS OF ELASTICITY

Taking as input the stiffness results presented in section 3.6, in this section the fitted curves are defined for the two AGRAC mixes at each testing temperature with a non-linear regression analysis (non-linear least squares method). Then, starting from these functions, the E values at all other temperatures in the range 0-30°C are determined. At last, using the definition of temperature given in section 4.1, the stiffness of the base is given as a function of curing time only.

4.6.1. FITTED CURVES

It is found that Equation (4.16) fits well the stiffness values. To be noted that the chosen equation implies that the stiffness starts developing right after manufacturing (t=0).

$$f(t) = a \cdot \exp\left(-b \cdot \frac{t}{24}\right) - a \qquad \text{[MPa, t in hours]} \qquad (4.16)$$

By running a statistical analysis (non-linear least squares method), the stiffness data presented in section 3.6 are fitted with the the given conditions. The parameters obtained from the analysis for each curve are given in Table 4.2. The fitted curves for AGRAC 2% ($E_{2\%}(t,0)$, $E_{2\%}(t,15)$ and $E_{2\%}(t,30)$) and the ones for AGRAC 4% ($E_{4\%}(t,0)$, $E_{4\%}(t,15)$ and $E_{4\%}(t,30)$) are presented separately in Figures 4.14 and 4.15.

	AGRAC 2% cement			AGRAC 4% cement		
	0°C	15°C	30°C	0°C	15°C	30°C
a	-2232	-1405	-957	-3633	-2389	-1991
b	0.2305	0.1611	0.1613	0.2756	0.2130	0.2481
s*	162.0	181.5	100.4	442.3	197.7	98.9
R^{2}**	0.969	0.908	0.939	0.917	0.959	0.986

*Standard error of estimate   **R-squared: coefficient of determination

Table 4.2: Parameters for the fitted curves on the stiffness results
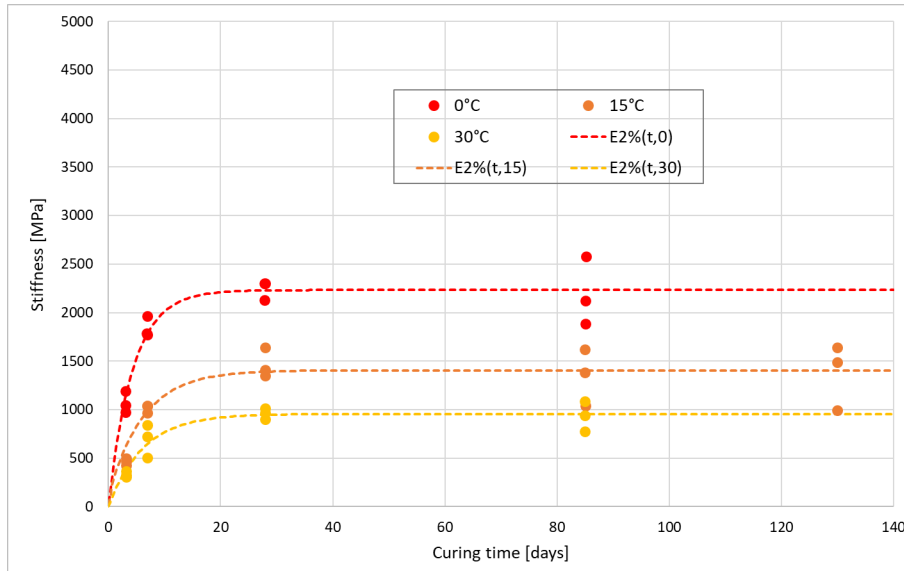
Figure 4.14: Fitted curves on the stiffness results for the AGRAC mix with 2% cement
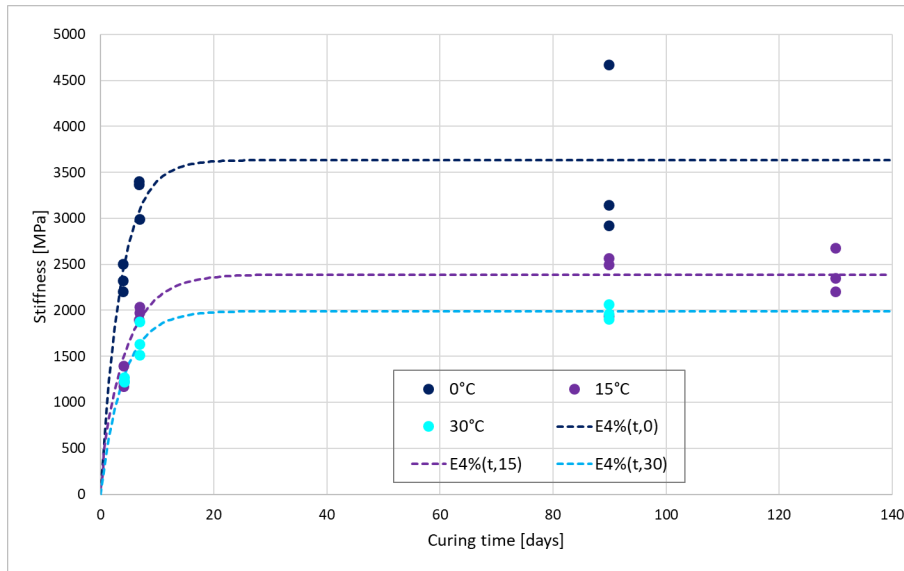
Figure 4.15: Fitted curves on the stiffness results for the AGRAC mix with 4% cement

4.6.2. STIFFNESS FUNCTION

The stiffness has now to be defined as a function of curing time. This process is now described:

As done for the ITS values in 4.2.2, for every fixed curing time the stiffness values E are considered to vary linearly between and 0 and 15°C and between 15 and 30°C (Figures 4.16 and 4.17). As a consequence the value of E at a given curing time t^* and temperature T^* between 0°C and 30°C is described by Equation (4.17).
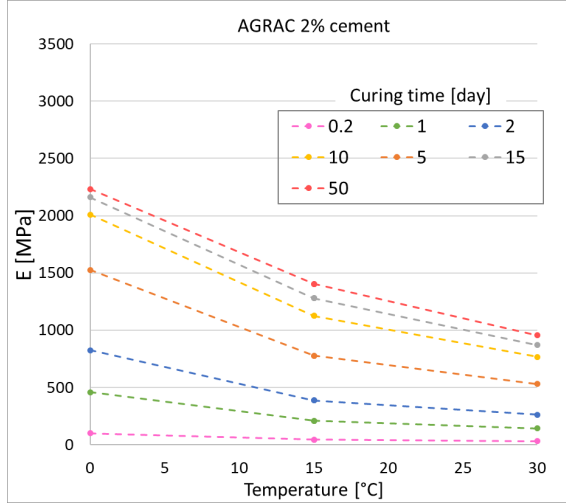
Figure 4.16: Linear variation of the E values with respect to the temperature at fixed curing times for the AGRAC mix with 2% cement. E values at 0, 15 and 30°C obtained from the fitted curves.
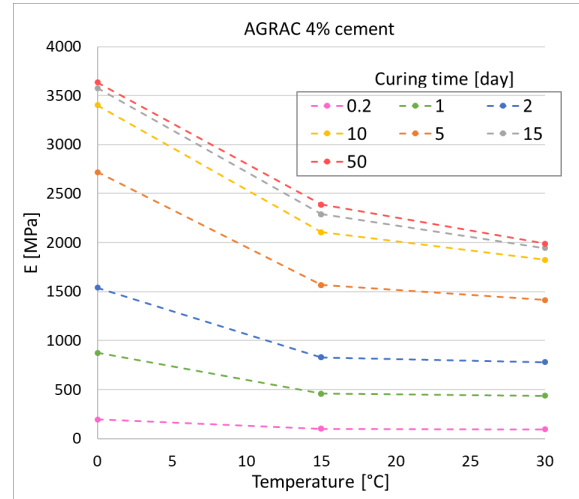
Figure 4.17: Linear variation of the E values with respect to the temperature at fixed curing times for the AGRAC mix with 4% cement. E values at 0, 15 and 30°C obtained from the fitted curves.

$$E(t^*, T^*) = \left(E(t^*, 0) - \left[E(t^*, 0) - E(t^*, 15)\right] \cdot \frac{T^*}{15}\right) \cdot p_{0-15}(T^*)$$
$$+ \left(E(t^*, 15) - \left[E(t^*, 15) - E(t^*, 30)\right] \cdot \frac{T^* - 15}{15}\right) \cdot p_{15-30}(T^*) \qquad \text{[MPa, T* in °C]} \quad (4.17)$$

Where p_{0-15} and p_{15-30} are the two piecewise functions already defined in 4.2.2.

The dependence of the modulus of elasticity on the curing time and temperature for the two mixes is also given in Appendix G in a format more convenient for practice usage.

The next step is to define the stiffness $E(t, T(t))$ of the AGRAC base as a function of curing time only (Equation (4.18)).

$$E(t, T(t)) = \left(E(t, 0) - \left[E(t, 0) - E(t, 15)\right] \cdot \frac{T(t)}{15}\right) \cdot p_{0-15}(T(t))$$
$$+ \left(E(t, 15) - \left[E(t, 15) - E(t, 30)\right] \cdot \frac{T(t) - 15}{15}\right) \cdot p_{15-30}(T(t)) \qquad \text{[MPa, T in °C]} \quad (4.18)$$

As an example the function $E(t, T(t))$ is plotted in Figures 4.18 and 4.19 for both AGRAC mixes for a base constructed on August 1st ($t_{0_{day}} = 90$) at 10:00 ($t_{0_{hour}} = 10$).
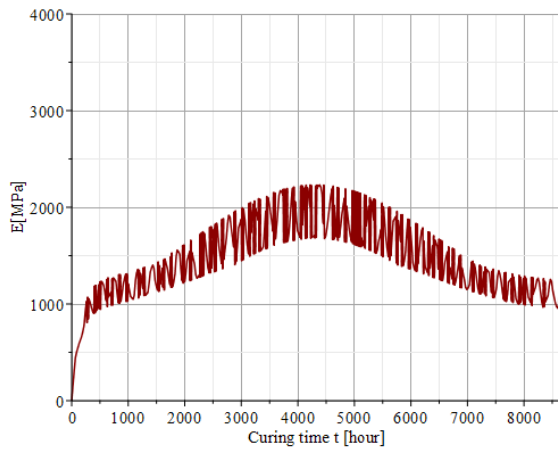
Figure 4.18: E function of AGRAC mix with 2% cement for a base constructed on August 1st at 10.00 (time up to 1 year)
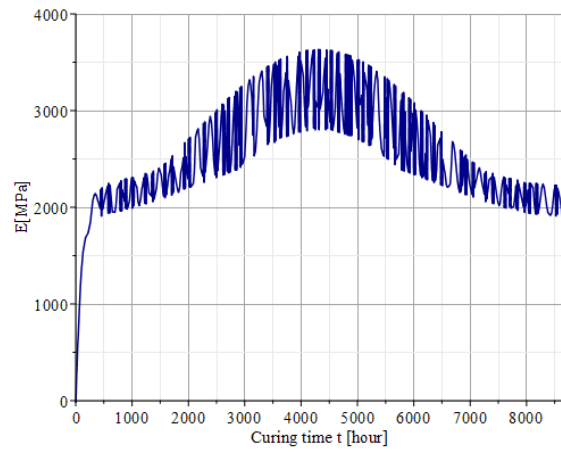
Figure 4.19: E function of AGRAC mix with 4% cement for a base constructed on August 1st at 10.00 (time up to 1 year)

4.7. RELAXATION

The relaxation coefficients for each AGRAC mix are taken as the average of the values presented in section 3.7. The resulting relaxation coefficients used in the model are given in Equation (4.19).

$$r_{2\%} = 30.67 \qquad r_{4\%} = 50.18 \qquad [\%] \qquad\qquad (4.19)$$

5

MODELLING

In this chapter the fitted curves defined in Chapter 4 are combined in order to construct, for a given time of construction, the occurring stresses $\sigma_{occ}(t, T(t))$ in the base. Then the occurring stresses are compared with the tensile strength $\sigma_{crack}(t, T(t))$. From the comparison it is determined whether the cracks occur and, if so, the crack pattern is analysed. The results are presented for both the AGRAC mixes for particular times of construction. The convention for the stresses is to consider positive the tensile stresses.

5.1. OCCURRING STRESSES

In this section the stresses due to shrinkage and thermal deformation are defined. The sum of these two stresses gives the total occurring stresses in the AGRAC base.

5.1.1. SHRINKAGE STRESSES

The shrinkage stresses $\sigma_{shr}(t, T(t))$ are given by (Equation (5.1)).

$$\sigma_{shr}(t, T(t)) = r \cdot E(t, T(t)) \cdot \epsilon_{shr}(t) \qquad \text{[MPa]} \qquad (5.1)$$

Where:

- r [-] is the relaxation coefficient as defined in 4.7.

- $E(t, T(t))$ [MPa] is the modulus of elasticity depending only on the curing time t by fixing the time of construction (4.6).

- $\epsilon_{shr}(t)$ [-] is the shrinkage strain, function of the curing time, as defined in 4.3.

Equation (5.1) is given separately for the each AGRAC mix in Equations (5.2) and (5.3).

$$\sigma_{2\%shr}(t, T(t)) = r_{2\%} \cdot E_{2\%}(t, T(t)) \cdot \epsilon_{shr} = 0.3067 \cdot E_{2\%}(t, T(t)) \cdot \epsilon_{shr}(t, 1.75) \qquad \text{[MPa]} \qquad (5.2)$$

$$\sigma_{4\%shr}(t, T(t)) = r_{4\%} \cdot E_{4\%}(t, T(t)) \cdot \epsilon_{shr} = 0.5018 \cdot E_{4\%}(t, T(t)) \cdot \epsilon_{shr}(t, 1.75) \qquad \text{[MPa]} \qquad (5.3)$$

The shrinkage stress function $\sigma_{shr}(t, T(t))$ is shown for the two AGRAC mixes in Figures 5.1 and 5.2 for a base constructed on August 1st at 10:00.
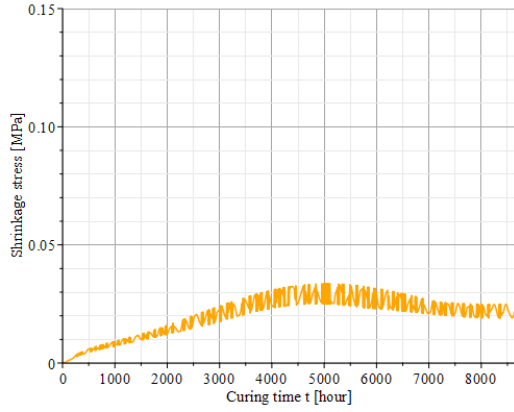
Figure 5.1: $\sigma_{shr}(t, T(t))$ function AGRAC 2% for a base constructed on August 1st at 10.00 (time up to 1 year)
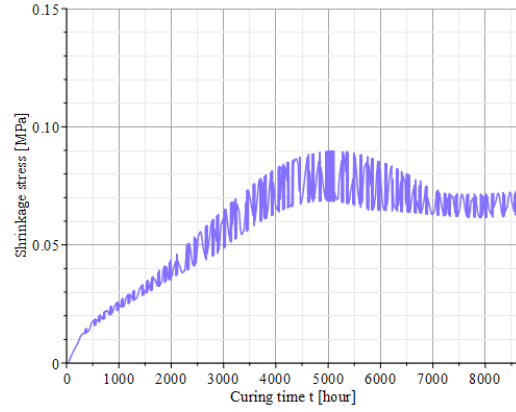
Figure 5.2: $\sigma_{shr}(t, T(t))$ function for AGRAC 4% for a base constructed on August 1st at 10.00 (time up to 1 year)

5.1.2. THERMAL STRESSES

The thermal stresses $\sigma_{the}(t, T(t))$ are given by (Equation (5.4)).

$$\sigma_{the}(t, T(t)) = r \cdot E(t, T(t)) \cdot \alpha \cdot \Delta(T(t)) \qquad \text{[MPa]} \qquad (5.4)$$

Where:

- r [-] is the relaxation coefficient as defined in 4.7.

- $E(t, T(t))$ [MPa] is the modulus of elasticity depending only on the curing time t by fixing the time of construction (4.6).

- α [m/m/°C] is the thermal coefficient as defined in 4.4.

- $\Delta(T(t))$ is the difference between the temperature at the curing time t and the temperature at the time of construction.

Equation (5.4) is given separately for the each AGRAC mix in Equations (5.5) and (5.6).

$$\sigma_{2\%the}(t, T(t)) = r_{2\%} \cdot E_{2\%}(t, T(t)) \cdot \alpha_{2\%} \cdot \Delta(T(t)) = 0.3067 \cdot E_{2\%}(t, T(t)) \cdot 18.76 \cdot 10^{-6} \cdot \Delta(T(t)) \qquad \text{[MPa]} \quad (5.5)$$

$$\sigma_{4\%the}(t, T(t)) = r_{4\%} \cdot E_{4\%}(t, T(t)) \cdot \alpha_{4\%} \cdot \Delta(T(t)) = 0.5018 \cdot E_{4\%}(t, T(t)) \cdot 16.80 \cdot 10^{-6} \cdot \Delta(T(t)) \qquad \text{[MPa]} \quad (5.6)$$

The thermal stress function $\sigma_{the}(t, T(t))$ is shown for the two AGRAC mixes in Figures 5.3 and 5.4 for a base constructed on August 1st at 10:00.
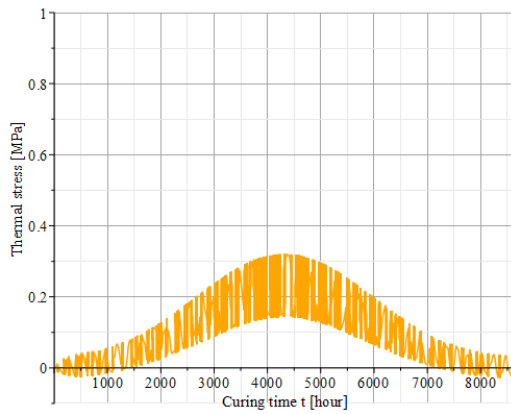
Figure 5.3: $\sigma_{the}(t, T(t))$ function for AGRAC 2% for a base constructed on August 1st at 10.00 (time up to 1 year)
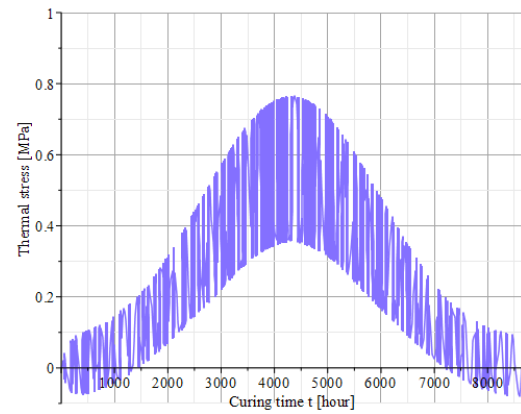
Figure 5.4: $\sigma_{the}(t, T(t))$ function for AGRAC 4% for a base constructed on August 1st at 10.00 (time up to 1 year)

5.1.3. OCCURRING STRESSES IN THE BASE

The occurring stresses $\sigma(t)$ in the base are given by the sum of the thermal and the shrinkage stresses (Equation (5.7)).

$$\sigma_{occ}(t, T(t)) = \sigma_{shr}(t, T(t)) + \sigma_{the}(t, T(t)) \qquad \text{[MPa]} \qquad (5.7)$$

The occurring stress function $\sigma(t, T(t))$ is shown for the two AGRAC mixes in Figures 5.5 and 5.6 for a base constructed on August 1st at 10:00.
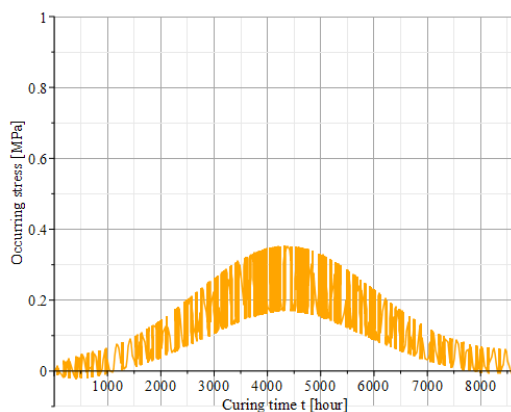
Figure 5.5: $\sigma_{occ}(t, T(t))$ function for AGRAC mix with 2% cement for a base constructed on August 1st at 10.00 (time up to 1 year)
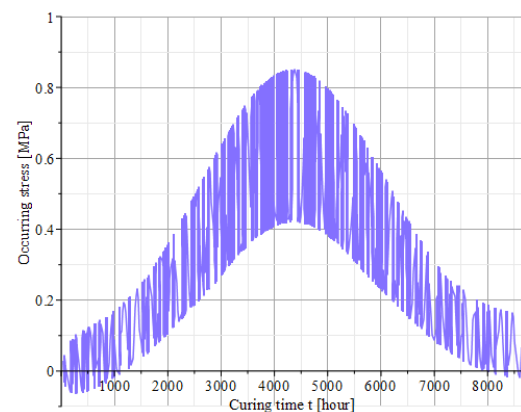
Figure 5.6: $\sigma_{occ}(t, T(t))$ function for AGRAC mix with 4% cement for a base constructed on August 1st at 10.00 (time up to 1 year)

5.2. COMPARISON

At this point the occurring stresses in the base $\sigma_{occ}(t, T(t))$ are compared with the tensile strength of the base $\sigma_{crack}(t, T(t))$. As an example the two functions are given in Figures 5.7 and 5.8 for the AGRAC mix with 2% cement for a road base constructed on August 1st at 16:00.
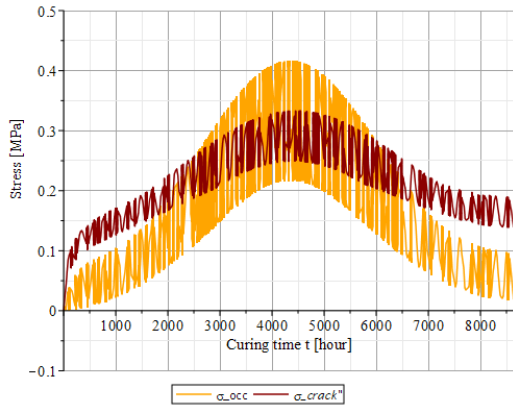
Figure 5.7: $\sigma_{occ}(t, T(t))$ and $\sigma_{crack}(t, T(t))$ of AGRAC 2% for a base constructed on August 1st at 16.00 (time up to 1 year)
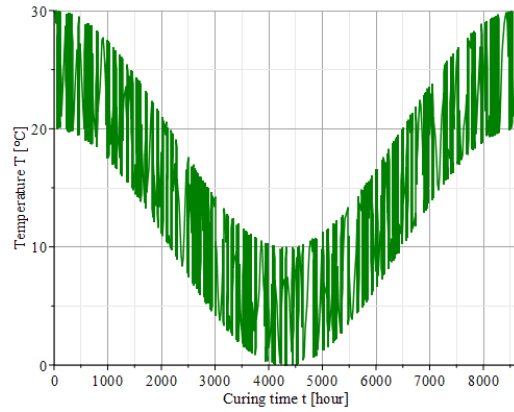
Figure 5.8: Base temperature for a base constructed on August 1st at 16.00 (time up to 1 year)

5.3. CRACK FORMATION: NON–WEAKENED AGRAC BASE

For non–weakened base it is here meant a base without transversal joints (saw–cuts). From the comparison of the two functions, it is possible to determine whether cracks occur and, if so, to characterise the crack pattern in terms of time of occurrence the cracks (more than one series of cracks might develop), crack spacing and crack width. An example of the determination of the crack width and the consequent stress reduction is given in Figures 5.9 and 5.10 for a non–weakened base constructed with AGRAC 2% on August 1st at 16:00. All equations used to characterize the crack pattern in the case of a non–weakened AGRAC base are give in section F.1 (Appendix F).
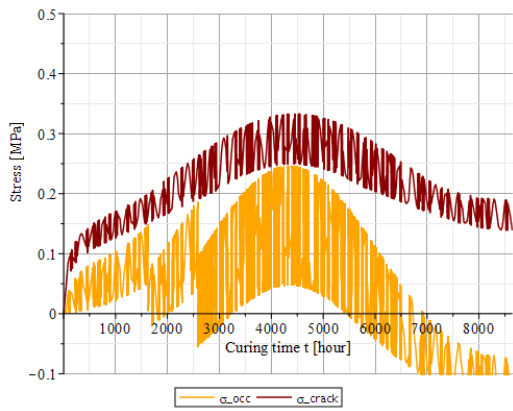
Figure 5.9: $\sigma_{occ}(t, T(t))$ and $\sigma_{crack}(t, T(t))$ of AGRAC 2% for a non-weakened base constructed on August 1st at 16.00 (time up to 1 year)
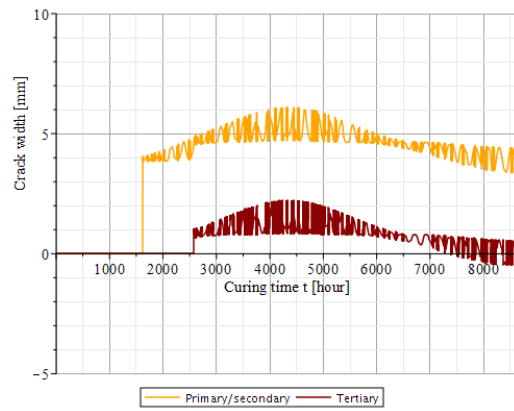
Figure 5.10: Crack width of AGRAC 2% for a non-weakened base constructed on August 1st at 16.00 (time up to 1 year)

5.4. CRACK FORMATION: WEAKENED AGRAC BASE

The analysis of the crack formation in the case of weakened (with saw-cuts) AGRAC base is similar to the one described for the non-weakened base with two major differences. Firstly, the stress is amplified in the weakened sections through a parameter depending on the thickness of the base and the depth of the saw-cut. Second, it is assumed that the cracks occur at the weakened location (at least until all weakened locations are cracked through). All equations used to characterize the crack pattern in the case of a weakened AGRAC base are given in section F.2 (Appendix F).

5.5. Crack formation results

The results presented in this section are obtained through the equations given in section F.1 (Appendix F).

5.5.1. Non−weakened AGRAC base

The crack formation is analysed for some particular combinations of AGRAC mix and time of construction. Furthermore the following variations are considered:

- The temperature model so far described considers a seasonal variation (ΔT_{year}) of 10°C and a daily variation (ΔT_{day}) of 5°C. In order to simulate the case in which a layer is placed above the base layer (variation of the temperature is lower) two additional variation of temperatures are considered: $\Delta T_{year} = 8$ with $\Delta T_{day} = 3$ and $\Delta T_{year} = 6$ with $\Delta T_{day} = 1$.

- In order to evaluate the effect of a different friction coefficient, besides the value $f_2 = 10$ presented in Appendix F also the value $f_2 = 4$ is used.

All the combinations considered are given separately for the two AGRAC mixes in Tables 5.1 and 5.2 along with the crack formation results. For each combination the plots of the stresses are given in Appendix H.

Discussion on the results

On the results presented in this section the following is observed:

- The period of construction which leads to the formation of the greatest number of cracks is August. Indeed, the base is constructed when the temperature reaches its highest values. Therefore, the temperature drops as the curing time increases right after construction causing high positive (tensile) thermal deformations. As a consequence the risk for the occurring stresses to exceed the tensile strength within a relative short period is high, also taking into account that the tensile strength doesn't have enough time to develop. Once the primary/secondary cracks occur, the occurring stresses keep increasing (being the temperature of the base still decreasing) leading to other series of cracks. The fact that the cracks occur in a short time after construction is not a negative phenomenon in itself because in this way the crack pattern might develop quick enough to be extinguished when the overlying layers are paved. The fact is that in all cases the time needed for the crack pattern to fully develop is quite high (between 1.5 and 8 months) so, according to the model used, waiting until the cracks are developed to pave the overlying layers doesn't seem an option to consider. The way to control the crack formation according to the model used is either to choose a combination of parameters for which no cracks occur or apply joints (as it will be discussed later on in this chapter). From the results obtained, the worst scenario occurs when the base is constructed with AGRAC 4% on August 1st at 16:00. Indeed, in this case 4 series of cracks develop in the base leading to a crack pattern with final crack spacing of only 1.9 m. So closely spaced cracks might lead to a disintegration of the base (material becomes unbound). More favourable seem the usage of AGRAC 2%. Indeed, according to the model cracks occur only for the two cases in which the base is constructed in August.

- Four different times of construction are analysed in August 1st. This is done to see whether constructing the AGRAC base during night time could reduce the problems related to crack formation. It is noted that in all cases shifting the construction of the base from 16:00 to 10:00 and 04:00 leads to a reduction in the crack series which take place in the base. The behaviour of the AGRAC base for the cases of construction on August 1st 22:00 is almost the same as the case of construction at 10:00. This is due to the fact that the temperature of construction is the same.

AGRAC mix	Time of construction	Case ID	ΔT$_{year}$	ΔT$_{day}$	f$_2$	Type of cracks	Time after construction	Time after construction	Crack spacing	Max crack width*
			°C	°C	-		hours	days	m	mm
2%	May 1st at 10.00	N2_May10_10-5	10	5	-	-	-	-	-	-
		N2_May10_8-3	8	3	-	-	-	-	-	-
		N2_May10_6-1	6	1	-	-	-	-	-	-
2%	August 1st at 04.00	N2_Aug04_10-5_10	10	5	10	Prim/Sec	3096	129.0	35.1	6.6
		N2_Aug04_10-5_4	10	5	4	Prim/Sec	3096	129.0	35.1	7.2
		N2_Aug04_8-3	8	3	-	-	-	-	-	-
		N2_Aug04_6-1	6	1	-	-	-	-	-	-
2%	August 1st at 10.00	N2_Aug10_10-5_10	10	5	10	Prim/Sec	2298	95.8	29.2	6.1
						Tertiary	3618	150.8	14.6	1.5
		N2_Aug10_10-5_4	10	5	4	Prim/Sec	2298	95.8	29.2	8.0
						Tertiary	3618	150.8	14.6	3.8
		N2_Aug10_8-3	8	3	-	-	-	-	-	-
		N2_Aug10_6-1	6	1	-	-	-	-	-	-
2%	August 1st at 16.00	N2_Aug16_10-5_10	10	5	10	Prim/Sec	1620	67.5	24.4	6.1
						Tertiary	2580	107.5	12.2	2.2
		N2_Aug16_10-5_4	10	5	4	Prim/Sec	1620	67.5	24.4	9.1
						Tertiary	2580	107.5	12.2	5.6
		N2_Aug16_8-3_10	8	3	10	Prim/Sec	2940	122.5	34.6	7.1
		N2_Aug16_8-3_4	8	3	4	Prim/Sec	2940	122.5	34.6	7.9
		N2_Aug16_6-1	6	1	-	-	-	-	-	-
2%	August 1st at 22.00	N2_Aug22_10-5_10	10	5	10	Prim/Sec	2310	96.3	29.2	6.2
						Tertiary	3654	152.3	14.6	1.6
		N2_Aug22_10-5_4	10	5	4	Prim/Sec	2310	96.3	29.2	8.1
						Tertiary	3654	152.3	14.6	3.8
		N2_Aug22_8-3	8	3	-	-	-	-	-	-
		N2_Aug22_6-1	6	1	-	-	-	-	-	-
2%	November 1st at 10.00	N2_Nov10_10-5	10	5	-	-	-	-	-	-
		N2_Nov10_8-3	8	3	-	-	-	-	-	-
		N2_Nov10_6-1	6	1	-	-	-	-	-	-
2%	February 1st at 04.00	N2_Feb10_10-5	10	5	-	-	-	-	-	-
		N2_Feb10_8-3	8	3	-	-	-	-	-	-
		N2_Feb10_6-1	6	1	-	-	-	-	-	-

*In the first year

Table 5.1: Crack formation results for non–weakened base constructed with AGRAC 2%

- For the cases considered, the crack widths are generally high (up to 9.1 mm). It is here remarked that the trends should be regarded as of interest rather than the absolute values.

- The change in the temperature amplitude (ΔT_{year} and ΔT_{day}) has a huge effect on the crack formation. Indeed, even in the worst scenario (AGRAC 4%, construction in August) a reduction in the amplitudes leads to a redution of the crack series and even prevents their occurrence in the case $\Delta T_{year} = 6$ with $\Delta T_{day} = 1$.

- The change of the friction coefficient f_2 only affects the crack widths (they increase with a decrease of f_2). The value $f_2 = 4$ leads to an increase of the primary/secondary crack widths up to 50% (N4_Aug16_10-5) with respect to the case in which $f_2 = 10$ is used. The crack spacing is not affected by f_2 since at the time of occurrence of the primary/secondary it is calculated using the coefficient of friction f_1 (Equation (F.1)) and all other crack spacings are determined by division from the first one. The breathing lengths are only slightly affected and so are the stress reductions (see section F.1 of Appendix F).

AGRAC mix	Time of construction	Case ID	ΔT_{year}	ΔT_{day}	f_2	Type of cracks	Time after construction	Time after construction	Crack spacing	Max crack width*
			°C	°C	-		hours	days	m	mm
4%	May 1st at 10.00	N4_May10_10-5_10	10	5	10	Prim/Sec	5538	230.7	45.9	6.4
		N4_May10_10-5_4	10	5	4	Prim/Sec	5538	230.7	45.9	7.0
		N4_May10_8-3	8	3	-	-	-	-	-	-
		N4_May10_6-1	6	1	-		-	-	-	-
4%	August 1st at 04.00	N4_Aug04_10-5_10	10	5	10	Prim/Sec	2640	110.0	40.4	6.3
						Tertiary	3936	164.0	20.2	1.3
		N4_Aug04_10-5_4	10	5	4	Prim/Sec	2640	110.0	40.4	8.0
						Tertiary	3936	164.0	20.2	3.2
		N4_Aug04_8-3_10	8	3	10	Prim/Sec	3600	150	31.2	7.0
		N4_Aug04_8-3_4	8	3	4	Prim/Sec	3600	150	31.2	7.2
		N4_Aug04_6-1	6	1	-	-	-	-	-	-
4%	August 1st at 10.00	N4_Aug10_10-5_10	10	5	10	Prim/Sec	1914	79.8	33.6	6.1
						Tertiary	2778	115.8	16.8	2.0
		N4_Aug10_10-5_4	10	5	4	Prim/Sec	1914	79.8	33.6	8.8
						Tertiary	2778	115.8	16.8	5.1
		N4_Aug10_8-3_10	8	3	10	Prim/Sec	2826	117.8	42.0	6.7
		N4_Aug10_8-3_4	8	3	4	Prim/Sec	2826	117.8	42.0	7.6
		N4_Aug10_6-1	6	1	-	-	-	-	-	-
4%	August 1st at 16.00	N4_Aug16_10-5_10	10	5	10	Prim/Sec	156	6.5	15.0	4.2
						Tertiary	1716	71.5	7.5	3.0
						Quartary	2508	104.5	3.7	2.2
						Cinquary	3372	140.5	1.9	1.2
		N4_Aug16_10-5_4	10	5	4	Prim/Sec	156	6.5	15.0	8.6
						Tertiary	1716	71.5	7.5	7.2
						Quartary	2508	104.5	3.7	5.9
						Cinquary	3372	140.5	1.9	3.8
		N4_Aug16_8-3_10	8	3	10	Prim/Sec	2316	96.5	38.6	6.8
						Tertiary	3924	163.5	19.3	1.4
		N4_Aug16_8-3_4	8	3	4	Prim/Sec	2316	96.5	38.6	8.4
						Tertiary	3924	163.5	19.3	3.6
		N4_Aug16_6-1	6	1	-	-	-	-	-	-
4%	August 1st at 22.00	N4_Aug22_10-5_10	10	5	10	Prim/Sec	1926	80.3	34.0	6.1
						Tertiary	2766	115.3	17.0	2.0
		N4_Aug22_10-5_4	10	5	4	Prim/Sec	1926	80.3	34.0	8.9
						Tertiary	2766	115.3	17.0	5.1
		N4_Aug22_8-3_10	8	3	10	Prim/Sec	2814	117.3	41.8	6.7
		N4_Aug22_8-3_4	8	3	4	Prim/Sec	2814	117.3	41.8	7.6
		N4_Aug22_6-1	6	1	-	-	-	-	-	-
4%	November 1st at 10.00	N4_Nov10_10-5_10	10	5	10	Prim/Sec	1194	49.7	40.6	5.1
		N4_Nov10_10-5_4	10	5	4	Prim/Sec	1194	49.7	40.6	5.7
		N4_Nov10_8-3	8	3	-	-	-	-	-	-
		N4_Nov10_6-1	6	1	-	-	-	-	-	-
4%	February 1st at 04.00	N4_Feb04_10-5	10	5	-	-	-	-	-	-
		N4_Feb04_8-3	8	3	-	-	-	-	-	-
		N4_Feb04_6-1	6	1	-	-	-	-	-	-

*In the first year

Table 5.2: Crack formation results for non–weakened base constructed with AGRAC 4%

5.5.2. WEAKENED AGRAC BASE

The crack formation results in the case of weakened AGRAC base are presented in this section for some of the most unfavourable combinations analysed in the case of non-weakened base. In particular are considered all combinations for construction time on August 1st (apart for the case of construction at 22:00 since the behaviour is similar to the case of construction at 10:00):

- **W2_Aug04_10–5_10:** AGRAC base with 2% cement constructed on August 1st at 04:00.

- **W2_Aug10_10–5_10:** AGRAC base with 2% cement constructed on August 1st at 10:00.

- **W2_Aug16_10–5_10:** AGRAC base with 2% cement constructed on August 1st at 16:00.

- **W4_Aug04_10–5_10:** AGRAC base with 4% cement constructed on August 1st at 04:00.

- **W4_Aug10_10–5_10:** AGRAC base with 4% cement constructed on August 1st at 10:00.

- **W4_Aug16_10–5_10:** AGRAC base with 4% cement constructed on August 1st at 16:00.

In all the above cases the temperature variations considered are : ΔT_{year} = 10°C and ΔT_{day} = 5°C. The coefficient of friction is chosen as f_2 = 10. The base thickness is considered 300 mm and the saw-cut depth is assumed to be 20% of the base thickness (60 mm). The slabs are considered 5 m long (distance between two consecutive saw-cuts).

CASE W2_AUG04_10–5_10

By applying the equations in F.2 (Appendix F) we can see that in this case the value x is 4 (primary/secondary cracks occur every 4th joint). Furthermore, as the cracking process is completed, it is calculated that at the location of the primary/secondary and tertiary cracks the weakened sections crack through while they remain uncracked at the location of the quartary cracks. The occurring stresses before the crack process starts and as it is completed are given in Figures 5.11 and 5.12. The crack widths for the case considered and for the case in which the base is non-weakened are given in Figures 5.13 and 5.14.
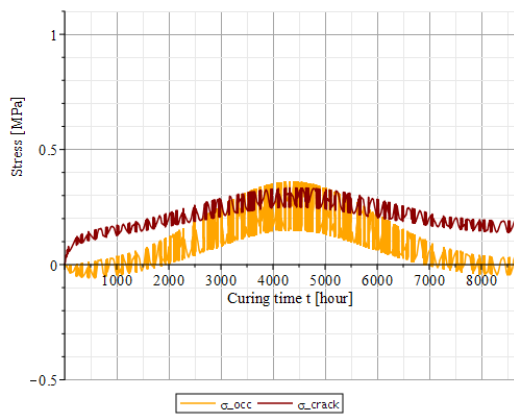
Figure 5.11: $\sigma_z(t)$ and $\sigma_{crack}(t)$ before t_{12}
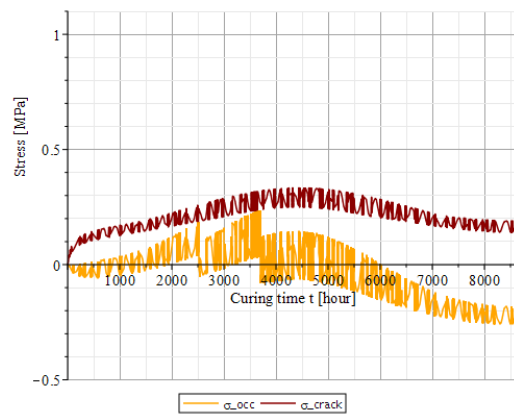
Figure 5.12: Maximum tensile stress and $\sigma_{crack}(t)$ after t_3
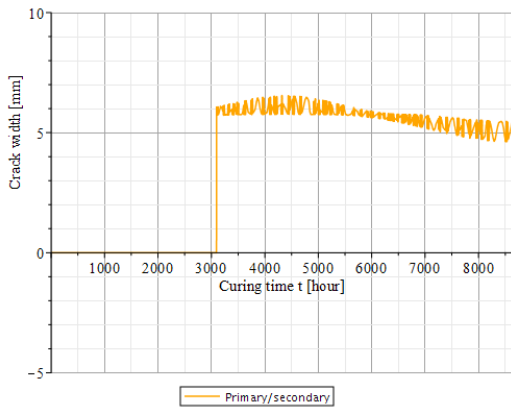
Figure 5.13: Crack widths for the non-weakened base (final crack spacing: 35.1 m)
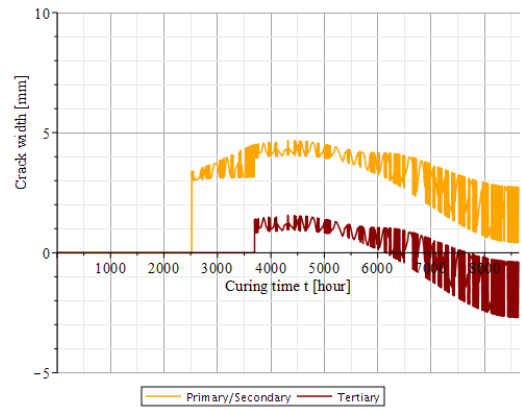
Figure 5.14: Crack widths for the weakened base (final crack spacing: 10 m)

CASE W2_AUG10_10–5_10

By applying the equations in F.2 (Appendix F) we can see that in this case the value x is 4 (primary/secondary cracks occur every 4th joint). Furthermore, as the cracking process is completed, it is calculated that all weakened sections have cracked through. The occurring stresses before the crack process starts and as it is completed are given in Figures 5.15 and 5.16. The crack widths for the case considered and for the case in which the base is non-weakened are given in Figures 5.17 and 5.18.
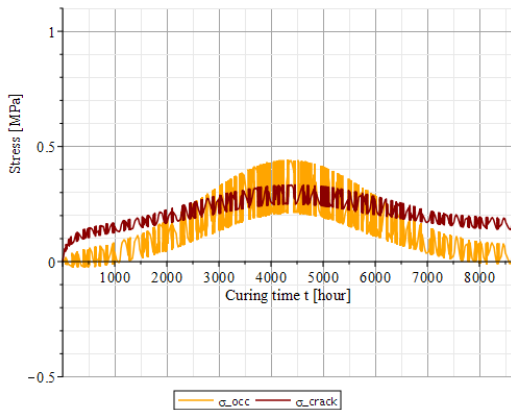
Figure 5.15: $\sigma_z(t)$ and $\sigma_{crack}(t)$ before t_{12}
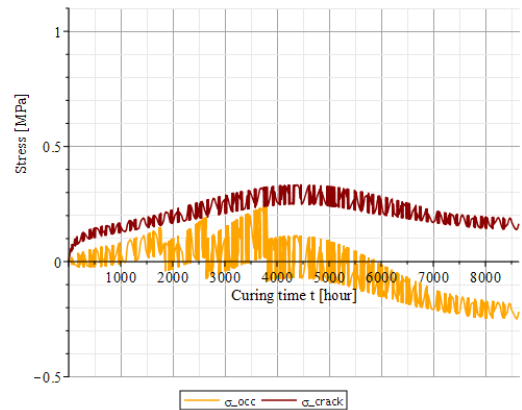
Figure 5.16: Maximum tensile stress and $\sigma_{crack}(t)$ after t_4
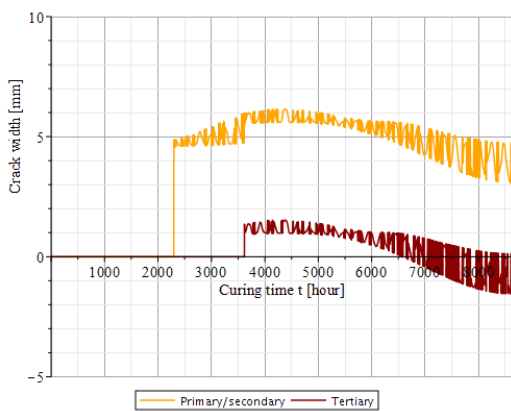
Figure 5.17: Crack widths for the non-weakened base (final crack spacing: 14.6 m)
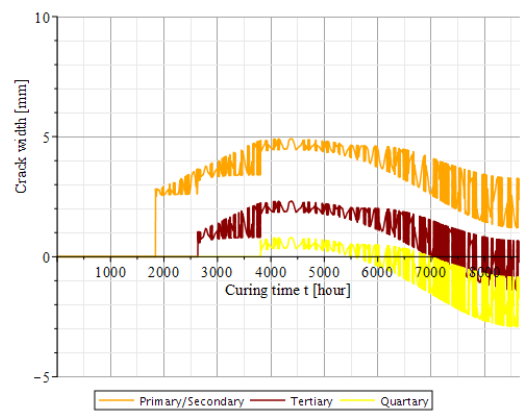
Figure 5.18: Crack widths for the weakened base (final crack spacing: 5 m)

CASE W2_AUG16_10–5_10

By applying the equations in F.2 (Appendix F) we can see that in this case the value x is 3 (Primary/secondary crack every 3rd joint). As the cracking process is completed all weakened sections crack through. After the tertiary cracks, the occurring stresses do not exceed any more the tensile strength. The occurring stresses before the crack process starts and as it is completed are given in Figures 5.19 and 5.20. The crack widths for the case considered and for the case in which the base is non-weakened are given in Figures 5.21 and 5.22.
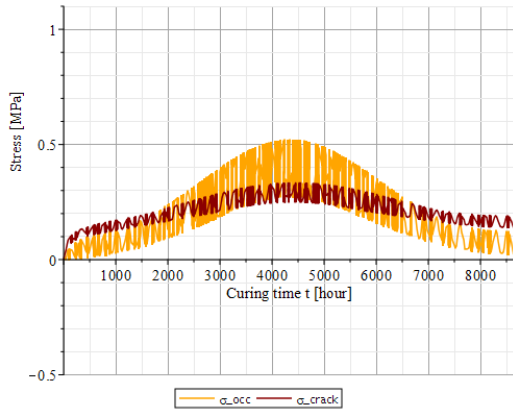
Figure 5.19: $\sigma_z(t)$ and $\sigma_{crack}(t)$ before t_{12}
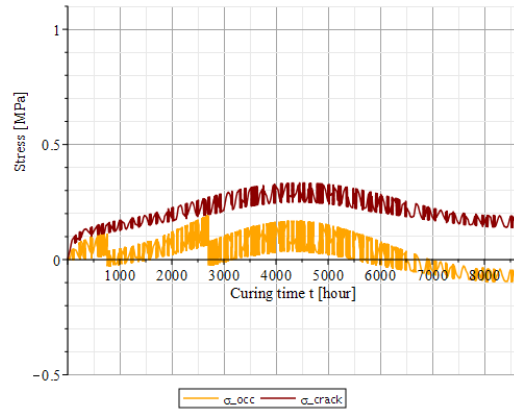
Figure 5.20: Maximum tensile stress and $\sigma_{crack}(t)$ after t_3
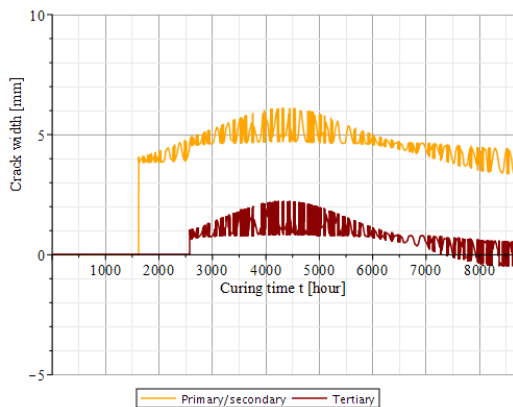
Figure 5.21: Crack widths for the non-weakened base (final crack spacing: 12.2 m)
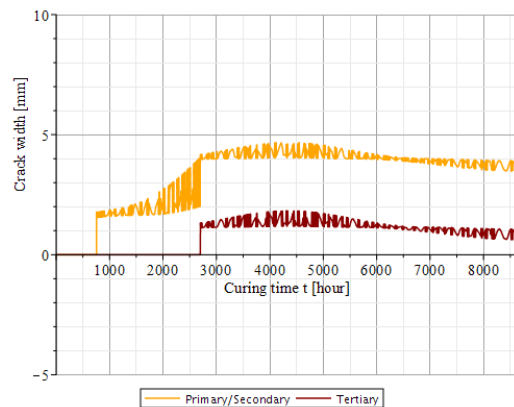
Figure 5.22: Crack widths for the weakened base (final crack spacing: 5 m)

CASE W4_AUG04_10–5_10

By applying the equations in F.2 (Appendix F) we can see that in this case the value x is 5 (Primary/secondary crack every 5th joint). The cracking process stops before the quartary cracks have cracked through. The occurring stresses before the crack process starts and as it is completed are given in Figures 5.23 and 5.24. The crack widths for the case considered and for the case in which the base is non-weakened are given in Figures 5.25 and 5.26.
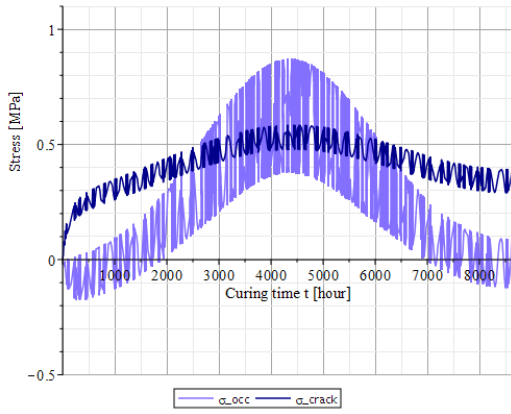
Figure 5.23: $\sigma_z(t)$ and $\sigma_{crack}(t)$ before t_{12}
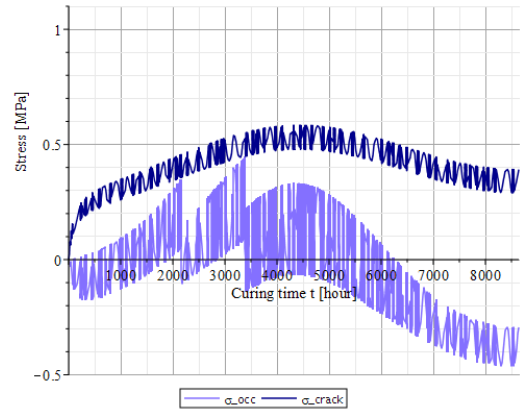
Figure 5.24: Maximum tensile stress and $\sigma_{crack}(t)$ after t_3
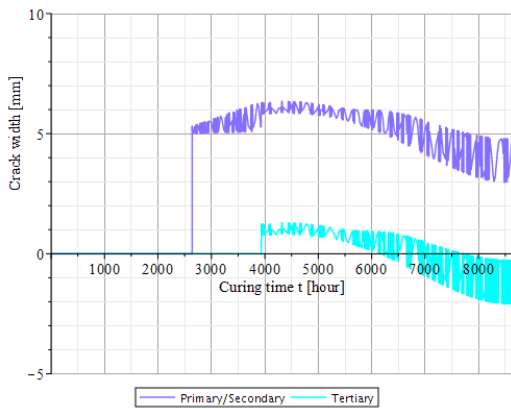
Figure 5.25: Crack widths for the non-weakened base (final crack spacing: 20.2 m)
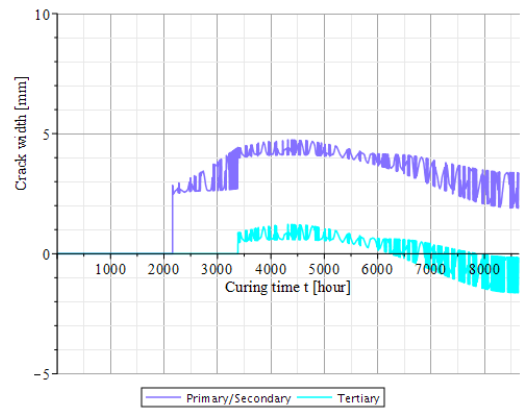
Figure 5.26: Crack widths for the weakened base (final crack spacing: 5 m)

Case W4_Aug10_10−5_10

By applying the equations in F.2 (Appendix F) we can see that in this case the value x is 4 (primary/secondary cracks occur every 4th joint). Furthermore, as the cracking process is completed, it is calculated that all weakened sections have cracked through. The occurring stresses before the crack process starts and as it is completed are given in Figures 5.27 and 5.28. The crack widths for the case considered and for the case in which the base is non-weakened are given in Figures 5.29 and 5.30.
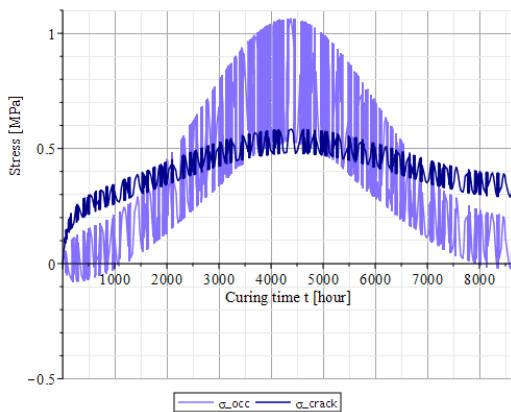
Figure 5.27: $\sigma_z(t)$ and $\sigma_{crack}(t)$ before t_{12}
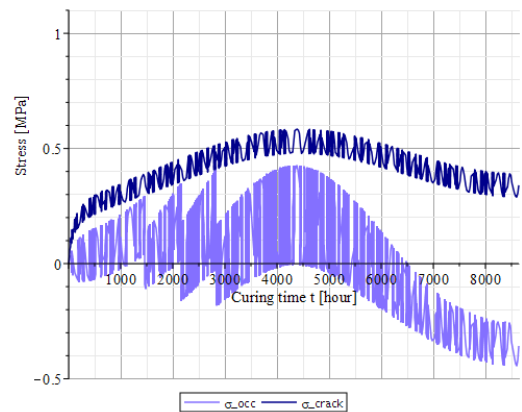
Figure 5.28: Maximum tensile stress and $\sigma_{crack}(t)$ after t_4
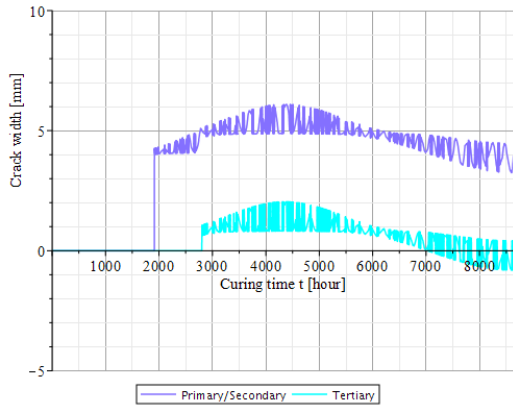
Figure 5.29: Crack widths for the non-weakened base (final crack spacing: 16.8 m)
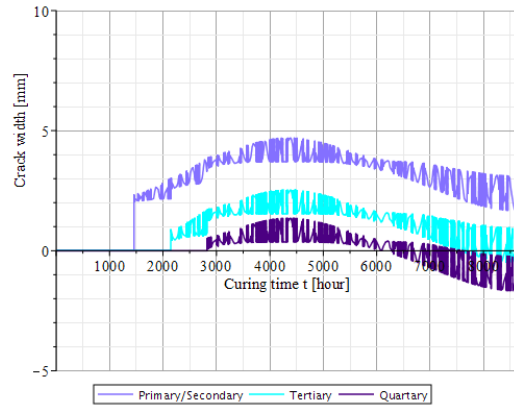
Figure 5.30: Crack widths for the weakened base (final crack spacing: 5 m)

CASE W4_AUG16_10–5_10

By applying the equations in F.2 (Appendix F) we can see that in this case the value x is 1. Therefore, at the time of occurrence of the primary/secondary all weakened sections crack through. The occurring stresses before the crack process starts and as it is completed are given in Figures 5.31 and 5.32. At this point the occurring stresses exceed again the tensile strength in non-weakened sections. Continuing the crack formation analysis it can be calculated that at the final stage each slab is divided in 8 parts (crack spacing 0.63 m). It has to be noted that for such small crack spacing the results might not be reliable because the breathing length is too small for the stress to increase as described by the model. Nevertheless, the results give an idea of the disintegration of the material that the AGRAC base would experience in this case. This is a very unfavourable situation even because the saw-cuts, which are meant to control the crack formation, prove to be ineffective.
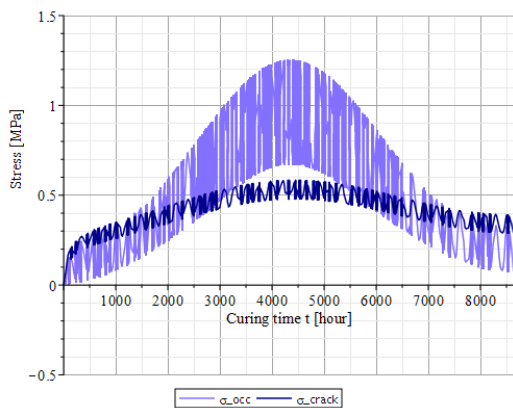
Figure 5.31: $\sigma_z(t)$ and $\sigma_{crack}(t)$ before t_{12}
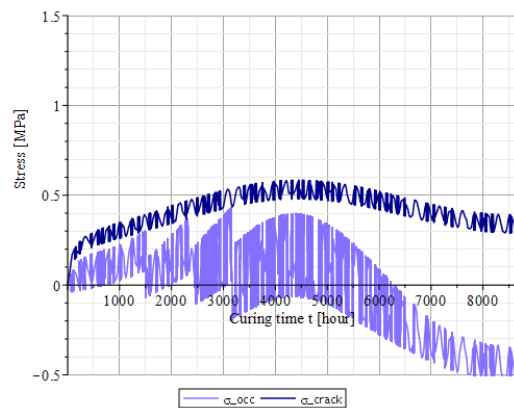
Figure 5.32: Maximum tensile stress and $\sigma_{crack}(t)$ after t_4

DISCUSSION ON THE RESULTS

On the results presented in this section the following is observed:

- The time of occurrence of the primary/secondary cracks is anticipated and the correspondent crack width is lower than in the case of a non-weakened AGRAC base. This is due to the fact that the occurring stresses reach the tensile strength earlier since they are amplified by the factor *g* (see Appendix F) in the weakened sections.

- In all considered cases apart from case W4_Aug16_10–5_10, cracks only develop in weakened sections. In case W4_Aug16_10–5_10 (construction with AGRAC 4% on August 1st at 16:00) cracks also occur in the middle of the cracks. The risk of this occurrence seems also possible for the case W4_Aug10_10–5_10 (construction with AGRAC 4% on August 1st at 10:00). Indeed, after the occurrence of the quartary cracks the occurring stress is close to reaching again the tensile strength.

6

CONCLUSIONS AND RECOMMENDATIONS

6.1. CONCLUSIONS

A first important result of this research, which is already visible from the testing phase, is that the material temperature has a significant effect on the mechanical behaviour of cement bound reclaimed asphalt (AGRAC), due to the presence of bitumen in the mix. This is especially evident from the Indirect Tensile Test results. Indeed, the tensile strength is found to decrease as the temperature increases. This decrease is quite considerable as for both AGRAC mixes tested (cement content 2% and 4% m/m) the strength at 0°C is more than double the strength at 30°C. Another important outcome of this research is the relaxation test which is specifically designed for this project in order to evaluate the relaxation in the same conditions in which the tensile strength is measured (ITT set-up). It seems that the test, as it was designed, has some potential and might be regarded in the future as an efficient way of estimating relaxation properties of cement bound materials.

The properties of AGRAC, retrieved through laboratory tests, are used as input in a model which predicts the occurrence of cracks in an AGRAC base. The occurrence of cracks is evaluated through a comparison between the occurring stresses in the base (sum of thermal and shrinkage stresses) and the tensile strength of the material. From the results obtained through the model the following is observed:

The results clearly show the influence of the time of construction on the crack formation process in a base constructed with AGRAC. According to the model developed, the time in the year which leads to the greater number of cracks in a non-weakened (without joints) AGRAC base is August (hottest period in the year according to the temperature model considered). Indeed, after the base is constructed the temperature decreases as the winter approaches with consequent early tensile thermal stresses which exceed in a relatively early stage the tensile strength. After the first series of cracks the tensile stresses keep increasing with possible occurrence of other crack series before the cold season is over. This trend is very clear for the AGRAC mix with 2% cement m/m for which, among all construction times in the year considered in the calculations, the only ones which lead to occurrence of cracks are the ones in August. More severe is the situation for AGRAC 4% for which crack series are observed also for construction times in May and November. Nevertheless, also for the AGRAC mix with 4% cement m/m the worst scenario remains August for which the calculated crack spacing, as the crack process fully develops, is so close (around 2 m) that one might think of a tendency of the material to disintegrate in the cracking process. This is in agreement with observations in practice. Indeed, during the last decades the cement content was decreased from 4-5% to 2-2.5% m/m precisely to reduce the risk of reflective cracking.

Not only the temperature at the time of construction but the material temperature itself has a big effect on

the results. This is due to the fact that the thermal stresses contribute to the occurring stresses in much greater portion compared to the shrinkage stresses. A consequence of this is the effect of the amplitudes of the seasonal and daily temperature of the base. This effect is studied to simulate the situation in which an overlying layer is placed on the base (with consequent reduction of the temperature variation of the AGRAC material). A decrease in the temperature amplitudes leads to a significant decrease of the risk of cracks in the non-weakened base.

In the case of construction in August, the calculations are also done for a weakened base in order to check whether by applying joints the crack formation process can be better controlled. In the calculations the saw-cuts are considered to be 60 mm deep and applied every 5 m in a 300 mm thick base. The results show that the saw-cuts cause a decrease of the time of occurrence of the first series of cracks and a reduction of their crack widths compared to the non-weakened case. Using AGRAC 2% it is calculated that the cracks only occur at weakened sections. This situation is favourable as the saw-cuts are meant to control the cracking process localizing and anticipating the cracks in a way that the crack formation process has fully developed at the time the above layer is constructed. This reduces the risk of reflective cracking. Instead, it seems that in the case of an AGRAC base constructed with 4% cement the saw-cuts could be inefficient for the highest construction temperatures, in the sense that cracks might appear also at non weakened sections, i.e. similar to the case of the non-weakened base.

6.2. RECOMMENDATIONS ON THE TEST PROGRAMME

In this research quite some effort was devoted into the manufacturing of the specimens. Indeed, this is believed to have a substantial effect on the results (especially the strength results). The method used for the compaction (Gyratory Compactor) has proved to be efficient in terms of ease of operating the equipment and control of the dimensions of the sample. Nevertheless, quite some care is necessary at the moment when the sample is extracted from the mould, being the material still fresh. Much better would be using a mould which allows the sample to cure for at least one day in the mould itself before being extracted. This would improve the uniformity of the specimens produced.

For the relaxation it is decided to use the ITT set-up. This is justified by the choice of testing the relaxation in the same conditions in which the tensile strength of the material is evaluated. From the results obtained it seems that the testing procedure used has some potential for its short time required and its relatively ease to perform. Nevertheless, some issues are observed as the stiffness of the material tested increases. It would be interesting for future research to improve the test procedure in a way that it can be applied to a wider range of materials.

6.3. RECOMMENDATIONS FOR PRACTICE

Giving recommendations for practice at this stage is a difficult task. This is manly due to the fact that the absolute values obtained from the model cannot be considered as reliable as the trends. For this reason, here two different approaches are considered favourable for practice.

- No cracks occur in the base

  As stated before, it is noticed that the AGRAC mix with 4% cement leads to a higher risk of cracks in a non-weakened base compared to the AGRAC mix with 2% cement. Nevertheless, according to the model it seems that by taking some measures also AGRAC 4% can be used without occurrence of cracks in the base. These measures first concern the construction time in the year. Indeed, warm

construction days (in summer) are unfavourable. Second, the seasonal and daily amplitudes of the temperatures have a great impact on the cracking risk. Therefore, paving the overlying layers as soon as possible (with consequent reduction of the temperature amplitudes) has to be regarded as beneficial in terms of avoiding the formation of cracks in the base.

- Widest cracks occur as early as possible

  According to the model cracks occur quite late in the base (even months after construction) so waiting until the cracks have fully developed before constructing the overlying layers doesn't seem an option to consider. Nevertheless, since absolute values are less reliable than trends in this model, this approach is here considered as possible. With this regard it is noted that by applying saw-cuts the first series of cracks (the widest cracks) do occur earlier and their width is reduced. Calculations are presented for a 300 mm thick base with 60 mm deep saw-cuts (20% of the base thickness), but it is noticed that the trends do not change for saw-cuts in the range 15-25% of the base thickness. In order to anticipate the occurrence of cracks it is convenient that the joints are made as soon as the hardening of the material allows it (starting from around a day from construction). It also has to be noted that waiting until the cracks occur before paving the overlying layers allows the base to be exposed to the atmosphere with consequent high temperature amplitudes. This also contributes in anticipating the occurrence of the crack series.

As stated before, the trends rather than the results are of interest from the results presented. Nevertheless, it is believed that this research could be useful in practice once field data are gathered and compared with the results obtained from the model. This is the main goal of this work.

BIBLIOGRAPHY

[1] CROW-Information and Technology Centre for Transport and Infrastructure, "*RAW - Standard conditions of contract for works of civil engineering construction*", 2010.

[2] NEN-EN 13286-2, "*Unbound and hydraulically bound mixtures - Part 2: Test methods for laboratory reference density and water content - Proctor compaction*", 2015.

[3] NEN-EN 14227-1, "*Unbound and hydraulically bound mixtures - Part 1: Cement bound granular mixtures*", 2013.

[4] Huurman M, Poot M., "*Determination of the Burgers' parameters by application of the dynamic ITT*".

[5] van Gurp C.A.P.M., "*TU Delft report 7-87-113-10, Proeven voor Wegenbouwmaterialen*", 1987.

[6] Saloua El et al., "*Laboratory Investigation of Cement-Treated Reclaimed Asphalt Pavement Material*", J. Mater. Civ. Eng., vol. 27, no. 6, pp. 1–7, 2015.

[7] Houben L.J.M., "*Model for transversal cracking (at joints) in plain concrete pavements*", TU Delft report 7-08-216-5, 2008.

[8] NEN-EN 1992-1-1, "*Eurocode 2: Design of concrete structures - Part 1-1: General rules and rules for buildings*", 2002.

[9] NEN-EN 13286-42, "*Unbound and hydraulically bound mixtures - Part 42: Test method for the determination of the indirect tensile strength of hydraulically bound mixtures*", 2003.

[10] Grilli A., Bocci E., Graziani A., "*Influence of reclaimed asphalt content on the mechanical behaviour of cement-treated mixtures*", Road Materials and Pavement Design, 2013.

[11] Kolias S., "*Mechanical properties of cement-treated mixtures of milled bituminous concrete and crushed aggregates*", Materials and Structures Vol. 29 pp 411-417, 1996.

[12] Yuan D., Nazarian S., Hoyos L.R., Puppala A.J., "*Cement Treated RAP Mixes for Roadway Bases*", 2010

[13] Videla C.C. et al.,"*Guide for Modelling and Calculating Shrinkage and Creep in Hardened Concrete*", ACI Committee report, 2009.

[14] Zhou C. et at., "*Micromechanical Model for Predicting Coefficient of Thermal Expansion of Concrete*", Journal of Materials in Civil Engineering, Vol. 25, No. 9, 2013.

A

APPENDIX A: MANUFACTURING

	Mass on total mineral aggregates	
	Extraction 1/2	Extraction 2/2
Aggregates >2mm [%]	53.7	52.7
Sand [%]	37.7	38.5
Filler [%]	8.7	8.8
Bitumen [%]	5.6	5.4

	Percentage passing [mass on total min. aggr.]	
Sieve [mm]	Extraction 1/2	Extraction 2/2
22.4	100.0	100.0
16	98.7	99.6
11.2	94.2	94.6
8.0	81.0	82.2
5.6	67.6	68.7
4	58.1	59.0
2.0	46.3	47.3
0.5	33.4	34.2
0.18	18.4	18.9
0.063	8.7	8.8
PAN	0.0	0.0

Table A.1: Components mass and passing percentages from the two extractions

Test on extracted bitumen	
Ring and ball softening point [°C]	67.1
Penetration [0.1mm]	25
PI - index [-]	- 0.72

Table A.2: Properties of the extracted bitumen

	Percentages [% m/m]			
	Retained (on single sieve)		Passing	
Sieve	RAP before extraction	design curve (max 63 mm)	RAP before extraction	design curve (max 63 mm)
63	0.0	0.0	100.0	100.0
45	1.4	1.2	98.6	98.8
31.5	2.2	1.8	96.4	97.0
22.4	7.0	5.9	89.3	91.1
16	9.0	7.5	80.3	83.6
11.2	10.8	9.0	69.5	74.6
8	11.6	9.7	57.9	64.9
5.6	12.6	10.5	45.3	54.4
4	10.1	8.5	35.1	45.9
2	12.9	10.7	22.2	35.2
1	6.5	7.6	15.7	27.6
0.063	15.7	27.4	0.0	0.2
PAN	0.0	0.2	0.0	0.0
tot:	100.00	100.00		

Table A.3: Retained and passing percentages for the "RAP before extraction" and "design (max 63 mm)" grading curves

Mould		Rammer			Procedure		Compaction energy [MJ/m³]
Diameter [mm]	Height [mm]	Mass [kg]	Diameter [mm]	Height of fall [mm]	Layers number	Blow numbers per layer	
152.4	116.4	2.5	50	300	3	56	0.5821

Table A.4: Standard Proctor parameters

B

APPENDIX B: ITT TEST

ITT results for AGRAC mix with **2%** cement tested at **0°C**								
Specimen ID	Curing time	h*	Mass*	Density	σ_{crack}	S_h	R^{2**}	E
	days	mm	g	kg/m³	MPa	N/mm	-	MPa
55	3.06	98.0	3504.7	2024.2	0.090	225826	0.914	855.8
56	3.06	97.9	3516.6	2033.2	0.081	243815	0.887	924.9
57	3.08	98.2	3521.4	2029.2	0.095	277870	0.880	1050.6
64	6.88	97.9	3499.9	2022.5	0.194	415070	0.940	1573.7
65	6.90	97.9	3502.0	2024.8	0.210	412362	0.959	1564.3
66	6.90	98.0	3502.6	2023.5	0.161	456115	0.933	1728.9
28	27.85	98.2	3476.7	2003.0	0.278	536552	0.972	2028.1
29	27.90	98.4	3481.6	2002.7	0.299	536864	0.962	2026.2
30	27.88	98.4	3472.6	1996.5	0.302	497572	0.952	1876.9
19	85.08	99.1	3478.0	1985.5	0.235	444131	0.943	1663.5
20	85.10	98.8	3484.0	1996.0	0.381	604905	0.977	2273.7
21	85.08	98.8	3479.3	1993.8	0.286	497237	0.984	1869.5
1	129.90	97.8	3465.0	2005.9	#N/A***	#N/A	#N/A	#N/A
2	129.92	98.2	3497.0	2016.2	0.277	#N/A	#N/A	#N/A
3	129.96	98.3	3476.0	2000.5	#N/A	#N/A	#N/A	#N/A

*measurements taken before testing   **R^2 for the determination of S_h *** #N/A: value not determined

ITT results for AGRAC mix with **2%** cement tested at **15°C**								
Specimen ID	Curing time	h*	Mass*	Density	σ_{crack}	S_h	R²**	E
	days	mm	g	kg/m³	MPa	N/mm	-	MPa
58	3.17	98.1	3504.0	2021.3	0.083	99436	0.904	376.3
59	3.17	98.3	3508.3	2020.7	0.079	108565	0.923	410.3
60	3.17	98.3	3509.5	2020.8	0.080	116062	0.944	438.5
67	6.94	98.0	3493.7	2018.4	0.131	241920	0.956	917.0
68	6.94	97.8	3485.2	2016.6	0.144	225270	0.947	855.2
69	6.94	97.9	3491.8	2018.3	0.124	242069	0.935	918.0
31	27.92	98.2	3468.5	1999.3	0.175	315157	0.953	1191.9
32	27.94	98.2	3485.1	2009.3	0.195	327877	0.957	1240.3
33	27.94	98.3	3479.2	2003.9	0.201	382978	0.953	1447.2
22	85.00	98.8	3487.8	1998.2	0.175	243929	0.962	916.9
23	84.98	98.8	3479.4	1993.9	0.219	379794	0.964	1427.9
24	84.98	98.4	3471.2	1995.7	0.231	323257	0.962	1219.4
4	129.94	98.4	3471.2	1995.7	0.231	323257	0.962	1383.4
5	129.94	98.5	3485.0	2003.2	0.180	232423	0.945	994.4
6	129.94	98.1	3471.0	2002.2	0.170	347054	0.947	1490.2

ITT results for AGRAC mix with **2%** cement tested at **30°C**								
Specimen ID	Curing time	h*	Mass*	Density	σ_{crack}	S_h	R²**	E
	days	mm	g	kg/m³	MPa	N/mm	-	MPa
61	3.23	98.0	3509.1	2026.3	0.047	71839	0.905	272.2
62	3.23	98.0	3506.6	2025.9	0.040	84538	0.922	320.4
63	3.23	97.9	3503.9	2025.9	0.052	76626	0.923	290.7
70	6.94	97.9	3500.9	2024.6	0.080	195254	0.918	740.9
71	6.98	97.8	3493.0	2020.6	0.070	117547	0.955	446.1
72	6.98	97.7	3499.1	2026.2	0.083	167691	0.938	637.1
34	27.96	98.3	3476.0	2000.5	0.116	209881	0.941	786.7
35	27.98	98.4	3473.8	1998.7	0.124	226444	0.966	854.8
36	27.96	98.1	3476.0	2004.6	0.117	235788	0.926	892.2
25	84.90	98.3	3474.9	1999.9	0.123	181045	0.951	683.6
26	84.90	98.3	3465.1	1994.8	0.116	253197	0.964	956.3
27	84.90	98.2	3472.6	2002.1	0.137	219934	0.949	832.0
7	130.00	98.2	3480.0	2005.9	0.121	#N/A	#N/A	#N/A
8	130.00	98.3	3482.0	2005.0	0.124	#N/A	#N/A	#N/A
9	130.00	97.8	3461.0	2002.6	0.120	#N/A	#N/A	#N/A

ITT results for AGRAC mix with **4%** cement tested at **0°C**								
Specimen ID	Curing time	h*	Mass*	Density	σ_{crack}	S_h	R^2**	E
	days	mm	g	kg/m³	MPa	N/mm	-	MPa
37	3.96	98.0	3496.0	2018.7	0.305	541225	0.960	2050.5
38	3.98	98.5	3530.9	2029.0	0.310	584895	0.965	2205.2
39	3.98	98.4	3513.5	2020.6	0.261	515407	0.963	1944.7
82	6.81	97.6	3510.1	2035.2	0.413	788268	0.961	2998.6
83	6.83	97.8	3512.0	2032.6	0.450	695165	0.974	2639.7
84	6.77	97.7	3524.9	2041.6	0.419	781056	0.963	2968.2
46	28.96	98.2	3500.8	2018.4	0.511	#N/A	#N/A	#N/A
47	28.96	98.5	3500.1	2010.3	0.533	#N/A	#N/A	#N/A
48	28.96	98.5	3492.8	2007.1	0.501	#N/A	#N/A	#N/A
73	89.90	97.6	3485.8	2021.6	0.538	677268	0.981	2577.1
74	89.90	97.7	3516.8	2038.0	0.539	729021	0.983	2771.8
75	89.90	98.0	3495.6	2018.5	0.545	1086340	0.973	4115.7
10	129.94	98.2	3486.0	2008.8	#N/A	#N/A	#N/A	#N/A
11	129.96	98.4	3502.0	2015.0	#N/A	#N/A	#N/A	#N/A
12	129.98	98.7	3493.0	2003.7	#N/A	#N/A	#N/A	#N/A

ITT results for AGRAC mix with **4%** cement tested at **15°C**								
Specimen ID	Curing time	h*	Mass*	Density	σ_{crack}	S_h	R^2**	E
	days	mm	g	kg/m³	MPa	N/mm	-	MPa
40	4.08	98.2	3513.1	2024.4	0.204	273629	0.954	1034.6
41	4.10	98.2	3508.5	2021.3	0.186	326033	0.913	1232.4
42	4.10	97.9	3512.6	2030.4	0.224	282290	0.957	1070.6
85	6.81	97.9	3504.7	2025.3	0.267	440776	0.963	1671.2
86	6.85	98.0	3507.9	2026.6	0.273	458976	0.959	1739.8
87	6.83	98.3	3518.7	2026.6	0.279	475421	0.956	1796.6
49	28.85	98.1	3476.4	2005.9	0.305	#N/A	#N/A	#N/A
50	28.85	98.6	3495.7	2007.3	0.300	#N/A	#N/A	#N/A
51	28.85	98.3	3494.8	2011.9	0.337	#N/A	#N/A	#N/A
76	89.85	97.6	3497.7	2027.4	0.379	449867	0.960	1710.9
77	89.83	97.6	3498.2	2028.8	0.448	594225	0.958	2261.1
78	89.88	97.8	3498.2	2024.1	0.440	580647	0.952	2204.3
13	129.94	98.3	3486.0	2007.8	0.416	514691	0.957	2206.6
14	129.92	98.5	3490.0	2005.0	0.437	549355	0.973	2349.2
15	129.90	98.6	3492.0	2004.1	0.409	627479	0.954	2680.6

ITT results for AGRAC mix with **4%** cement tested at **30°C**								
Specimen ID	Curing time	h*	Mass*	Density	σ_{crack}	S_h	R²**	E
	days	mm	g	kg/m³	MPa	N/mm	-	MPa
43	4.17	98.2	3522.5	2029.9	0.125	296863	0.937	1122.4
44	4.17	98.1	3519.9	2029.9	0.118	284134	0.936	1075.1
45	4.17	98.0	3509.8	2027.2	0.125	285320	0.960	1081.2
88	6.83	97.8	3508.2	2029.9	0.157	436631	0.964	1657.6
89	6.85	97.9	3503.1	2025.9	0.164	379565	0.947	1440.2
90	6.83	98.0	3502.2	2021.8	0.133	352572	0.953	1335.4
52	28.98	98.3	3502.5	2017.3	0.199	#N/A	#N/A	#N/A
53	28.96	98.5	3495.1	2007.4	0.228	#N/A	#N/A	#N/A
54	28.98	98.4	3498.5	2011.9	0.208	#N/A	#N/A	#N/A
79	89.85	97.7	3497.1	2026.1	0.291	441589	0.949	1678.6
80	89.88	97.7	3502.6	2028.2	0.280	455542	0.938	1730.7
81	89.88	97.9	3498.1	2022.0	0.320	479365	0.942	1818.0
16	129.96	97.9	3489.0	2016.2	0.260	#N/A	#N/A	#N/A
17	129.98	98.2	3491.0	2012.2	0.235	#N/A	#N/A	#N/A
18	129.98	98.1	3473.0	2004.4	0.232	#N/A	#N/A	#N/A

C

APPENDIX C: THERMAL DEFORMATION TEST

Specimen ID	Cement percentage	Curing time	h*	Mass*	Density	$T_{initial}$	T_{final}	Thermal strain	Thermal coefficient
	%	days	mm	g	kg/m³	°C	°C	m/m	m/m/°C
T-1	2	6.9	194.7	3086	2018.1	24.0	0.0	4.50E-04	18.75E-06
T-1	2	13.9	194.7	3086	2018.1	22.6	0.0	4.02E-04	17.77E-06
T-1	2	98.9	194.7	3086	2018.1	22.4	0.0	3.69E-04	16.46E-06
T-2	4	7.0	194.7	3098	2025.9	24.0	0.0	3.97E-04	16.55E-06
T-2	4	13.9	194.7	3098	2025.9	22.6	0.0	3.72E-04	16.45E-06
T-2	4	98.9	194.7	3098	2025.9	22.4	0.0	3.37E-04	15.05E-06
S-1	2	107.9	194.0	3084	2024.1	22.2	0.0	4.27E-04	19.23E-06
S-2	4	107.9	194.6	3084	2017.8	22.2	0.0	3.97E-04	17.88E-06
S-3	2	107.8	195.2	3091	2016.2	22.0	0.0	4.03E-04	18.34E-06
S-4	4	107.8	195.2	3095	2018.8	22.0	0.0	3.66E-04	16.64E-06
S-5	2	24.0	195.1	3092	2017.9	22.8	0.0	4.50E-04	19.72E-06
S-6	4	24.0	195.0	3109	2030.0	22.8	0.0	3.76E-04	16.50E-06

*measurement taken before testing

Table C.1: Thermal deformation measurements

D

APPENDIX D: POISSON'S RATIO TEST

Sample ID	Cement	Curing time	Temperature	Load	Radial strain	Axial strain 1	Axial strain 2	Axial strain 3	Axial strain average	Poisson's ratio
	%	days	°C	kN	-	-	-	-	-	-
S-3	2	104	25	1.5	-1.01E-05	5.15E-05	1.14E-04	5.84E-05	7.47E-05	**0.135**
S-3	2	104	15	1.5	-7.22E-06	4.23E-05	6.62E-05	4.71E-05	5.19E-05	**0.139**
S-3	2	104	15	3.0	-1.90E-05	8.51E-05	1.58E-04	9.98E-05	1.14E-04	**0.166**
S-4	4	104	15	3.0	-1.05E-05	4.77E-05	7.69E-05	8.21E-05	6.89E-05	**0.153**

Table D.1: Poisson's ratio measurements

E

APPENDIX E: RELAXATION TEST

Sample ID	Cement percentage	h*	Mass*	Density	Curing time at beginning of test	Applied horizontal displacement	Initial force	Final force	r
	%	mm	g	Kg/m³	days	mm	kN	kN	%
R-1	2%	97.9	3474.9	2008.1	8.08	0.0384	1.7830	0.5183	29.07
R-3	2%	98.1	3473.6	2003.7	1.96	0.0301	1.0338	0.3337	32.28
R-5	4%	97.8	3504.6	2027.3	1.98	0.0567	2.2820	1.1451	50.18

**measurement taken before testing*

Table E.1: Relaxation test parameters

APPENDIX F: CRACK FORMATION

F.1. NON-WEAKENED AGRAC BASE

In this section the equations used for determining the crack pattern are given for the case of a non-weakened (without joints) AGRAC base. The equations are taken from Report 7-08-216-5 [7]. All the equation presented in this section are valid for both AGRAC mixes.

BEFORE THE PRIMARY/SECONDARY CRACKS ($t < t_{12}$)

It is assumed that the base is fully restrained in the longitudinal direction. Therefore, all strains turn into stresses because of the obstructed deformation. Before the occurrence of the primary cracks the base in integer. The occurring stress $\sigma_{occ}(t) = r \cdot E(t) \cdot \epsilon(t) = \sigma(t)$ are smaller than the tensile strength $\sigma_{crack}(t)$ (Figure F.1).
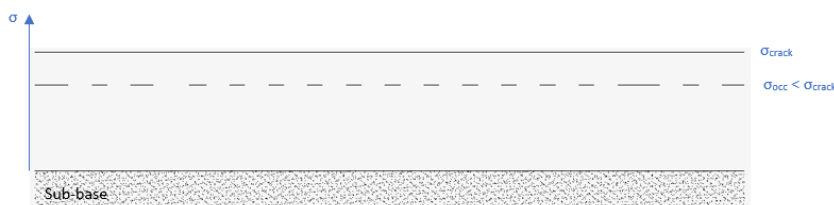
Figure F.1: Base before the occurrence of the cracks

PRIMARY/SECONDARY CRACKS ($t = t_{12}$)

As considered in Report 7-08-216-5 it is assumed that the primary and the secondary cracks occur at the same time. This assumption is justified by the fact that the reduction of stress between the primary and the secondary cracks is very small and therefore also small is the time interval required for the material to reach again the tensile strength. The primary/secondary cracks occur at a certain time t_{12} when $\sigma(t_{12}) = \sigma_{crack}(t_{12})$ (Figure F.2).

As the cracks occur, the breathing length L_{a12}, the crack distance L_{w12}, the initial crack width of the primary/secondary cracks w_{12i} and the reduction of stress $\Delta\sigma_{12}$ are given in Equations (F.1) to (F.4).

$$L_{a12} = \frac{1000 \cdot E(t_{12}) \cdot \epsilon(t_{12})}{\gamma \cdot f_1} \qquad \text{[m]} \qquad \text{(F.1)}$$
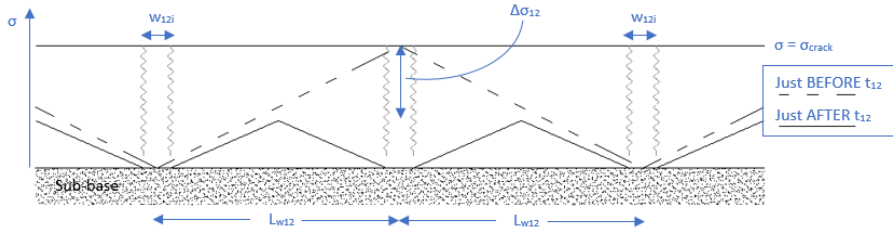
Figure F.2: Base at the time of occurrence of the primary/secondary cracks

$$L_{w12} = L_{a12} \qquad \text{[m]} \qquad (F.2)$$

$$w_{12i} = \frac{10^6 \cdot E(t_{12}) \cdot \epsilon(t_{12})^2}{2 \cdot \gamma \cdot f_1} \qquad \text{[mm]} \qquad (F.3)$$

$$\Delta\sigma_{12} = 0.5 \cdot \sigma(t_{12}) \cdot \left[1 + \frac{w_{12i}}{1000 \cdot L_{a12}}\right] \qquad \text{[MPa]} \qquad (F.4)$$

Where:

- $E(t_{12})$ [MPa] is the modulus of elasticity of the AGRAC material at the time t_{12}

- $\epsilon(t_{12})$ [-] is the deformation in the base at the time t_{12}

- $\sigma(t_{12})$ [MPa] is the occurring stress in the base at the time t_{12}

- f_1 [-] friction coefficient between the base and the surrounding layers before the occurrence of the primary/secondary cracks, considered as 1.0 [7].

- γ [kN/m^3] is the specific gravity of the AGRAC material, considered as 20.0.

After t_{12} (and before the tertiary cracks) the maximum tensile stress $\sigma_2(t)$, the maximum tensile strain in the base $\epsilon_2(t)$, the change of width of the primary/secondary cracks $\Delta_{w_{12}}(t)$ and the crack width of the primary/secondary cracks $w_{12}(t)$ are given in Equations (F.5) to (F.8).

$$\sigma_2(t) = \sigma(t) - \Delta\sigma_{12} \qquad \text{[MPa]} \qquad (F.5)$$

$$\epsilon_2(t) = \frac{\sigma_2(t)}{r \cdot E(t)} \qquad \text{[-]} \qquad (F.6)$$

$$\Delta_{w_{12}}(t) = \frac{10^6 \cdot E(t) \cdot \epsilon_2(t)^2 \cdot \text{sign}(\epsilon_2(t))}{\gamma \cdot f_2} - c_{12} \qquad \text{[mm]} \qquad (F.7)$$

$$w_{12}(t) = w_{12i} + \Delta_{w_{12}}(t) \qquad \text{[mm]} \qquad (F.8)$$

Where:

- r [-] is the relaxation coefficient (varying according to the AGRAC mix considered)

- f_2 [-] is the friction coefficient between the base and the surrounding layers after the occurrence of the primary/secondary cracks, arbitrary considered as 10.0 [7].

- c_{12} [mm] is a constant coefficient determined from the equation $\Delta_{w_{12}}(t_{12}) = 0$

- $\text{sign}(\epsilon_2(t))$ is the sign function of $\epsilon_2(t)$

Tertiary cracks ($t = t_3$)

At the time t_3 the maximum stress in the base $\sigma_2(t)$ reaches the tensile strength of the material: $\sigma_2(t_3) = \sigma_{crack}(t_3)$.

The initial width of the tertiary cracks w_{3i}, the breathing length L_{a3}, the crack distance between a tertiary and a primary/secondary crack L_{w3} and the decrease of the maximum stress $\Delta\sigma_3$ are given in Equations (F.9) to (F.12).

$$w_{3i} = \frac{10^6 \cdot E(t_3) \cdot \epsilon_2(t_3)^2}{\gamma \cdot f_2} \qquad [\text{mm}] \qquad (\text{F.9})$$

$$L_{a3} = 0.25 \cdot L_{a1} - 0.5 \cdot \frac{w_{12}(t_3)}{1000} - 0.5 \cdot \frac{w_{3i}}{1000} \qquad [\text{m}] \qquad (\text{F.10})$$

$$L_{w3} = 0.5 \cdot L_{w12} \qquad [\text{m}] \qquad (\text{F.11})$$

$$\Delta\sigma_3 = 0.5 \cdot \sigma_2(t_3) \cdot \left[1 + \frac{w_{3i}}{1000 \cdot L_{a3}} \right] \qquad [\text{MPa}] \qquad (\text{F.12})$$

After t_3 (and before the quartary cracks) the maximum tensile stress $\sigma_3(t)$, the maximum tensile strain in the base $\epsilon_3(t)$, the change of width of the tertiary cracks $\Delta_{w_3}(t)$, the crack width of the primary/secondary cracks $w_{12_3}(t)$ and the crack width of the tertiary cracks $w_3(t)$ are given in Equations (F.13) to (F.17).

$$\sigma_3(t) = \sigma_2(t) - \Delta\sigma_3 \qquad [\text{MPa}] \qquad (\text{F.13})$$

$$\epsilon_3(t) = \frac{\sigma_3(t)}{r \cdot E(t)} \qquad [\text{-}] \qquad (\text{F.14})$$

$$\Delta_{w_3}(t) = \frac{10^6 \cdot E(t) \cdot \epsilon_3(t)^2 \cdot \text{sign}(\epsilon_3(t))}{\gamma \cdot f_2} - c_3 \qquad [\text{mm}] \qquad (\text{F.15})$$

$$w_{12_3}(t) = w_{12}(t_3) + \Delta_{w_3}(t) \qquad [\text{mm}] \qquad (\text{F.16})$$

$$w_3(t) = w_{3i} + \Delta_{w_3}(t) \qquad [\text{mm}] \qquad (\text{F.17})$$

Where:

- c_3 [mm] is a constant coefficient determined from the equation $\Delta_{w_3}(t_3) = 0$

Quartary cracks ($t = t_4$)

At the time t_4 the maximum stress in the base $\sigma_3(t)$ reaches the tensile strength of the material: $\sigma_3(t_4) = \sigma_{crack}(t_4)$.

The initial width of the quartary cracks w_{4i}, the breathing length L_{a4}, the crack distance between a quartary and a tertiary crack L_{w4} and the decrease of the maximum stress $\Delta\sigma_4$ are given in Equations (F.18) to (F.21).

$$w_{4i} = \frac{10^6 \cdot E(t_4) \cdot \epsilon_3(t_4)^2}{\gamma \cdot f_2} \qquad [\text{mm}] \qquad (\text{F.18})$$

$$L_{a4} = 0.125 \cdot L_{a1} - 0.25 \cdot \frac{w_{12_3}(t_4)}{1000} - 0.25 \cdot \frac{w_3(t_4)}{1000} - 0.5 \cdot \frac{w_{4i}}{1000} \qquad \text{[m]} \qquad (\text{F.19})$$

$$L_{w4} = 0.25 \cdot L_{w12} \qquad \text{[m]} \qquad (\text{F.20})$$

$$\Delta\sigma_4 = 0.5 \cdot \sigma_3(t_4) \cdot \left[1 + \frac{w_{4i}}{1000 \cdot L_{a4}} \right] \qquad \text{[MPa]} \qquad (\text{F.21})$$

After t_4 (and before the cinquary cracks) the maximum tensile stress $\sigma_4(t)$, the maximum tensile strain in the base $\epsilon_4(t)$, the change of width of the quartary cracks $\Delta_{w_4}(t)$, the crack width of the primary/secondary cracks $w_{12_4}(t)$, the crack width of the tertiary cracks $w_{3_4}(t)$ and the crack width of the quartary cracks $w_4(t)$ are given in Equations (F.22) to (F.27).

$$\sigma_4(t) = \sigma_3(t) - \Delta\sigma_4 \qquad \text{[MPa]} \qquad (\text{F.22})$$

$$\epsilon_4(t) = \frac{\sigma_4(t)}{r \cdot E(t)} \qquad \text{[-]} \qquad (\text{F.23})$$

$$\Delta_{w_4}(t) = \frac{10^6 \cdot E(t) \cdot \epsilon_4(t)^2 \cdot \text{sign}(\epsilon_4(t))}{\gamma \cdot f_2} - c_4 \qquad \text{[mm]} \qquad (\text{F.24})$$

$$w_{12_4}(t) = w_{12_3}(t_4) + \Delta_{w_4}(t) \qquad \text{[mm]} \qquad (\text{F.25})$$

$$w_{3_4}(t) = w_3(t_4) + \Delta_{w_4}(t) \qquad \text{[mm]} \qquad (\text{F.26})$$

$$w_4(t) = w_{4i} + \Delta_{w_4}(t) \qquad \text{[mm]} \qquad (\text{F.27})$$

Where:

- c_4 [mm] is a constant coefficient determined from the equation $\Delta_{w_4}(t_4) = 0$

CINQUARY CRACKS ($t = t_5$)

At the time t_5 the maximum stress in the base $\sigma_4(t)$ reaches the tensile strength of the material: $\sigma_4(t_5) = \sigma_{crack}(t_5)$.

The initial width of the cinquary cracks w_{5i}, the breathing length L_{a5}, the crack distance between a cinquary and a quartary crack L_{w5} and the decrease of the maximum stress $\Delta\sigma_5$ are given in Equations (F.28) to (F.31).

$$w_{5i} = \frac{10^6 \cdot E(t_5) \cdot \epsilon_4(t_5)^2}{\gamma \cdot f_2} \qquad \text{[mm]} \qquad (\text{F.28})$$

$$L_{a5} = 0.075 \cdot L_{a1} - 0.125 \cdot \frac{w_{12_4}(t_5)}{1000} - 0.125 \cdot \frac{w_{3_4}(t_5)}{1000} - 0.125 \cdot \frac{w_4(t_5)}{1000} - 0.5 \cdot \frac{w_{5i}}{1000} \qquad \text{[m]} \qquad (\text{F.29})$$

$$L_{w5} = 0.125 \cdot L_{w12} \qquad \text{[m]} \qquad (\text{F.30})$$

$$\Delta\sigma_5 = 0.5 \cdot \sigma_4(t_5) \cdot \left[1 + \frac{w_{5i}}{1000 \cdot L_{a5}} \right] \qquad \text{[MPa]} \qquad (\text{F.31})$$

After t_5 (and before other cracks occur) the maximum tensile stress $\sigma_5(t)$, the maximum tensile strain in the base $\epsilon_5(t)$, the change of width of the cinquary cracks $\Delta_{w_5}(t)$, the crack width of the primary/secondary cracks $w_{12_5}(t)$, the crack width of the tertiary cracks $w_{3_5}(t)$, the crack width of the quartary cracks $w_{4_5}(t)$ and the crack width of the cinquary cracks $w_5(t)$ are given in Equations (F.32) to (F.38).

$$\sigma_5(t) = \sigma_4(t) - \Delta\sigma_5 \qquad \text{[MPa]} \qquad (F.32)$$

$$\epsilon_5(t) = \frac{\sigma_5(t)}{r \cdot E(t)} \qquad \text{[-]} \qquad (F.33)$$

$$\Delta_{w_5}(t) = \frac{10^6 \cdot E(t) \cdot \epsilon_5(t)^2 \cdot \text{sign}(\epsilon_5(t))}{\gamma \cdot f_2} - c_5 \qquad \text{[mm]} \qquad (F.34)$$

$$w_{12_5}(t) = w_{12_4}(t_5) + \Delta_{w_5}(t) \qquad \text{[mm]} \qquad (F.35)$$

$$w_{3_5}(t) = w_{3_4}(t_5) + \Delta_{w_5}(t) \qquad \text{[mm]} \qquad (F.36)$$

$$w_{4_5}(t) = w_4(t_5) + \Delta_{w_4}(t) \qquad \text{[mm]} \qquad (F.37)$$

$$w_5(t) = w_{5i} + \Delta_{w_5}(t) \qquad \text{[mm]} \qquad (F.38)$$

Where:

- c_5 [mm] is a constant coefficient determined from the equation $\Delta_{w_5}(t_5) = 0$

Determination of t_{crack}

It is noted that before the occurring stresses $\sigma_{occ}(t) = \sigma(t)$ exceed the tensile strength $\sigma_{crack}(t)$ there is an interval in which the two functions overlap (Figure F.3). This is due to the fact that both functions increase with a decrease of the temperature and vice-versa. It is decided to consider as moment of cracking t_{crack} the time in which a local maximum of the occurring stresses function reach the lower boundary of the strength function. For the example in Figure F.3 the cracks occur at $t_{crack} = 1548$ hours.
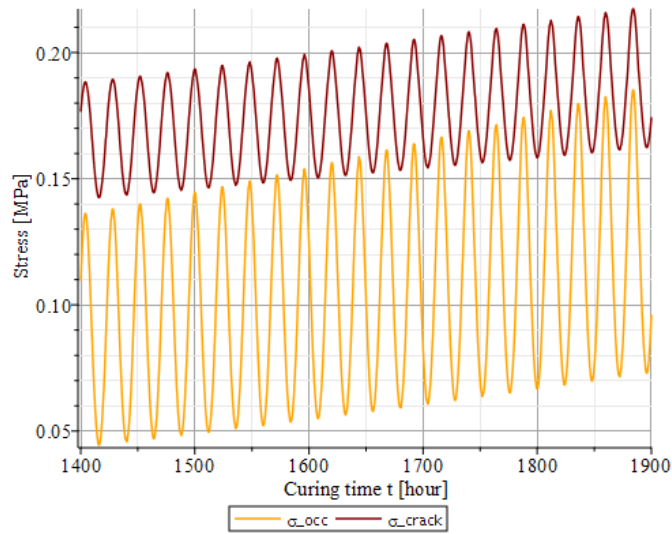
Figure F.3: Example of occurring stresses - strength overlapping

F.2. WEAKENED AGRAC BASE

Sometimes in practice joints (saw-cuts) are constructed in the AGRAC base in order to localize the cracks. This leads to a better control of the cracking process. In this section the equations used for determining the crack pattern are given for the case of a weakened (with joints/saw-cuts) AGRAC base. The equations are taken from Report 7-08-216-5 [7]. All the equation presented in this section are valid for both AGRAC mixes. To be noted in this section some of the parameters already introduced for the case of a non-weakened base (section F.1) will be used.

In order to model the crack formation for a weakened AGRAC base the following parameters have to be introduced:

- h [mm] is the thickness of the base

- z [mm] is the depth of the saw-cut

The tensile stresses in the base are greatest in the weakened cross-sections. Here the tensile stress $\sigma_z(t)$ is given by Equation (F.39).

$$\sigma_z(t) = g \cdot \sigma(t) \qquad \text{[MPa]} \qquad (F.39)$$

Where:

- $\sigma(t)$ [MPa] is the occurring stress in the base (Equation (5.7))

- g [-] is the enlargement factor given by $g = \frac{h}{h-z}$

Furthermore, the parameter "slab length" (distance between two consecutive saw-cuts) p [m] is also introduced.

PRIMARY/SECONDARY CRACKS

In a weakened base the location of the cracks is assumed to be limited to the weakened sections (at least until all weakened sections are cracked through). The number of primary/secondary cracks which develop are determined through parameter x (Equation (F.40)).

$$x \leq \frac{L_{a12_{app}}}{p} \qquad (F.40)$$

Where:

- x [greatest integer number]: cracks occur every x^{th} joint (i.e. $x = 3$ means saw-cuts 1,4,7.. crack through)

- $L_{a12_{app}}$ [m] apparent breathing length at the time t_{12} when the stress at the weakened sections $\sigma_z(t)$ exceeds for the first time the tensile strength $\sigma_{crack}(t)$, calculated through Equation (F.1). To be noted that t_{12} is smaller than the one calculated in the non-weakened case because the occurring tresses are enlarged through factor g. As a consequence also $L_{a12_{app}}$ will be smaller than L_{a12}.

Depending on the value of x the crack formation process is now analysed.

Primary/secondary cracks at the location of every joint ($x = 1$)

In this case all weakened sections crack through at the time t_{12} of occurrence of the primary/secondary cracks (P/S) (Figure F.4). Indeed, at this time the stress at the weakened sections $\sigma_z(t)$ reaches the tensile strength $\sigma_{crack}(t)$.
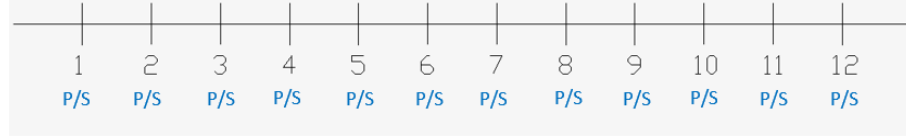
Figure F.4: Location of cracks for the case $x = 1$

The initial width of the primary/secondary cracks is determined through Equation (F.41).

$$w_{12i} = \frac{10^6 \cdot E(t_{12}) \cdot \epsilon(t_{12})^2}{2 \cdot \gamma \cdot f_1} \qquad \text{[mm]} \qquad (F.41)$$

The breathing length L_{a12z} is now equal to half of the slab length (Equation (F.42)).

$$L_{a12z} = 0.5 \cdot p \qquad \text{[m]} \qquad (F.42)$$

The stress reduction $\Delta\sigma_{12z}$ mid-way between two cracks due to the primary/secondary cracks is given by Equation (F.43).

$$\Delta\sigma_{12z} = 0.5 \cdot \sigma_z(t_{12}) \left[1 + \frac{w_{12i}}{1000 \cdot L_{a12z}} \right] \qquad \text{[MPa]} \qquad (F.43)$$

The stress $\sigma_2(t)$ mid-way two cracks is therefore given by Equation (F.44). To be noted that now this stress is calculated at a non-weakened section and therefore it is not enlarged by the factor g.

$$\sigma_2(t) = \frac{\sigma_z(t) - \Delta\sigma_{12z}}{g} \qquad \text{[MPa]} \qquad (F.44)$$

If the stress $\sigma_2(t)$ exceeds the tensile strength $\sigma_{crack}(t)$ the base will crack in a non-weakened section between the already existing cracks. This of course is a highly unfavourable situation.

Primary/secondary cracks at the location of every 3rd joint ($x = 3$)

When the primary/secondary cracks (P/S) occur at the location of every 3rd joint, for reasons of symmetry the possible tertiary cracks (T) occur together in the 2 joints lying in between (Figure F.5).

Figure F.5: Location of cracks for the case $x = 3$

At time t_{12} the amplified occurring stress $\sigma_z(t)$ reaches the tensile strength $\sigma_{crack}(t)$ leading to the occurrence of the primary/secondary cracks. The new breathing length L_{a12z}, the initial crack width of the primary/secondary cracks w_{12i} and the stress reduction at the location of the tertiary cracks $\Delta\sigma_{12z}$ are given in Equations (F.45) to (F.47) (Figure F.6).

$$L_{a12z} = 1.5 \cdot p \qquad \text{[m]} \qquad (F.45)$$

$$w_{12i} = \frac{10^6 \cdot E(t_{12}) \cdot \epsilon(t_{12})^2}{2 \cdot \gamma \cdot f_1} \qquad \text{[mm]} \qquad \text{(F.46)}$$

$$\Delta\sigma_{12z} = 1.333 \cdot 0.5 \cdot \sigma_z(t_{12}) \cdot \left[1 + \frac{w_{12i}}{1000 \cdot L_{a12z}}\right] \qquad \text{[MPa]} \qquad \text{(F.47)}$$
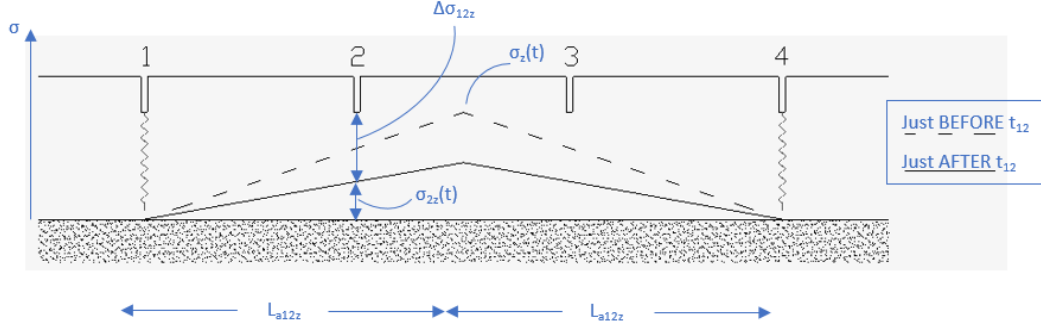
Figure F.6: Cracks at t_{12} for $x = 3$

The tensile stress at the location of the tertiary cracks after the occurrence of the primary/secondary cracks is therefore given by Equation (F.48).

$$\sigma_{2z}(t) = \frac{2}{3} \cdot \sigma_z(t) - \left[\Delta\sigma_{12z} - \frac{1}{3} \cdot \sigma_z(t_{12})\right] \qquad \text{[MPa]} \qquad \text{(F.48)}$$

The maximum tensile strain $\epsilon_{2z}(t)$ midway between the primary/secondary cracks is given by Equation (F.49).

$$\epsilon_{2z}(t) = \frac{3}{2} \cdot \frac{\sigma_{2z}(t)}{r \cdot E(t)} \qquad \text{[-]} \qquad \text{(F.49)}$$

At this point, if the stress at the location of the tertiary cracks $\sigma_{2z}(t)$ exceeds again the tensile strength $\sigma_{crack}(t)$, the tertiary cracks will occur at a time t_3. The new breathing length L_{a3z} and the initial width of the tertiary cracks w_{3i} are given in Equations (F.50) and (F.51).

$$L_{a3z} = 0.5 \cdot p \qquad \text{[m]} \qquad \text{(F.50)}$$

$$w_{3i} = \frac{10^6 \cdot E(t_3) \cdot \epsilon_{2z}(t_3)^2}{2 \cdot \gamma \cdot f_2} \qquad \text{[mm]} \qquad \text{(F.51)}$$

At this stage a crack has developed in every weakened section. The stress reduction $\Delta\sigma_{3z}$ mid-way between two cracks is given by Equation (F.52).

$$\Delta\sigma_{3z} = 0.5 \cdot \sigma_{2z}(t_3) \cdot \left[1 + \frac{w_{3i}}{1000 \cdot L_{a3z}}\right] \qquad \text{[MPa]} \qquad \text{(F.52)}$$

The maximum stress mid-way between two cracks $\sigma_3(t)$ is given by Equation (F.53). If the stress $\sigma_3(t)$ exceeds the tensile strength, then cracks will occur also in non-weakened sections.

$$\sigma_3(t) = \frac{\sigma_{2z} - \Delta\sigma_{3z}}{g} \qquad \text{[MPa]} \qquad \text{(F.53)}$$

PRIMARY/SECONDARY CRACKS AT THE LOCATION OF EVERY 4th JOINT ($x = 4$)

When the primary/secondary cracks (P/S) occur at the location of every 4th joint, the tertiary cracks (T) occur in the weakened sections mid-way between two primary/secondary cracks. Finally, the quartary cracks (Q) occur at the remaining uncracked weakened sections (Figure F.7).
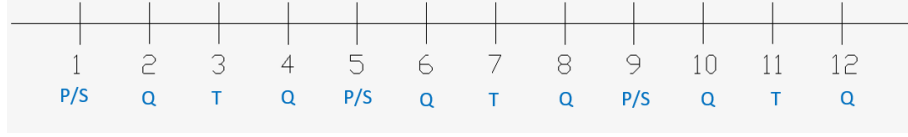
Figure F.7: Location of cracks for the case $x = 4$

At time t_{12} the amplified occurring stress $\sigma_z(t)$ reaches the tensile strength $\sigma_{crack}(t)$ leading to the occurrence of the primary/secondary cracks. The new breathing length L_{a12z}, the initial crack width of the primary/secondary cracks w_{12i} and the stress reduction at the location of the tertiary cracks $\Delta\sigma_{12z}$ are given in Equations (F.54) to (F.56).

$$L_{a12z} = 2 \cdot p \qquad\qquad \text{[m]} \qquad\qquad (\text{F.54})$$

$$w_{12i} = \frac{10^6 \cdot E(t_{12}) \cdot \epsilon(t_{12})^2}{2 \cdot \gamma \cdot f_1} \qquad\qquad \text{[mm]} \qquad\qquad (\text{F.55})$$

$$\Delta\sigma_{12z} = 0.5 \cdot \sigma_z(t_{12}) \cdot \left[1 + \frac{w_{12i}}{1000 \cdot L_{a12z}}\right] \qquad\qquad \text{[MPa]} \qquad\qquad (\text{F.56})$$

The tensile stress $\sigma_{2z}(t)$ at the location of the tertiary cracks after the occurrence of the primary/secondary cracks is therefore given by Equation (F.57).

$$\sigma_{2z}(t) = \sigma_z(t) - \Delta\sigma_{12z} \qquad\qquad \text{[MPa]} \qquad\qquad (\text{F.57})$$

The maximum tensile strain $\epsilon_{2z}(t)$ at the location of the tertiary cracks is given by Equation (F.58).

$$\epsilon_{2z}(t) = \frac{\sigma_{2z}(t)}{r \cdot E(t)} \qquad\qquad \text{[-]} \qquad\qquad (\text{F.58})$$

At this point, if the stress at the location of the tertiary cracks $\sigma_{2z}(t)$ exceeds again the tensile strength $\sigma_{crack}(t)$, the tertiary cracks will occur at time t_3. The new breathing length L_{a3z} and the initial width of the tertiary cracks w_{3i} are given in Equations (F.59) and (F.60).

$$L_{a3z} = 1.0 \cdot p \qquad\qquad \text{[m]} \qquad\qquad (\text{F.59})$$

$$w_{3i} = \frac{10^6 \cdot E(t_3) \cdot \epsilon_{2z}(t_3)^2}{\gamma \cdot f_2} \qquad\qquad \text{[mm]} \qquad\qquad (\text{F.60})$$

The stress reduction $\Delta\sigma_{3z}$ at the location of the quartary cracks is given by Equation (F.61).

$$\Delta\sigma_{3z} = 0.5 \cdot \sigma_{2z}(t_3) \cdot \left[1 + \frac{w_{3i}}{1000 \cdot L_{a3z}}\right] \qquad\qquad \text{[MPa]} \qquad\qquad (\text{F.61})$$

The maximum stress at the location of the quartary cracks $\sigma_{3z}(t)$ is given by Equation (F.62).

$$\sigma_{3z}(t) = \sigma_{2z} - \Delta\sigma_{3z} \qquad\qquad \text{[MPa]} \qquad\qquad (\text{F.62})$$

At this point, if the stress at the location of the quartary cracks $\sigma_{3z}(t)$ exceeds again the tensile strength $\sigma_{crack}(t)$, the quartary cracks will occur at time t_4. The new breathing length L_{a4z} and the initial width of the quartary cracks w_{4i} are given in Equations (F.63) and (F.64).

$$L_{a4z} = 0.5 \cdot p \qquad \text{[m]} \qquad\qquad (F.63)$$

$$w_{4i} = \frac{10^6 \cdot E(t_4) \cdot \epsilon_{3z}(t_4)^2}{2 \cdot \gamma \cdot f_2} \qquad \text{[mm]} \qquad\qquad (F.64)$$

At this stage all weakened sections are cracked through. The stress reduction $\Delta\sigma_{4z}$ mid-way two cracks is given by Equation (F.65).

$$\Delta\sigma_{4z} = 0.5 \cdot \sigma_{3z}(t_4) \cdot \left[1 + \frac{w_{4i}}{1000 \cdot L_{a4z}} \right] \qquad \text{[MPa]} \qquad\qquad (F.65)$$

The maximum stress mid-way two cracks $\sigma_4(t)$ is given by Equation (F.66). If this stress exceeds the tensile strength, then cracks will occur also in non-weakened sections.

$$\sigma_4(t) = \frac{\sigma_{3z} - \Delta\sigma_{4z}}{g} \qquad \text{[MPa]} \qquad\qquad (F.66)$$

PRIMARY/SECONDARY CRACKS AT THE LOCATION OF EVERY 5th JOINT ($x = 5$)

When the primary/secondary cracks (P/S) occur (at time t_{12}) at the location of every 5th joint, the tertiary (T) and quartary (Q) occur in the weakened sections according to the scheme in Figure F.8.
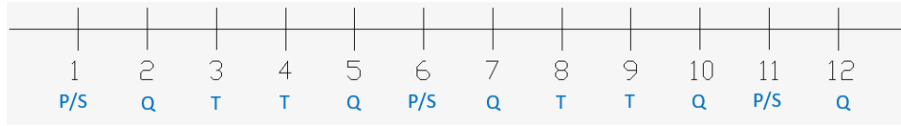
Figure F.8: Location of cracks for the case $x = 5$

At time t_{12} the amplified occurring stress $\sigma_z(t)$ reaches the tensile strength $\sigma_{crack}(t)$ leading to the occurrence of the primary/secondary cracks. The new breathing length L_{a12z}, the initial crack width of the primary/secondary cracks w_{12i} and the stress reduction at the location of the tertiary cracks $\Delta\sigma_{12z}$ are given in Equations (F.67) to (F.69).

$$L_{a12z} = 2.5 \cdot p \qquad \text{[m]} \qquad\qquad (F.67)$$

$$w_{12i} = \frac{10^6 \cdot E(t_{12}) \cdot \epsilon(t_{12})^2}{2 \cdot \gamma \cdot f_1} \qquad \text{[mm]} \qquad\qquad (F.68)$$

$$\Delta\sigma_{12z} = 1.2 \cdot 0.5 \cdot \sigma_z(t_{12}) \cdot \left[1 + \frac{w_{12i}}{1000 \cdot L_{a12z}} \right] \qquad \text{[MPa]} \qquad\qquad (F.69)$$

The tensile stress $\sigma_{2z}(t)$ at the location of the tertiary cracks after the occurrence of the primary/secondary cracks is therefore given by Equation (F.70).

$$\sigma_{2z}(t) = \frac{4}{5} \cdot \sigma_z(t) - \left[\Delta\sigma_{12z} - \frac{1}{5} \cdot \sigma_z(t_{12}) \right] \qquad \text{[MPa]} \qquad\qquad (F.70)$$

The maximum tensile strain $\epsilon_{2z}(t)$ midway between the primary/secondary cracks is given by Equation (F.71).

$$\epsilon_{2z}(t) = \frac{5}{4} \cdot \frac{\sigma_{2z}(t)}{r \cdot E(t)} \qquad \text{[-]} \qquad\qquad (F.71)$$

At this point, if the stress at the location of the tertiary cracks $\sigma_{2z}(t)$ exceeds again the tensile strength $\sigma_{crack}(t)$, the tertiary cracks will occur at a time t_3. The new breathing length L_{a3z} and the initial width of the tertiary cracks w_{3i} are given in Equations (F.72) and (F.73).

$$L_{a3z} = 1.0 \cdot p \qquad \text{[m]} \qquad (F.72)$$

$$w_{3i} = \frac{10^6 \cdot E(t_3) \cdot \epsilon_{2z}(t_3)^2}{2 \cdot \gamma \cdot f_2} \qquad \text{[mm]} \qquad (F.73)$$

The stress reduction $\Delta\sigma_{3z}$ at the location of the quartary cracks is given by Equation (F.74).

$$\Delta\sigma_{3z} = 0.5 \cdot \sigma_{2z}(t_3) \cdot \left[1 + \frac{w_{3i}}{1000 \cdot L_{a3z}}\right] \qquad \text{[MPa]} \qquad (F.74)$$

The maximum stress at the location of the quartary cracks $\sigma_{3z}(t)$ is given by Equation (F.75).

$$\sigma_{3z}(t) = \sigma_{2z} - \Delta\sigma_{3z} \qquad \text{[MPa]} \qquad (F.75)$$

At this point, if the stress at the location of the quartary cracks $\sigma_{3z}(t)$ exceeds again the tensile strength $\sigma_{crack}(t)$, the quartary cracks will occur at time t_4. The new breathing length L_{a4z} and the initial width of the tertiary cracks w_{4i} are given in Equations (F.76) and (F.77).

$$L_{a4z} = 0.5 \cdot p \qquad \text{[m]} \qquad (F.76)$$

$$w_{4i} = \frac{10^6 \cdot E(t_3) \cdot \epsilon_2(t_3)^2}{2 \cdot \gamma \cdot f_2} \qquad \text{[mm]} \qquad (F.77)$$

At this point all weakened sections have cracked through. The stress reduction $\Delta\sigma_{4z}$ mid-way two cracks is given by Equation (F.78).

$$\Delta\sigma_{4z} = 0.5 \cdot \sigma_{3z}(t_4) \cdot \left[1 + \frac{w_{4i}}{1000 \cdot L_{a4z}}\right] \qquad \text{[MPa]} \qquad (F.78)$$

The maximum stress mid-way two cracks $\sigma_4(t)$ is given by Equation (F.79). If this stress exceeds the tensile strength, then cracks will occur also in non-weakened sections.

$$\sigma_4(t) = \frac{\sigma_{3z} - \Delta\sigma_{4z}}{g} \qquad \text{[MPa]} \qquad (F.79)$$

G

APPENDIX G: FORMULAE FOR PRACTICE

In this appendix the equations used in the model for the AGRAC tensile strength (ITS) and the AGRAC modulus of elasticity (E) are given in a more convenient format for practice usage.

AGRAC 2% CEMENT

$$ITS_{2\%} = 0.143 \cdot \exp\left[1 - \sqrt{\left(\frac{4.491}{t/24}\right)}\right] \cdot \left(1 + 3.676 \cdot 10^{-4} \cdot T^2 - 3.103 \cdot 10^{-2} \cdot T\right) \qquad \text{[MPa]} \qquad \text{(G.1)}$$

$$E_{2\%} = \left(-2223 \cdot \exp\left[-\frac{0.231 \cdot t}{24}\right] + 2223\right) \cdot \left(1 + 3.778 \cdot 10^{-4} \cdot T^2 - 3.033 \cdot 10^{-2} \cdot T\right) \qquad \text{[MPa]} \qquad \text{(G.2)}$$

AGRAC 4% CEMENT

$$ITS_{4\%} = 0.237 \cdot \exp\left[1 - \sqrt{\left(\frac{1.755}{t/24}\right)}\right] \cdot \left(1 + 4.444 \cdot 10^{-5} \cdot T^2 - 1.867 \cdot 10^{-2} \cdot T\right) \qquad \text{[MPa]} \qquad \text{(G.3)}$$

$$E_{4\%} = \left(-3633 \cdot \exp\left[-\frac{0.276 \cdot t}{24}\right] + 3633\right) \cdot \left(1 + 4.667 \cdot 10^{-4} \cdot T^2 - 2.967 \cdot 10^{-2} \cdot T\right) \qquad \text{[MPa]} \qquad \text{(G.4)}$$

Where:

- t [hours] is the curing time (interval from time of construction)

- T [°C] is the temperature of the AGRAC. The above equations are valid for temperatures in the range 0-30°C.

The statistical parameters obtained by comparing the measured data with the prediction given by the above equations are given in Tables G.1 and G.2.

	ITS - AGRAC 2% cement			E - AGRAC 2% cement		
	0°C	15°C	30°C	0°C	15°C	30°C
s*	0.0410	0.0225	0.0090	151	199.3	120.4
R²**	0.8776	0.9152	0.9622	0.9691	0.8746	0.9057

*Standard error of estimate   **R-squared: coefficient of determination

Table G.1: Statistical parameters for AGRAC 2%

	ITS - AGRAC 4% cement			E - AGRAC 4% cement		
	0°C	15°C	30°C	0°C	15°C	30°C
s^*	0.0245	0.0326	0.0325	434.3	174.1	113.9
R^{2**}	0.9857	0.9496	0.8857	0.9112	0.9634	0.9774

*Standard error of estimate   **R-squared: coefficient of determination

Table G.2: Statistical parameters for AGRAC 4%

H

APPENDIX H: NON–WEAKENED BASE RESULTS

H.1. N2_MAY10_10–5
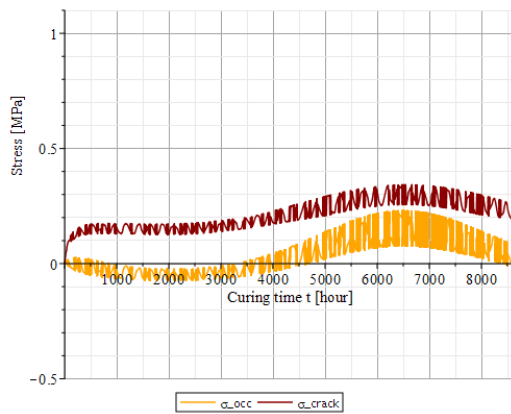
Figure H.1: N2_May10_10–5 σ_{occ} vs σ_{crack}
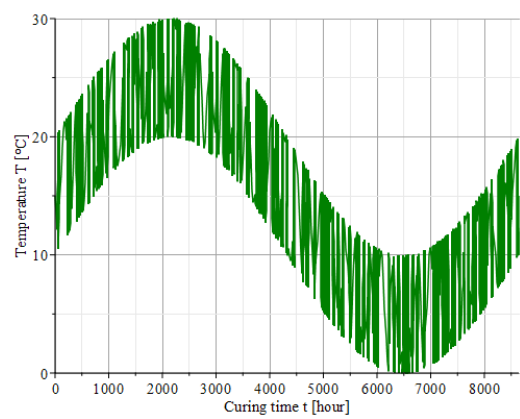
Figure H.2: N2_May10_10–5 Base temperature

H.2. N2_MAY10_8–3
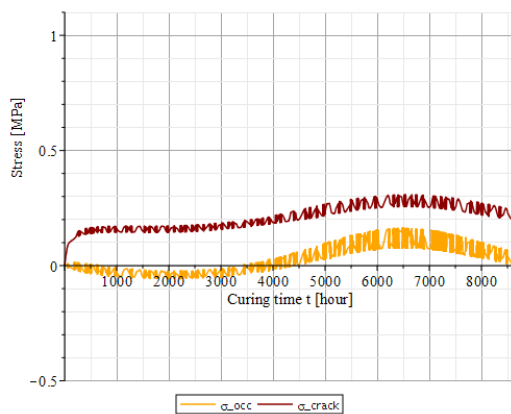
Figure H.3: N2_May10_8–3 σ_{occ} vs σ_{crack}
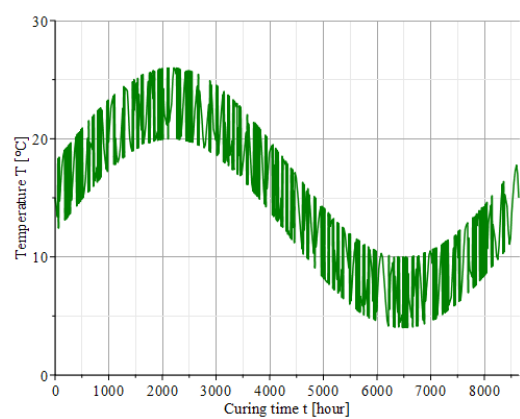
Figure H.4: N2_May10_8–3 Base temperature

H.3. N2_May10_6–1
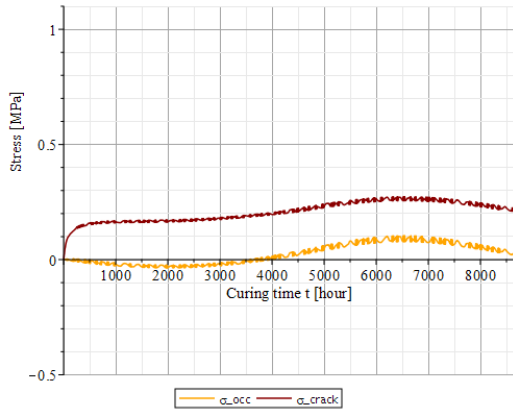
Figure H.5: N2_May10_6–1 σ_{occ} vs σ_{crack}
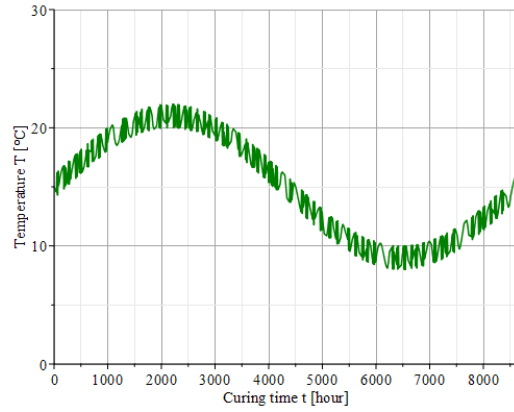
Figure H.6: N2_May10_6–1 Base temperature

H.4. N2_Aug04_10–5_10
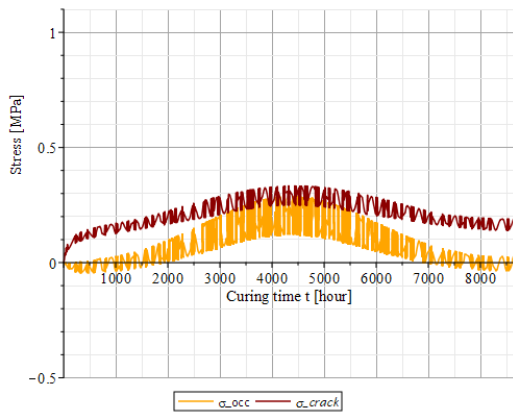
Figure H.7: N2_Aug04_10–5_10 σ_{occ} vs σ_{crack}
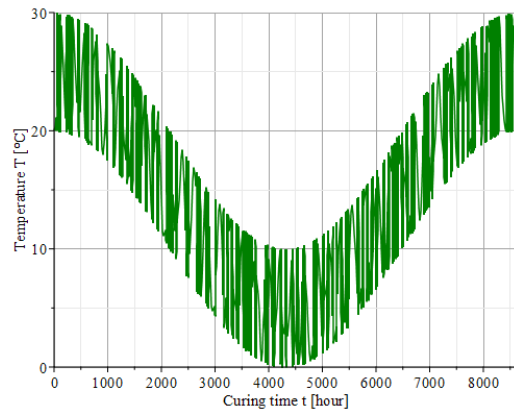
Figure H.8: N2_Aug04_10–5_10 Base temperature
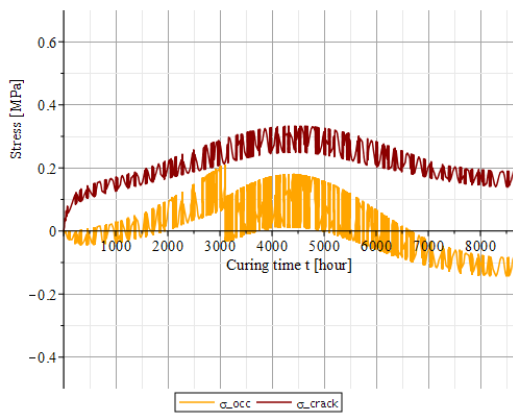
Figure H.9: N2_Aug04_10–5_10 σ_{occ} vs σ_{crack}
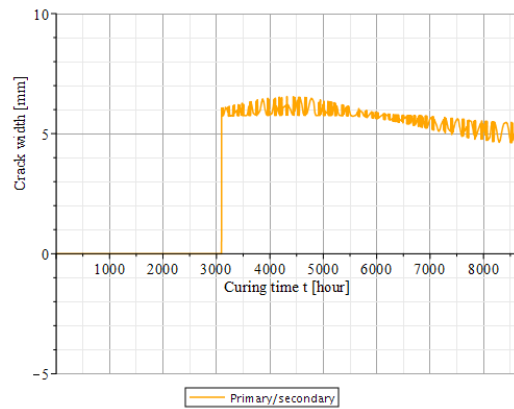
Figure H.10: N2_Aug04_10–5_10 Crack width

H.5. N2_Aug04_10–5_4
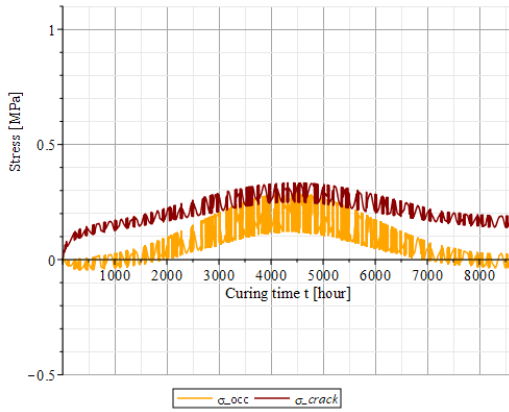
Figure H.11: N2_Aug04_10–5_4 σ_{occ} vs σ_{crack}
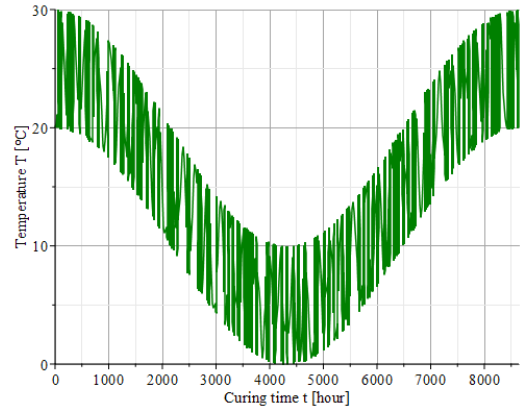
Figure H.12: N2_Aug04_10–5_4 Base temperature
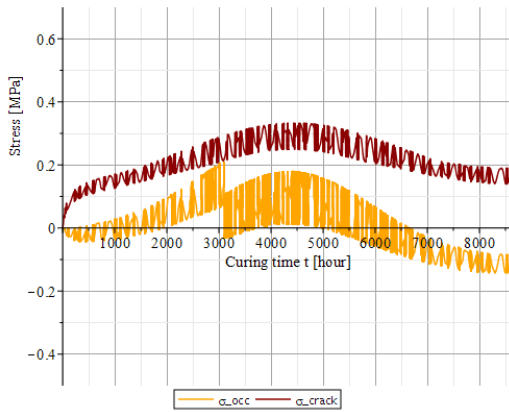
Figure H.13: N2_Aug04_10–5_4 σ_{occ} vs σ_{crack}
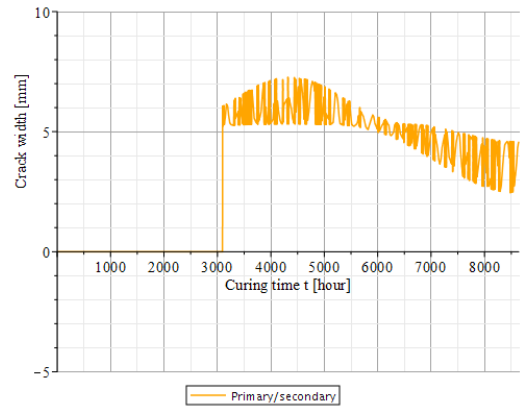
Figure H.14: N2_Aug04_10–5_4 Crack width

H.6. N2_Aug04_8–3
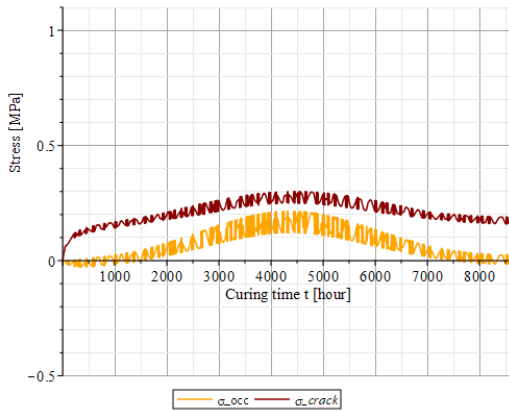
Figure H.15: N2_Aug04_8–3 σ_{occ} vs σ_{crack}
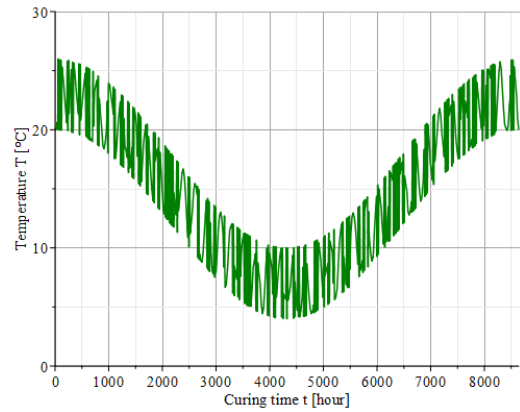
Figure H.16: N2_Aug04_8–3 Base temperature

H.7. N2_AUG04_6–1
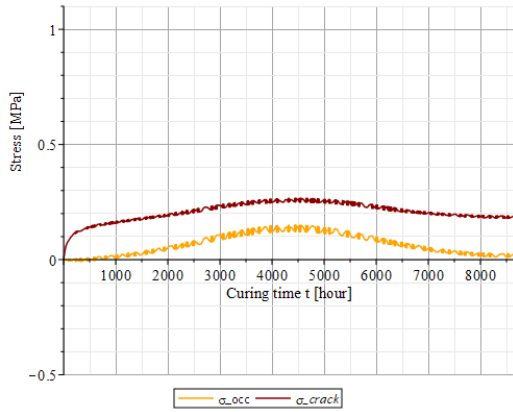
Figure H.17: N2_Aug04_6–1 σ_{occ} vs σ_{crack}
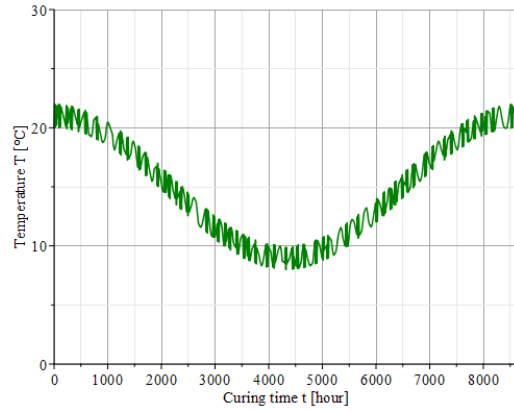
Figure H.18: N2_Aug04_6–1 Base temperature

H.8. N2_AUG10_10–5_10
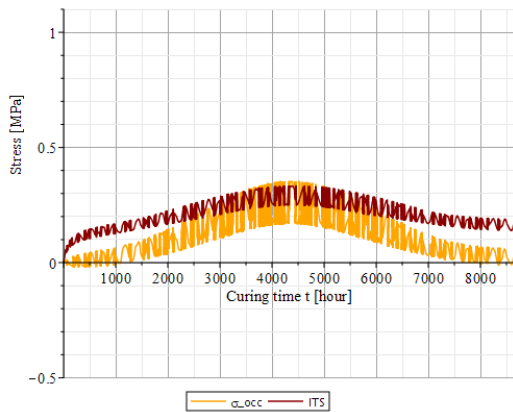
Figure H.19: N2_Aug10_10–5_10 σ_{occ} vs σ_{crack}
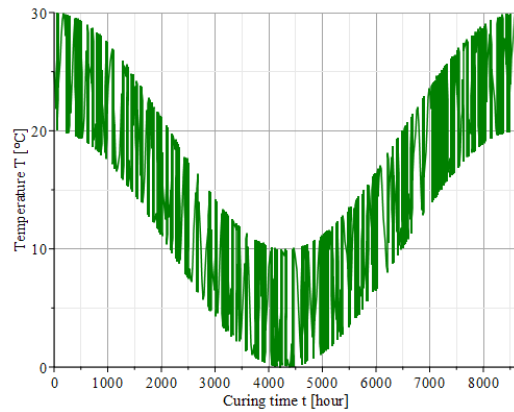
Figure H.20: N2_Aug10_10–5_10 Base temperature
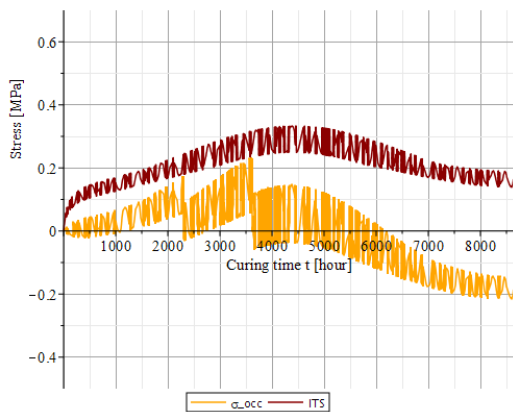
Figure H.21: N2_Aug10_10–5_10 σ_{occ} vs σ_{crack}
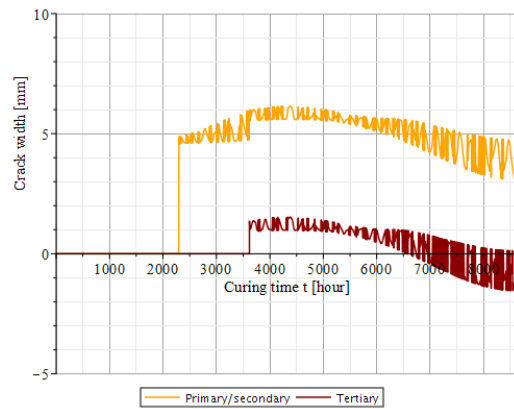
Figure H.22: N2_Aug10_10–5_10 Crack width

H.9. N2_Aug10_10–5_4
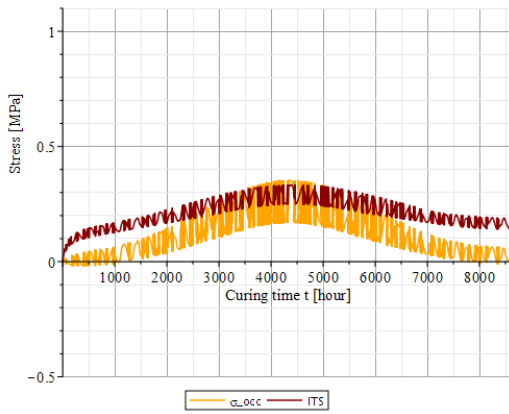
Figure H.23: N2_Aug10_10–5_4 σ_{occ} vs σ_{crack}
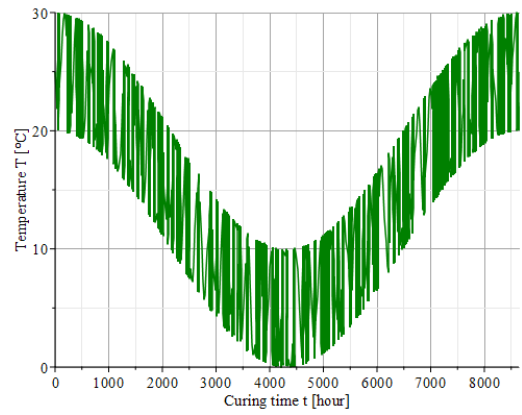
Figure H.24: N2_Aug10_10–5_4 Base temperature
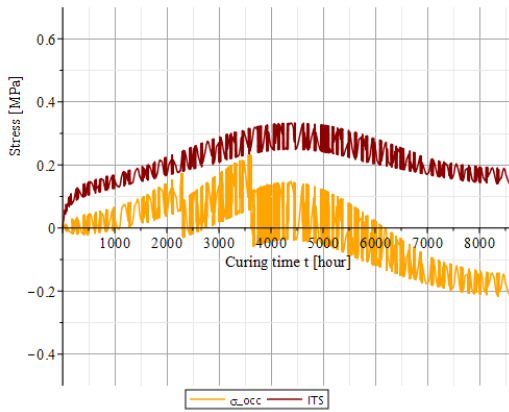
Figure H.25: N2_Aug10_10–5_4 σ_{occ} vs σ_{crack}
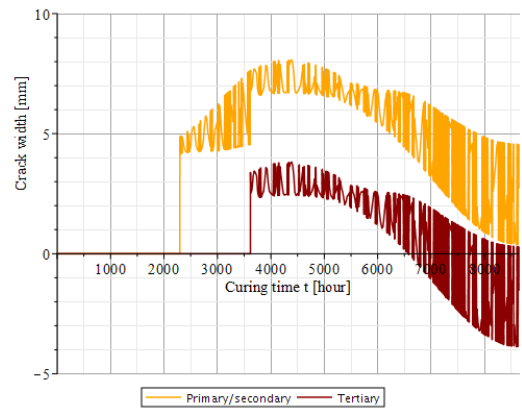
Figure H.26: N2_Aug10_10–5_4 Crack width

H.10. N2_Aug10_8–3
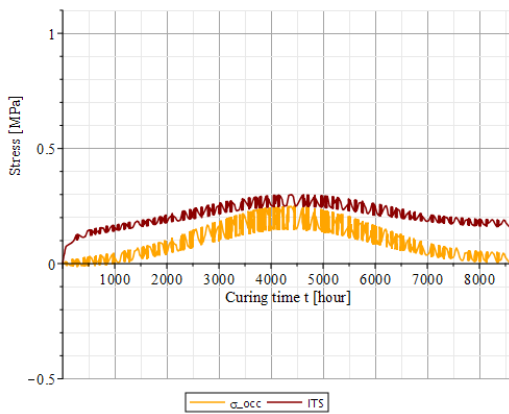
Figure H.27: N2_Aug10_8–3 σ_{occ} vs σ_{crack}
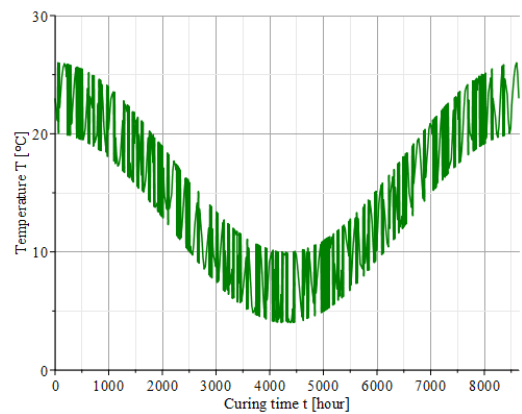
Figure H.28: N2_Aug10_8–3 Base temperature

H.11. N2_AUG10_6–1
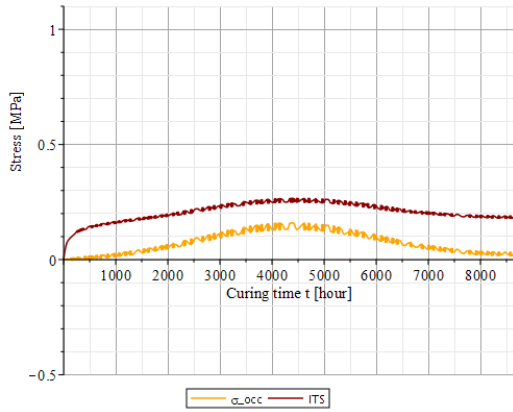
Figure H.29: N2_Aug10_6–1 σ_{occ} vs σ_{crack}
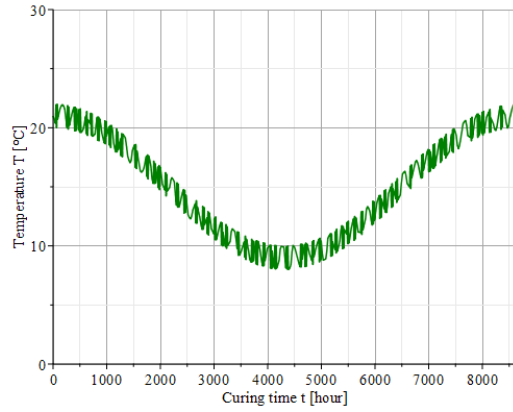
Figure H.30: N2_Aug10_6–1 Base temperature

H.12. N2_AUG16_10–5_10
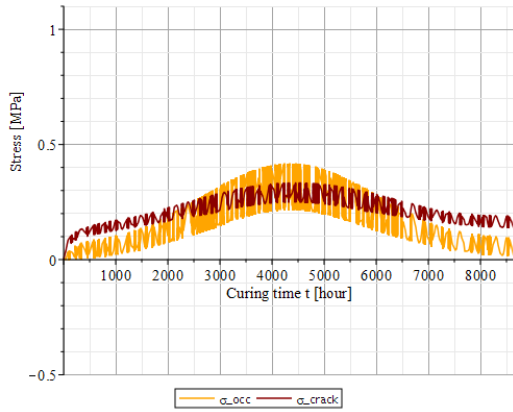
Figure H.31: N2_Aug16_10–5_10 σ_{occ} vs σ_{crack}
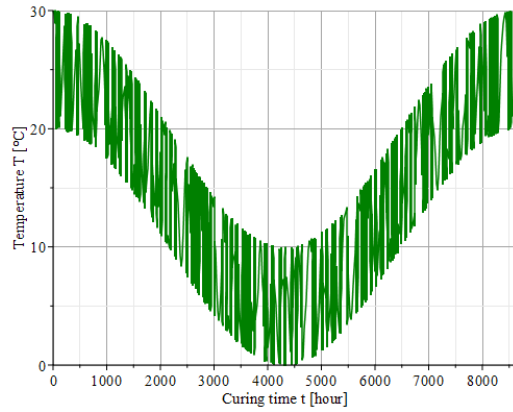
Figure H.32: N2_Aug16_10–5_10 Base temperature
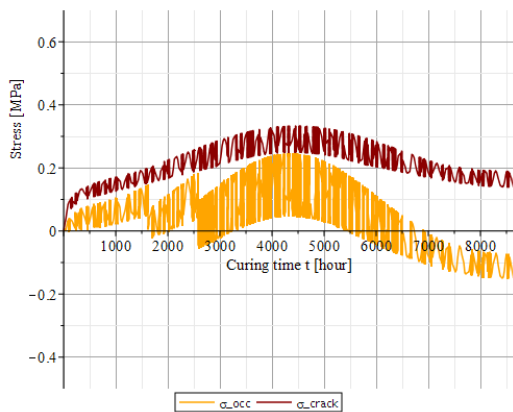
Figure H.33: N2_Aug16_10–5_10 σ_{occ} vs σ_{crack}
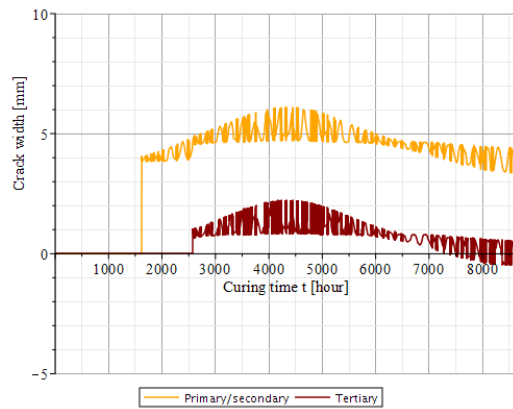
Figure H.34: N2_Aug16_10–5_10 Crack width

H.13. N2_Aug16_10–5_4
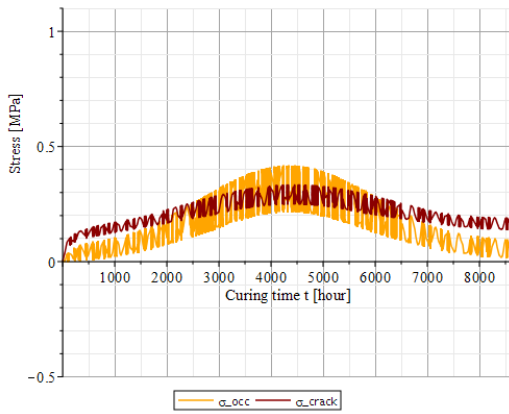
Figure H.35: N2_Aug16_10–5_4 σ_{occ} vs σ_{crack}
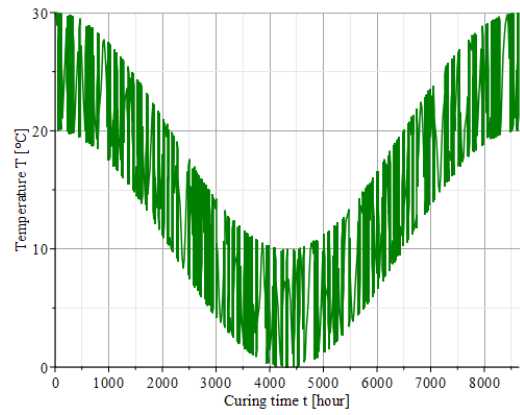
Figure H.36: N2_Aug16_10–5_4 Base temperature
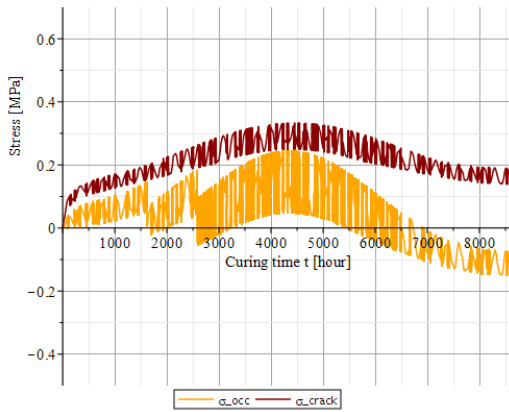
Figure H.37: N2_Aug16_10–5_4 σ_{occ} vs σ_{crack}
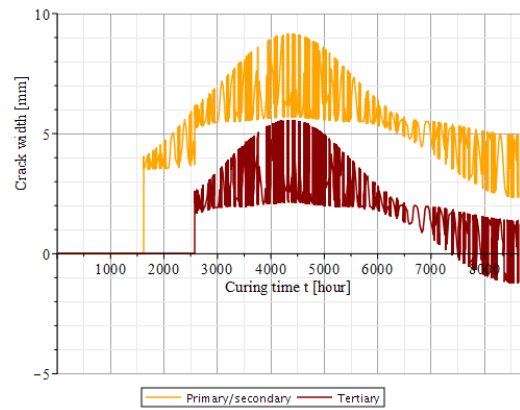
Figure H.38: N2_Aug16_10–5_4 Crack width

H.14. N2_Aug16_8–3_10
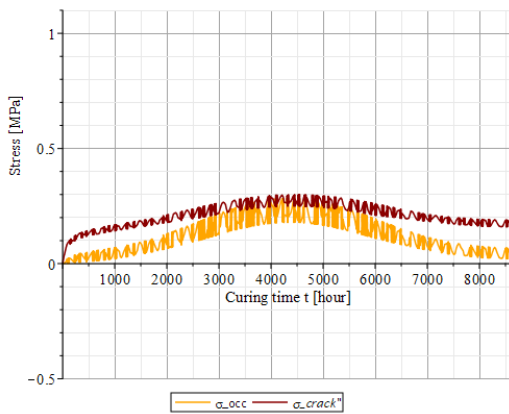
Figure H.39: N2_Aug16_8–3_10 σ_{occ} vs σ_{crack}
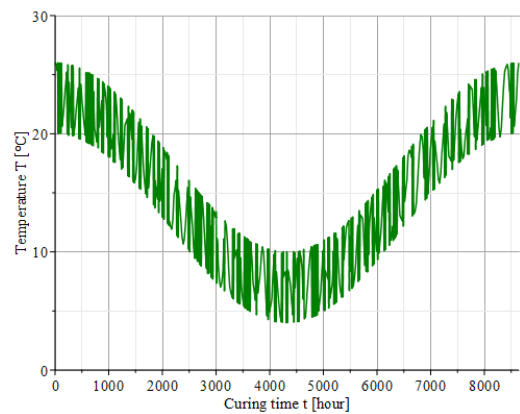
Figure H.40: N2_Aug16_8–3_10 Base temperature
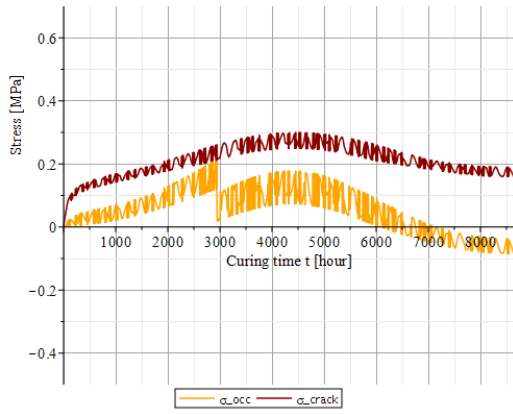
Figure H.41: N2_Aug16_8–3_10 σ_{occ} vs σ_{crack}
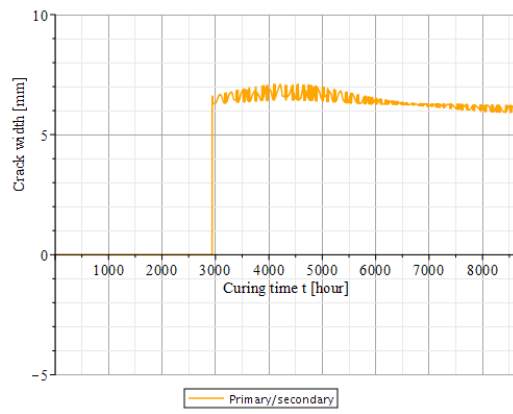
Figure H.42: N2_Aug16_8–3_10 Crack width

H.15. N2_AUG16_8–3_4
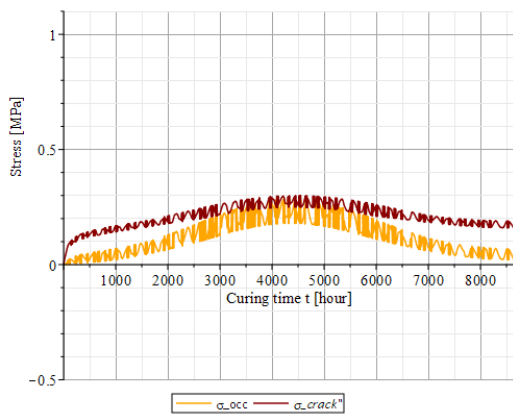
Figure H.43: N2_Aug16_8–3_4 σ_{occ} vs σ_{crack}
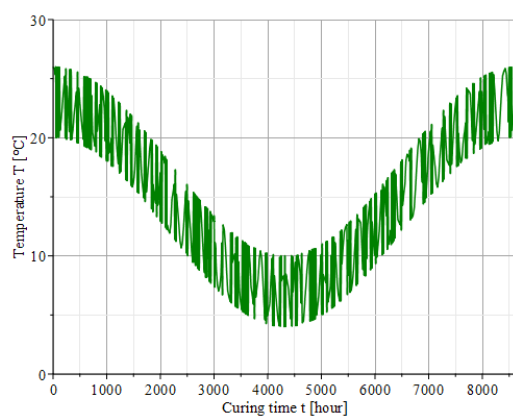
Figure H.44: N2_Aug16_8–3_4 Base temperature
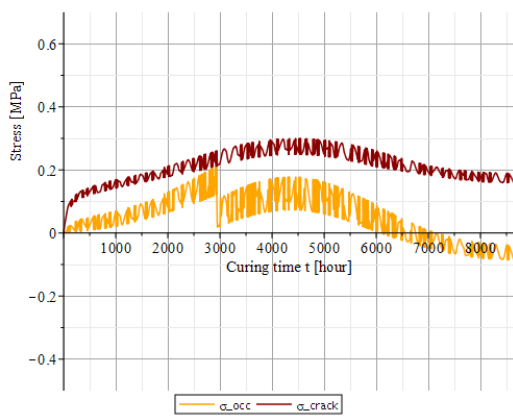
Figure H.45: N2_Aug16_8–3_4 σ_{occ} vs σ_{crack}
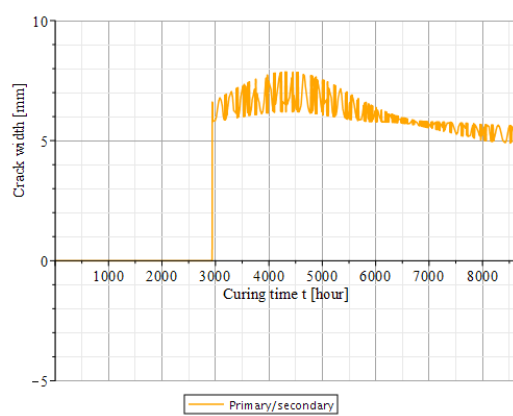
Figure H.46: N2_Aug16_8–3_4 Crack width

H.16. N2_Aug16_6–1
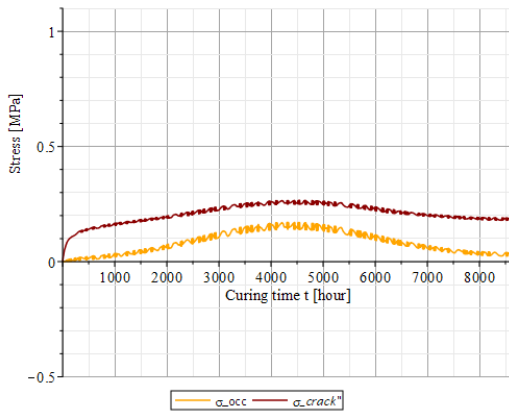
Figure H.47: N2_Aug16_6–1 σ_{occ} vs σ_{crack}
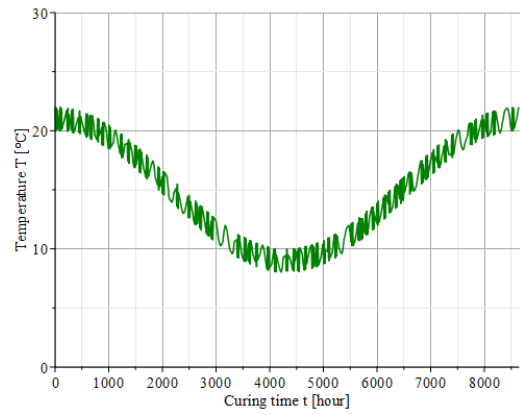
Figure H.48: N2_Aug16_6–1 Base temperature

H.17. N2_Aug22_10–5_10
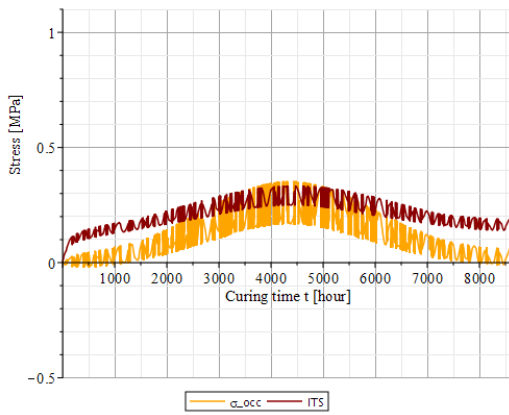
Figure H.49: N2_Aug22_10–5_10 σ_{occ} vs σ_{crack}
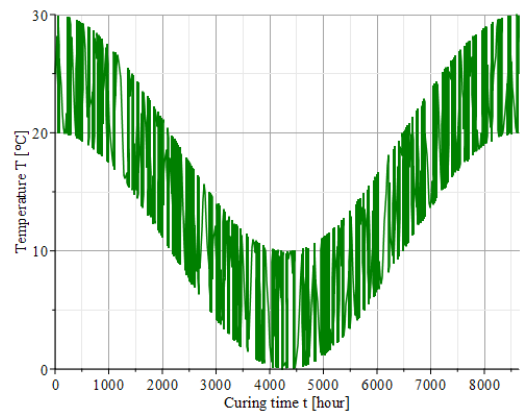
Figure H.50: N2_Aug22_10–5_10 Base temperature
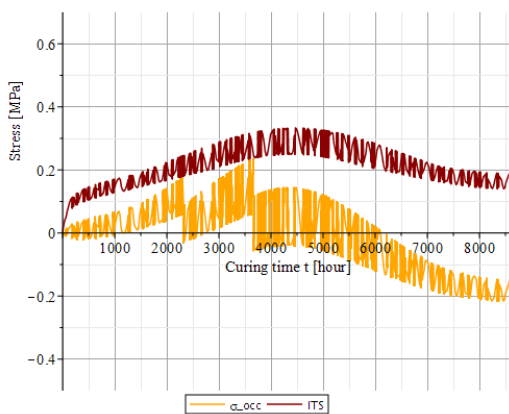
Figure H.51: N2_Aug22_10–5_10 σ_{occ} vs σ_{crack}
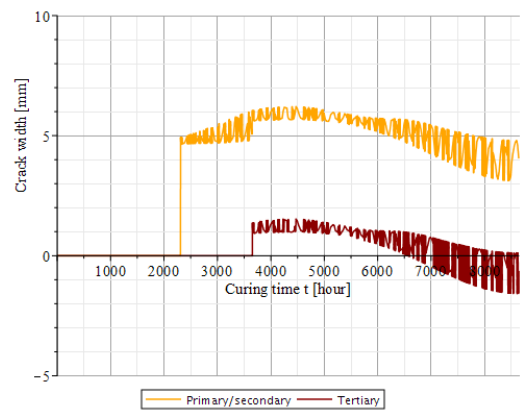
Figure H.52: N2_Aug22_10–5_10 Crack width

H.18. N2_AUG22_10–5_4
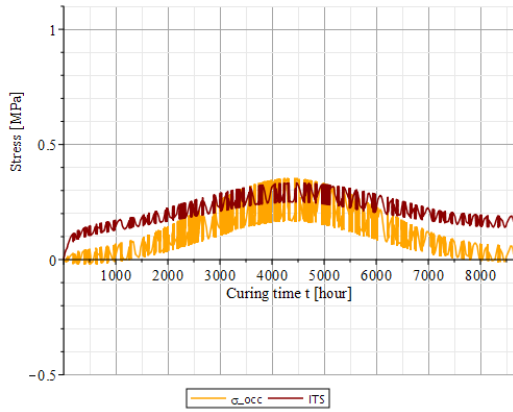
Figure H.53: N2_Aug22_10–5_4 σ_{occ} vs σ_{crack}
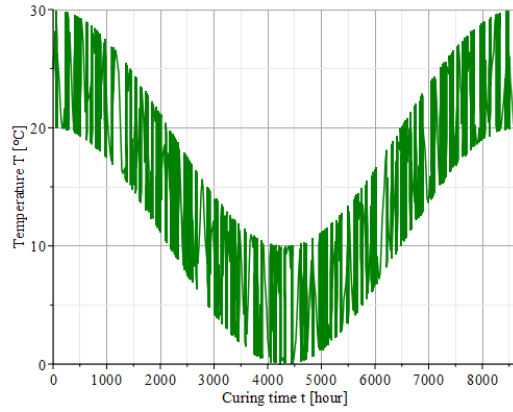
Figure H.54: N2_Aug22_10–5_4 Base temperature
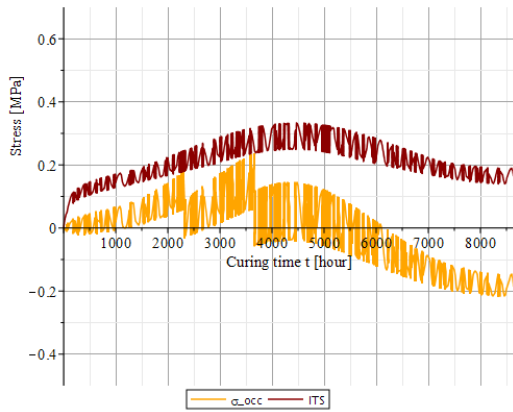
Figure H.55: N2_Aug22_10–5_4 σ_{occ} vs σ_{crack}
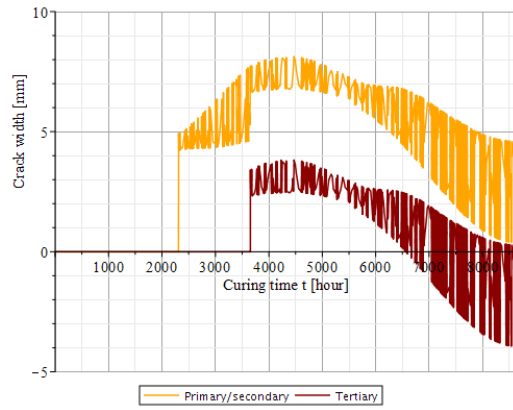
Figure H.56: N2_Aug22_10–5_4 Crack width

H.19. N2_AUG22_8–3
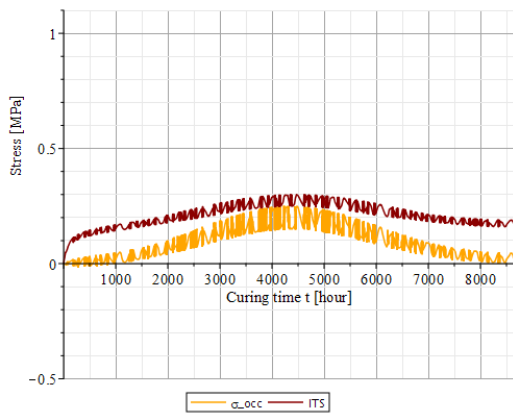
Figure H.57: N2_Aug22_8–3 σ_{occ} vs σ_{crack}
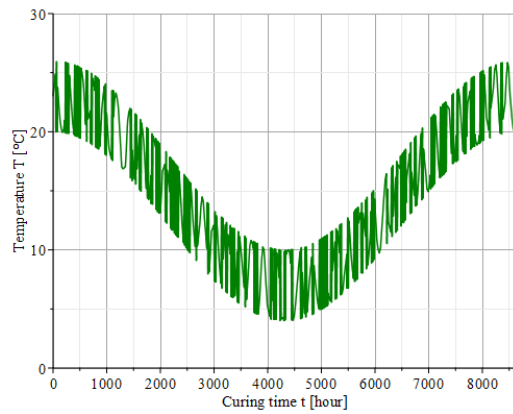
Figure H.58: N2_Aug22_8–3 Base temperature

H.20. N2_Aug22_6–1
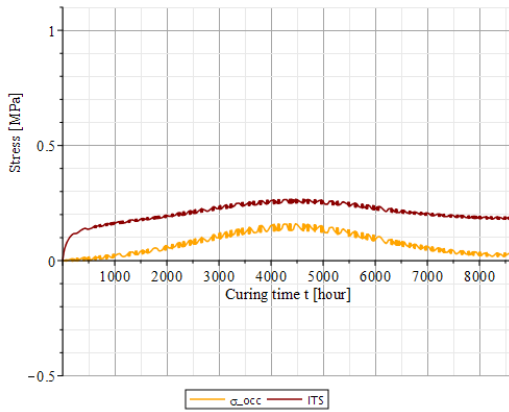
Figure H.59: N2_Aug22_6–1 σ_{occ} vs σ_{crack}
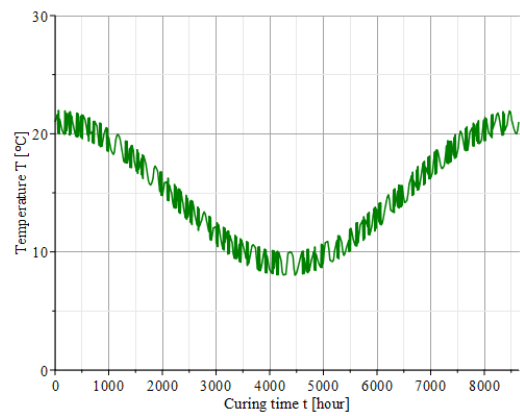
Figure H.60: N2_Aug22_6–1 Base temperature

H.21. N2_Nov10_10–5
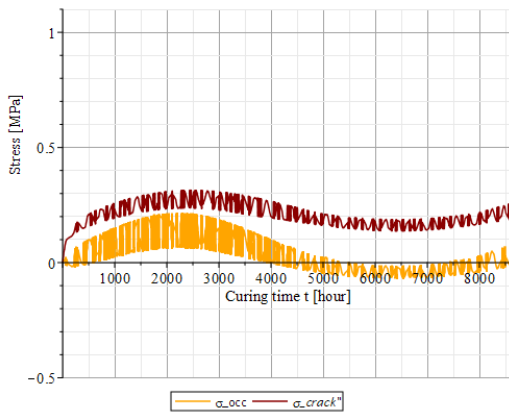
Figure H.61: N2_Nov10_10–5 σ_{occ} vs σ_{crack}
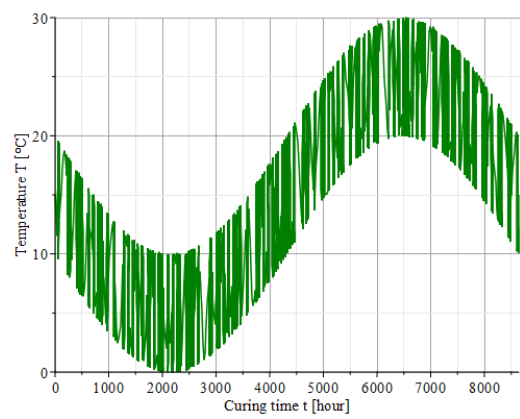
Figure H.62: N2_Nov10_10–5 Base temperature

H.22. N2_Nov10_8–3
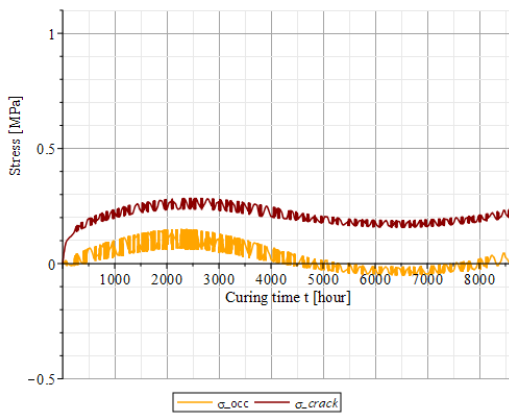
Figure H.63: N2_Nov10_8–3 σ_{occ} vs σ_{crack}
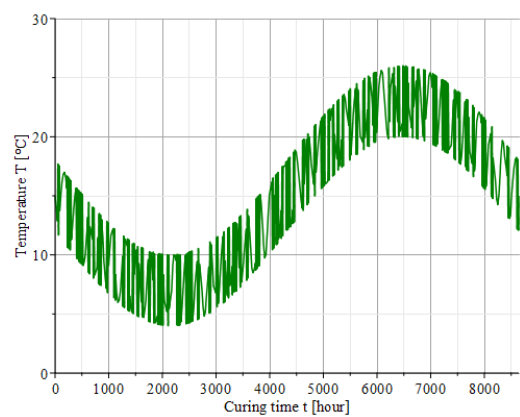
Figure H.64: N2_Nov10_8–3 Base temperature

H.23. N2_Nov10_6–1
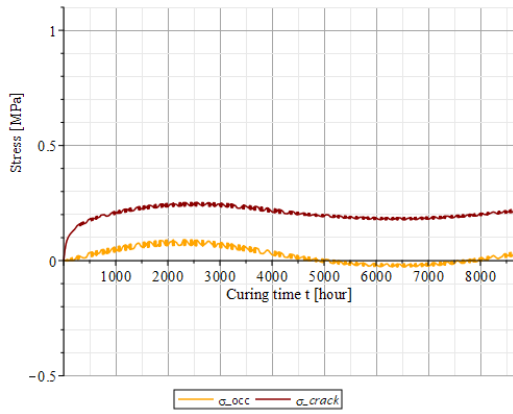
Figure H.65: N2_Nov10_6–1 σ_{occ} vs σ_{crack}
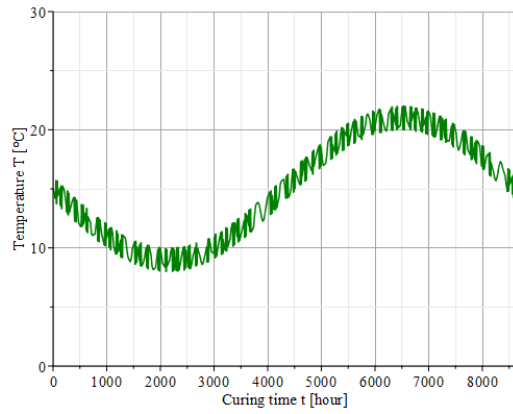
Figure H.66: N2_Nov10_6–1 Base temperature

H.24. N2_Feb04_10–5
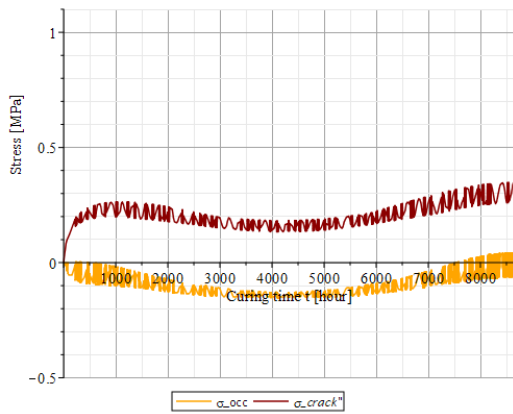
Figure H.67: N2_Feb04_10–5 σ_{occ} vs σ_{crack}
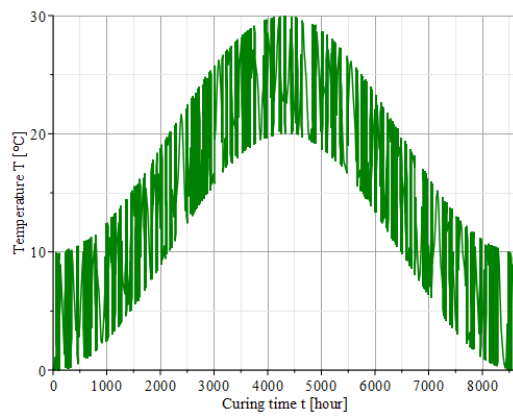
Figure H.68: N2_Feb04_10–5 Base temperature

H.25. N2_Feb04_8–3
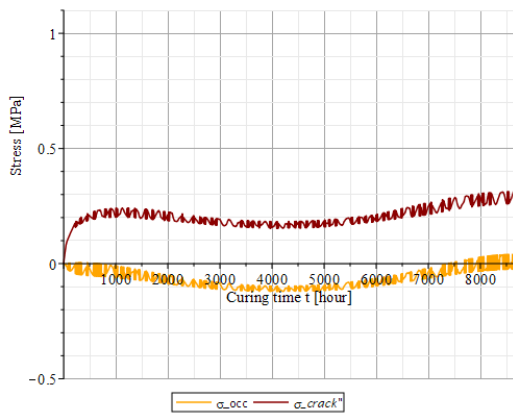
Figure H.69: N2_Feb04_8–3 σ_{occ} vs σ_{crack}
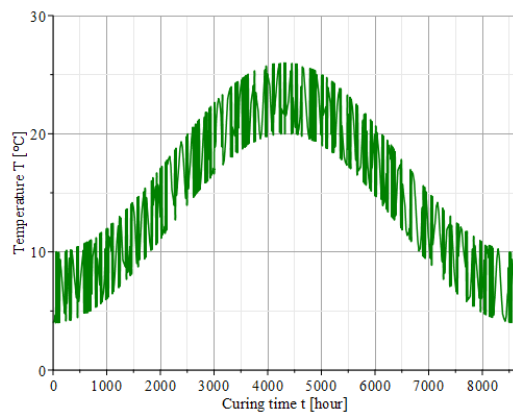
Figure H.70: N2_Feb04_8–3 Base temperature

H.26. N2_Feb04_6–1
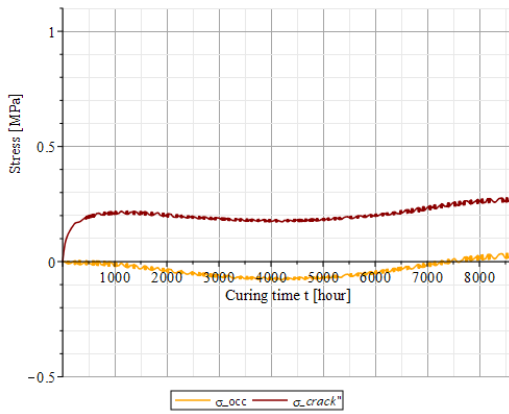
Figure H.71: N2_Feb04_6–1 σ_{occ} vs σ_{crack}
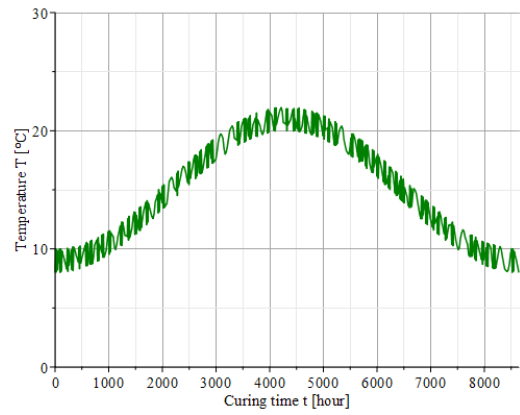
Figure H.72: N2_Feb04_6–1 Base temperature

H.27. N4_May10_10–5_10
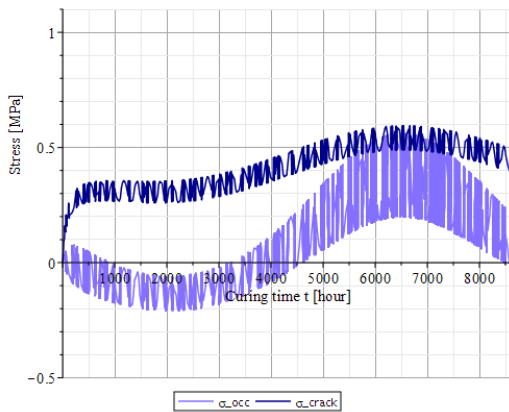
Figure H.73: N4_May10_10–5_10 σ_{occ} vs σ_{crack}
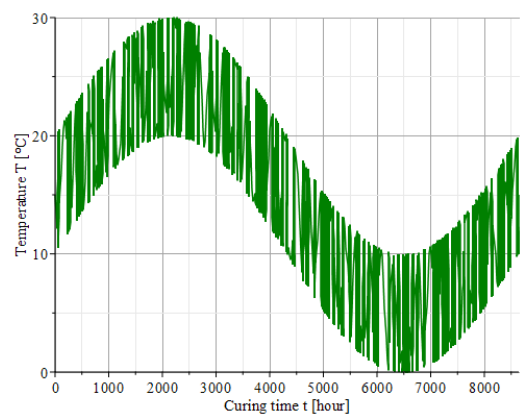
Figure H.74: N4_May10_10–5_10 Base temperature
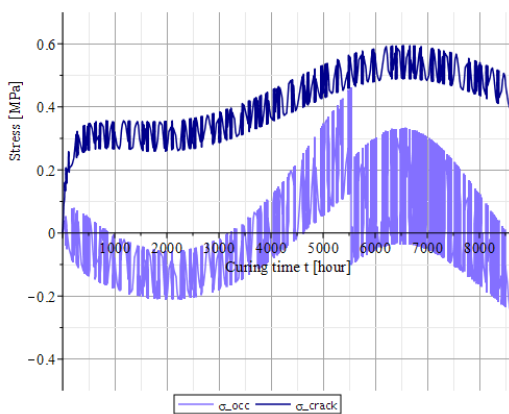
Figure H.75: N4_May10_10–5_10 σ_{occ} vs σ_{crack}
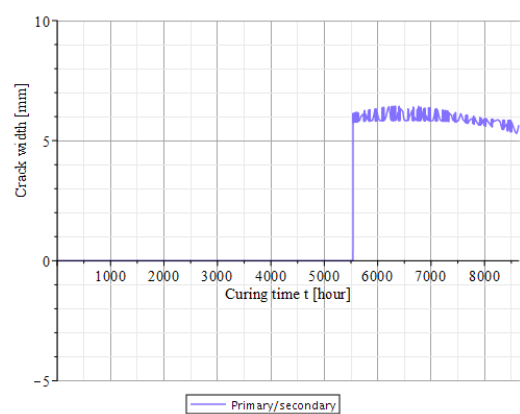
Figure H.76: N4_May10_10–5_10 Crack width

H.28. N4_May10_10–5_4
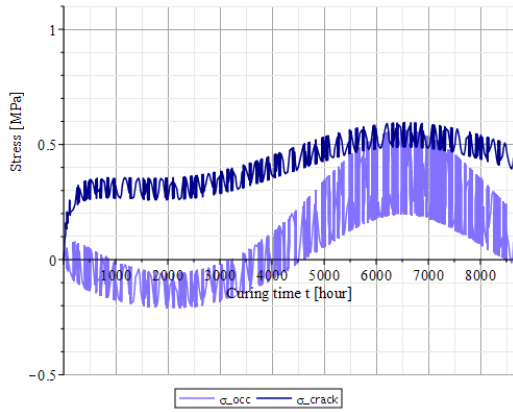
Figure H.77: N4_May10_10–5_4 σ_{occ} vs σ_{crack}
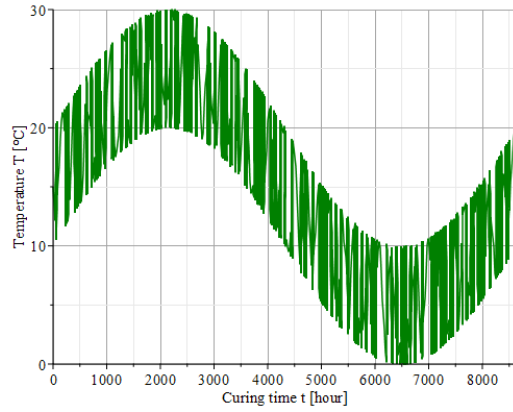
Figure H.78: N4_May10_10–5_4 Base temperature
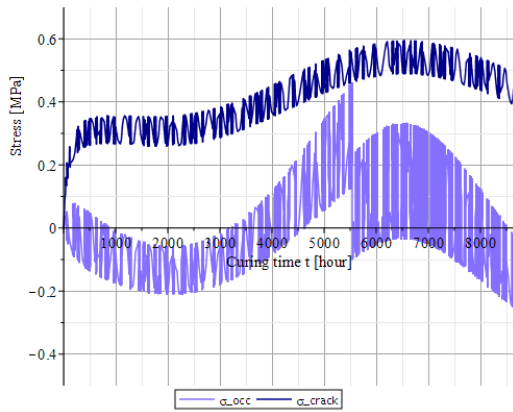
Figure H.79: N4_May10_10–5_4 σ_{occ} vs σ_{crack}
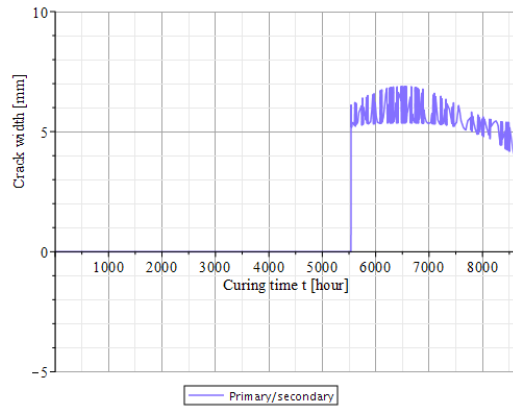
Figure H.80: N4_May10_10–5_4 Crack width

H.29. N4_May10_8–3
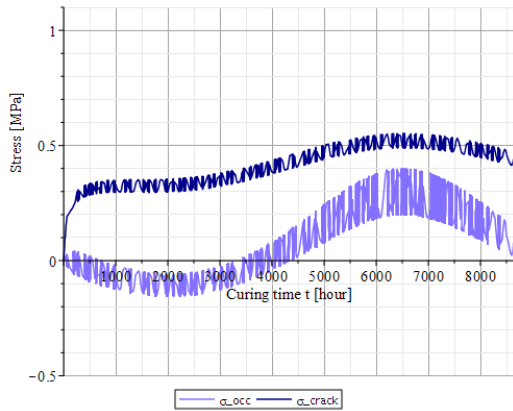
Figure H.81: N4_May10_8–3 σ_{occ} vs σ_{crack}
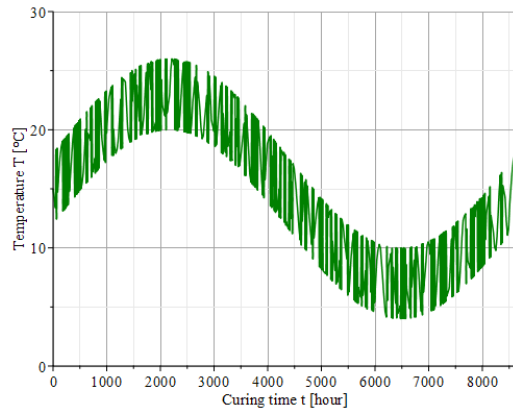
Figure H.82: N4_May10_8–3 Base temperature

H.30. N4_MAY10_6–1
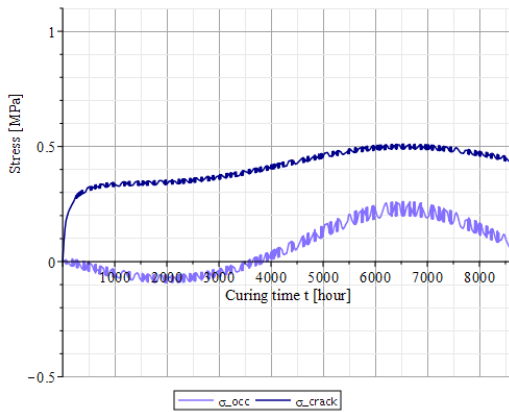
Figure H.83: N4_May10_6–1 σ_{occ} vs σ_{crack}
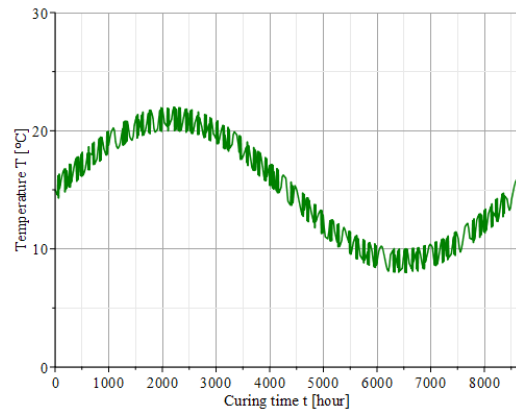
Figure H.84: N4_May10_6–1 Base temperature

H.31. N4_AUG04_10–5_10
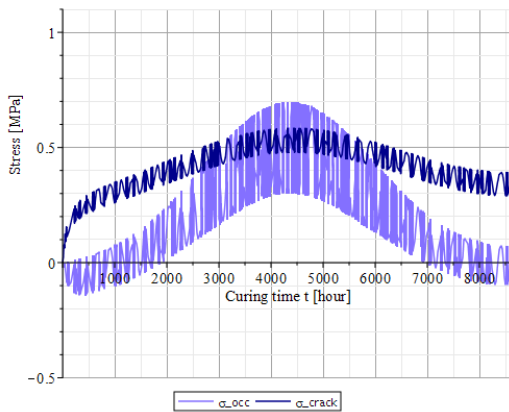
Figure H.85: N4_Aug04_10–5_10 σ_{occ} vs σ_{crack}
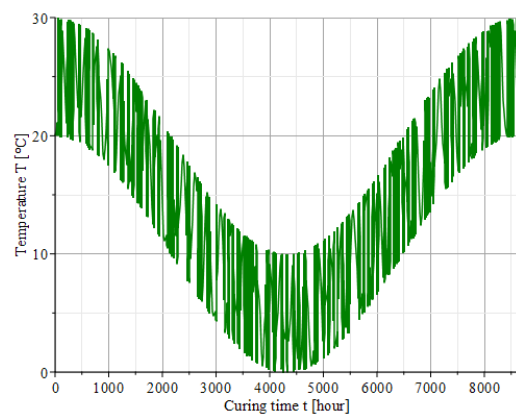
Figure H.86: N4_Aug04_10–5_10 Base temperature
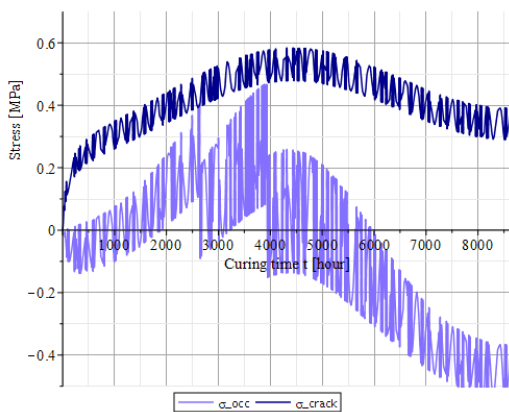
Figure H.87: N4_Aug04_10–5_10 σ_{occ} vs σ_{crack}
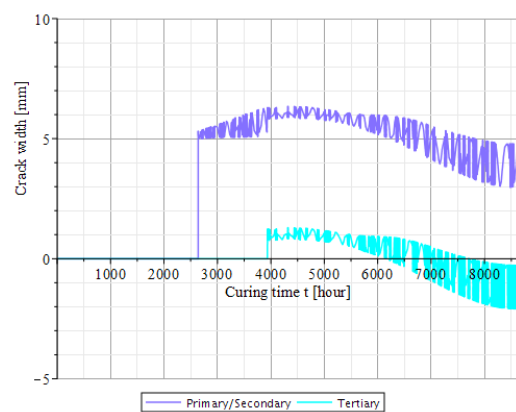
Figure H.88: N4_Aug04_10–5_10 Crack width

H.32. N4_Aug04_10−5_4
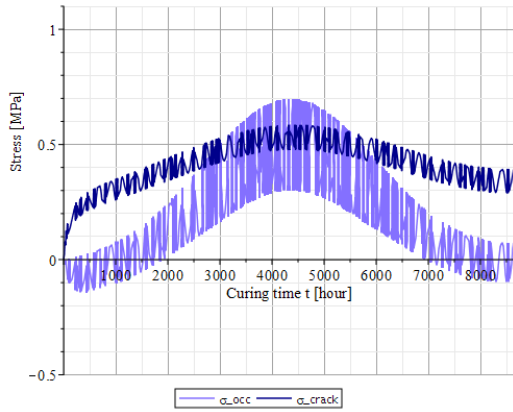
Figure H.89: N4_Aug04_10−5_4 σ_{occ} vs σ_{crack}
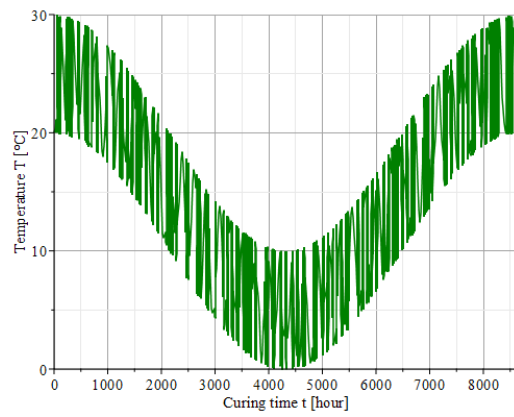
Figure H.90: N4_Aug04_10−5_4 Base temperature
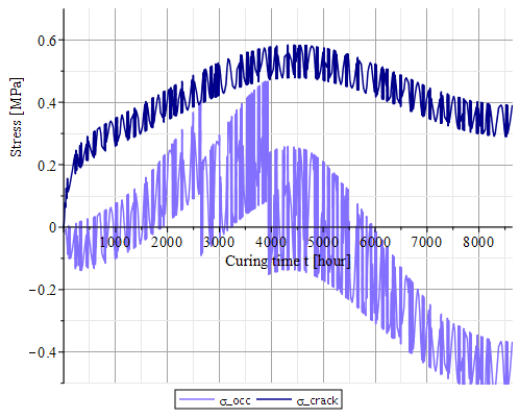
Figure H.91: N4_Aug04_10−5_4 σ_{occ} vs σ_{crack}
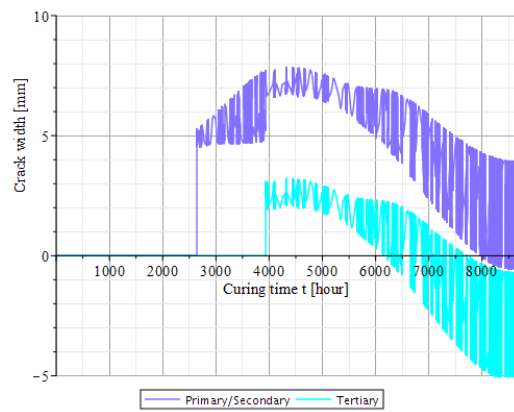
Figure H.92: N4_Aug04_10−5_4 Crack width

H.33. N4_Aug04_8−3_10
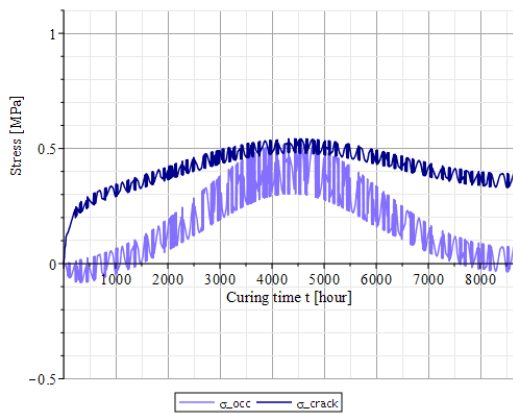
Figure H.93: N4_Aug04_8−3_10 σ_{occ} vs σ_{crack}
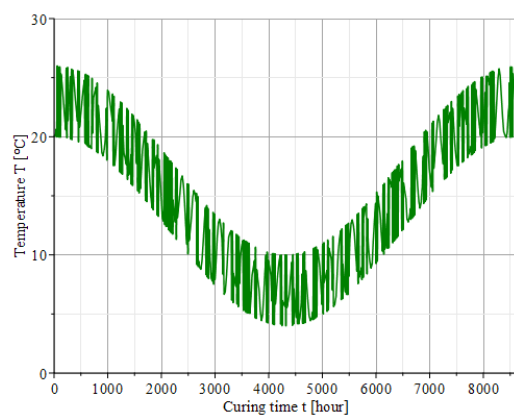
Figure H.94: N4_Aug04_8−3_10 Base temperature
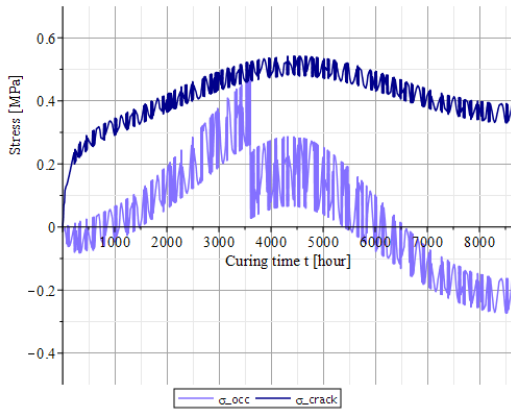
Figure H.95: N4_Aug04_8–3_10 σ_{occ} vs σ_{crack}
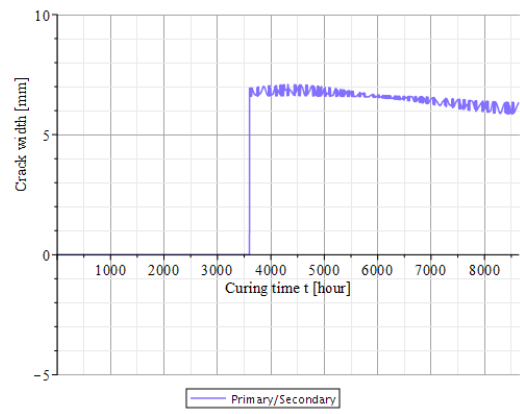
Figure H.96: N4_Aug04_8–3_10 Crack width

H.34. N4_Aug04_8–3_4
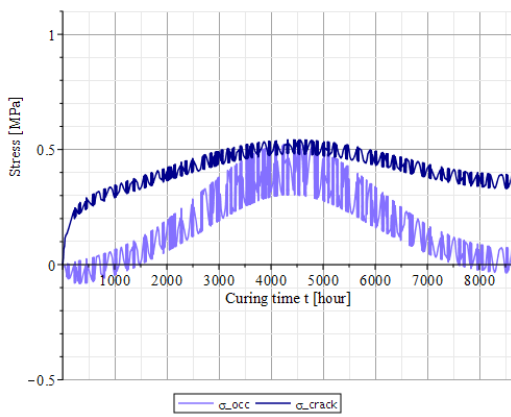
Figure H.97: N4_Aug04_8–3_4 σ_{occ} vs σ_{crack}
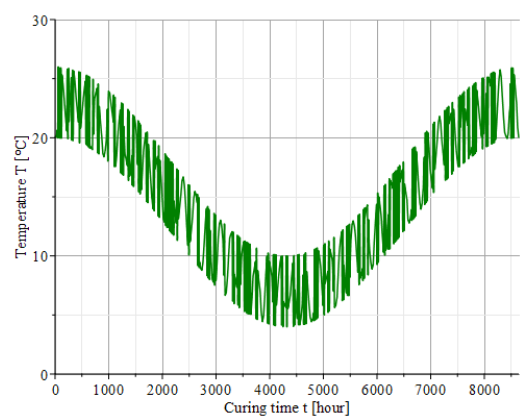
Figure H.98: N4_Aug04_8–3_4 Base temperature
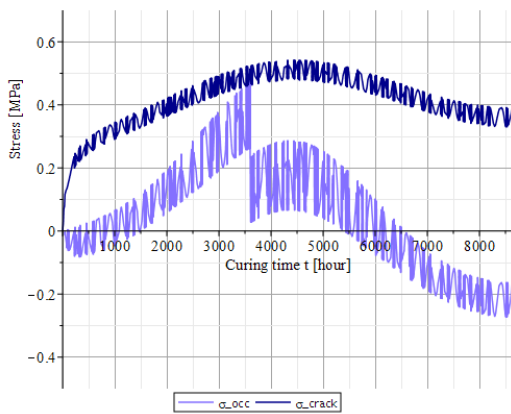
Figure H.99: N4_Aug04_8–3_4 σ_{occ} vs σ_{crack}
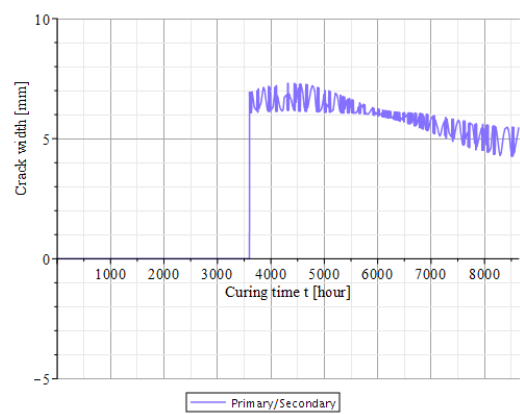
Figure H.100: N4_Aug04_8–3_4 Crack width

H.35. N4_Aug04_6–1
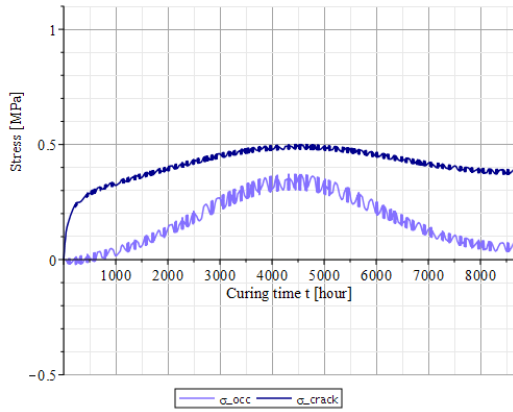
Figure H.101: N4_Aug04_6–1 σ_{occ} vs σ_{crack}
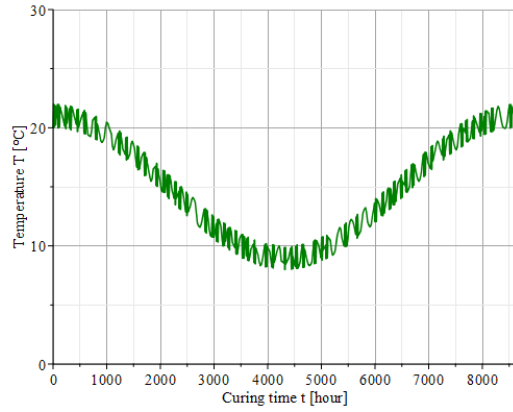
Figure H.102: N4_Aug04_6–1 Base temperature

H.36. N4_Aug10_10–5_10
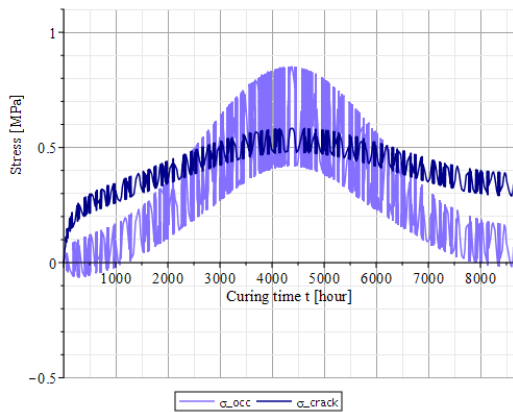
Figure H.103: N4_Aug10_10–5_10 σ_{occ} vs σ_{crack}
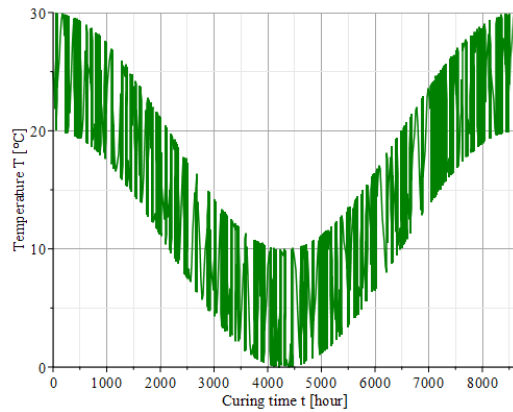
Figure H.104: N4_Aug10_10–5_10 Base temperature
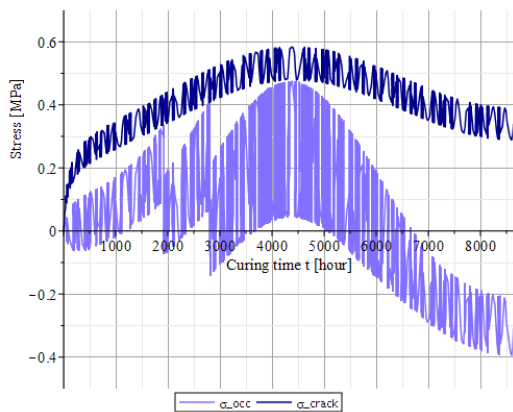
Figure H.105: N4_Aug10_10–5_10 σ_{occ} vs σ_{crack}
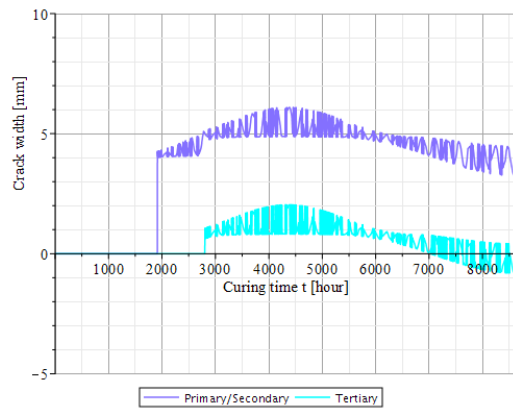
Figure H.106: N4_Aug10_10–5_10 Crack width

H.37. N4_Aug10_10–5_4
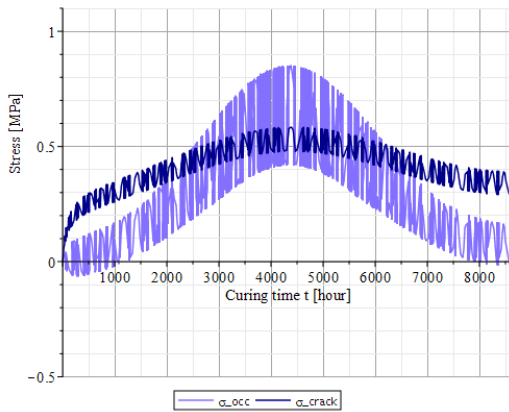
Figure H.107: N4_Aug10_10–5_4 σ_{occ} vs σ_{crack}
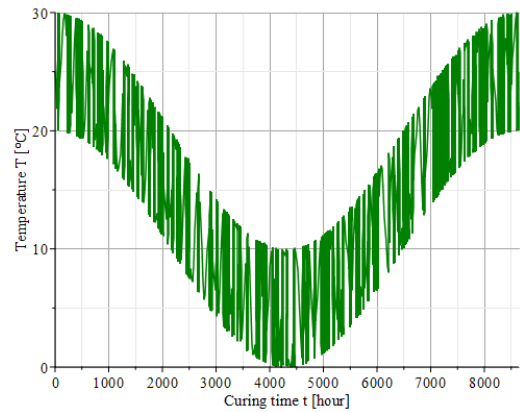
Figure H.108: N4_Aug10_10–5_4 Base temperature
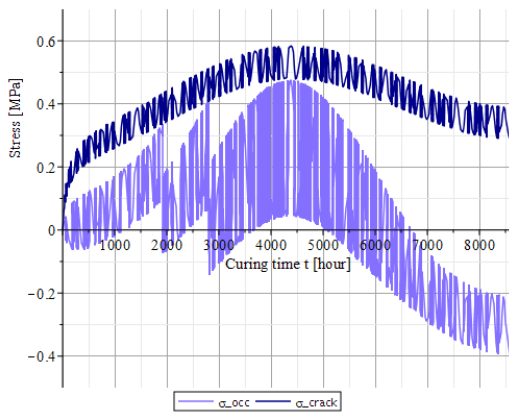
Figure H.109: N4_Aug10_10–5_4 σ_{occ} vs σ_{crack}
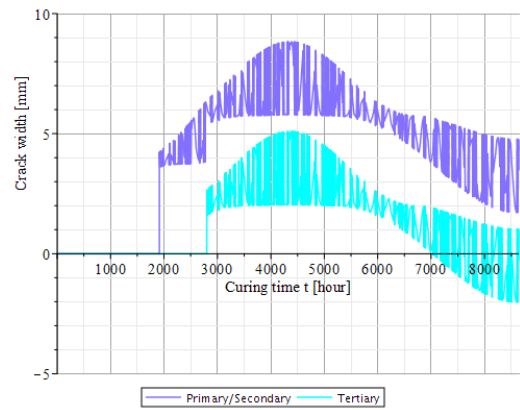
Figure H.110: N4_Aug10_10–5_4 Crack width

H.38. N4_Aug10_8–3_10
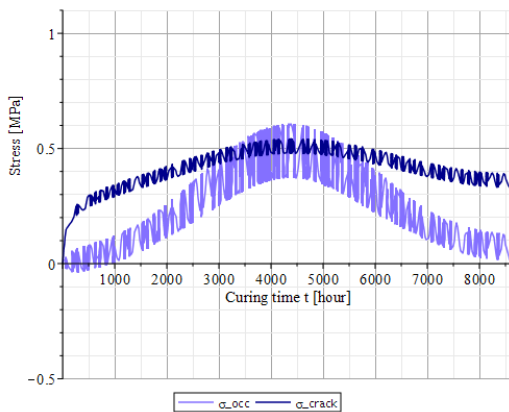
Figure H.111: N4_Aug10_8–3_10 σ_{occ} vs σ_{crack}
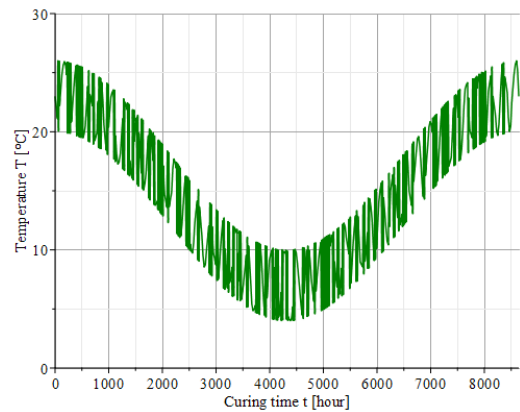
Figure H.112: N4_Aug10_8–3_10 Base temperature
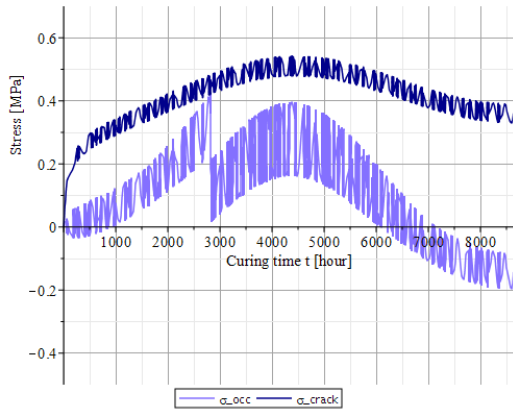
Figure H.113: N4_Aug10_8–3_10 σ_{occ} vs σ_{crack}
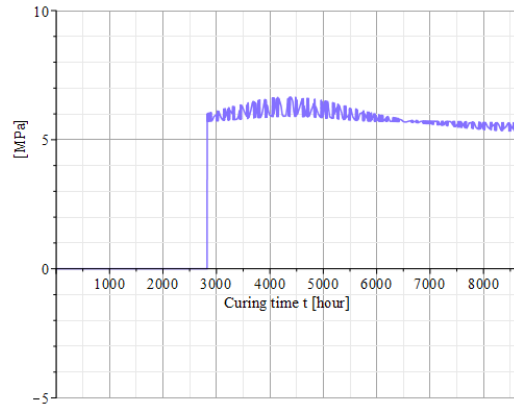
Figure H.114: N4_Aug10_8–3_10 Crack width

H.39. N4_AUG10_8–3_4
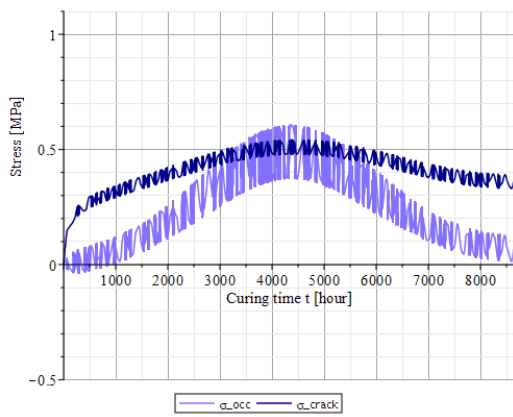
Figure H.115: N4_Aug10_8–3_4 σ_{occ} vs σ_{crack}
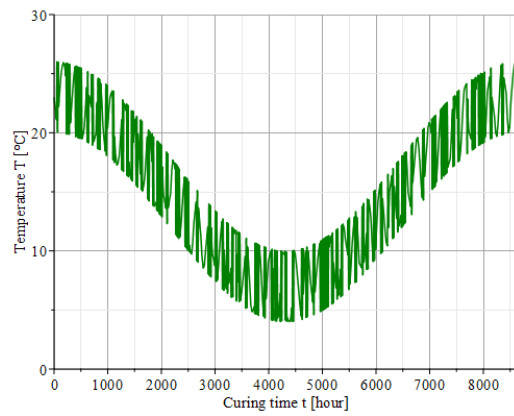
Figure H.116: N4_Aug10_8–3_4 Base temperature
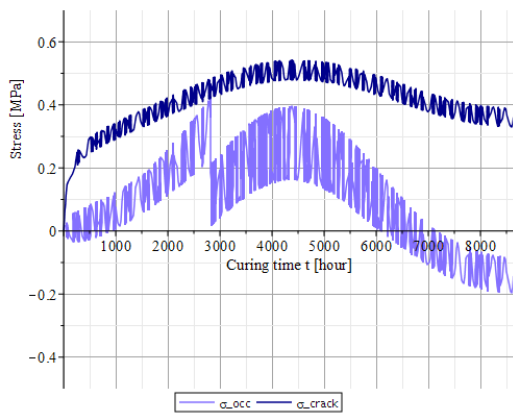
Figure H.117: N4_Aug10_8–3_4 σ_{occ} vs σ_{crack}
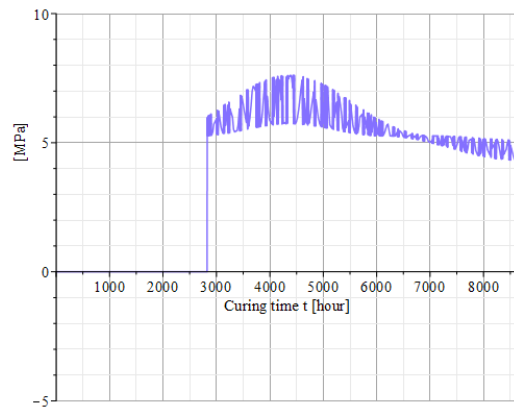
Figure H.118: N4_Aug10_8–3_4 Crack width

H.40. N4_Aug10_6–1
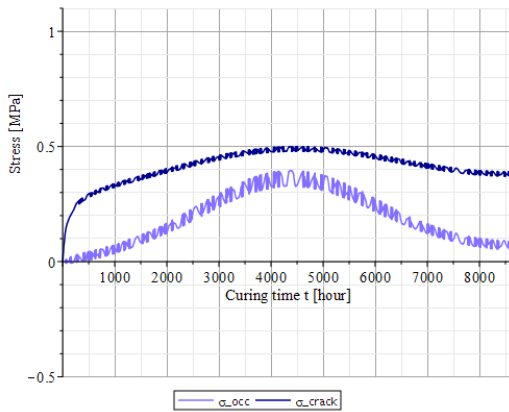
Figure H.119: N4_Aug10_6–1 σ_{occ} vs σ_{crack}
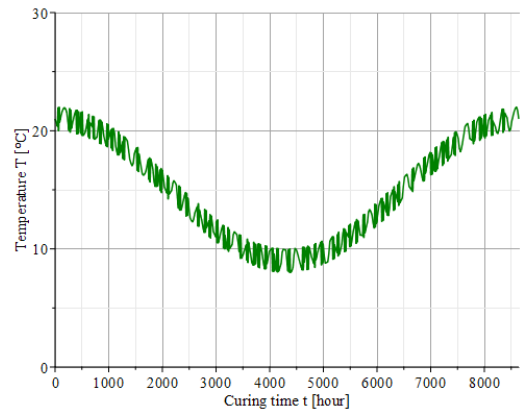
Figure H.120: N4_Aug10_6–1 Base temperature

H.41. N4_Aug16_10–5_10
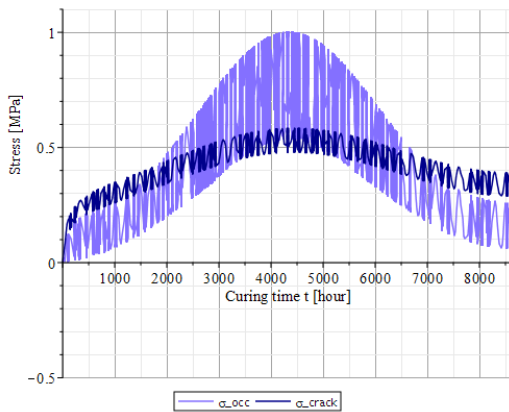
Figure H.121: N4_Aug16_16–5_10 σ_{occ} vs σ_{crack}
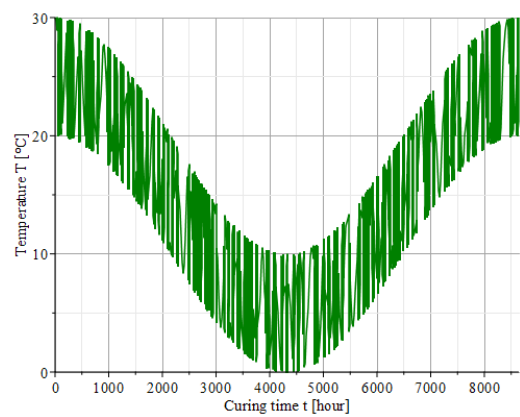
Figure H.122: N4_Aug16_10–5_10 Base temperature
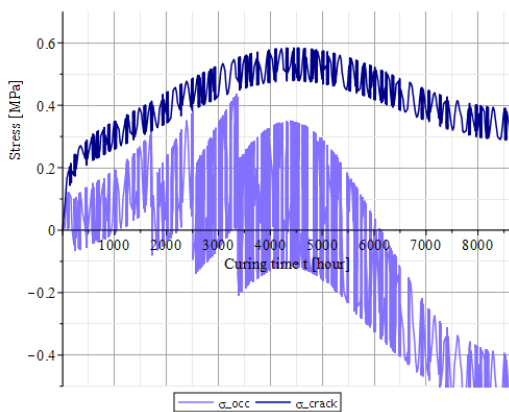
Figure H.123: N4_Aug16_10–5_10 σ_{occ} vs σ_{crack}
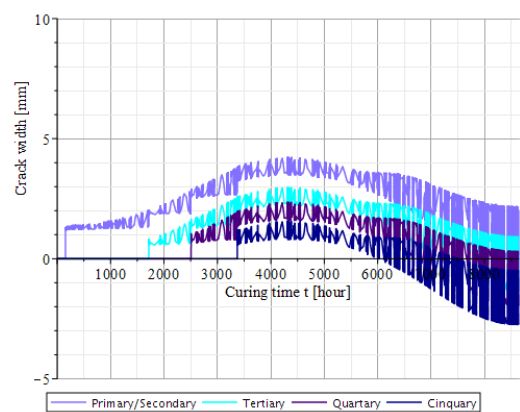
Figure H.124: N4_Aug16_10–5_10 Crack width

H.42. N4_Aug16_10−5_4
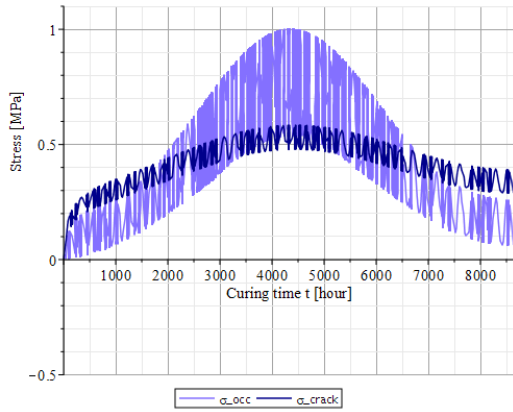
Figure H.125: N4_Aug16_16−5_4 σ_{occ} vs σ_{crack}
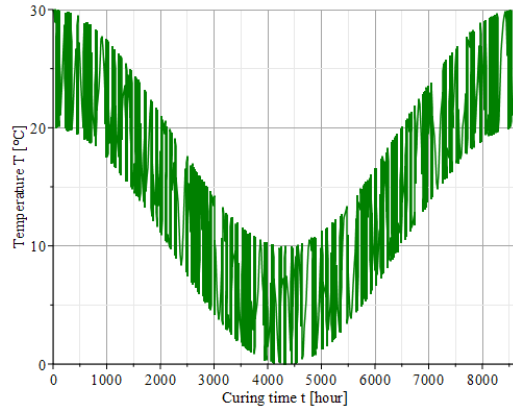
Figure H.126: N4_Aug16_10−5_4 Base temperature
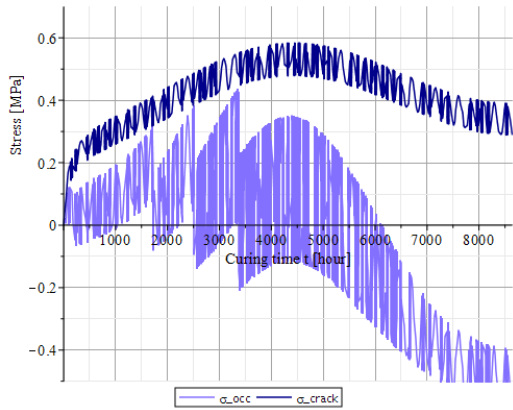
Figure H.127: N4_Aug16_10−5_4 σ_{occ} vs σ_{crack}
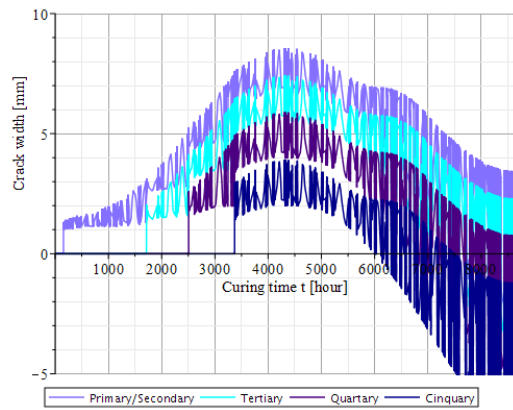
Figure H.128: N4_Aug16_10−5_4 Crack width

H.43. N4_Aug16_8−3_10
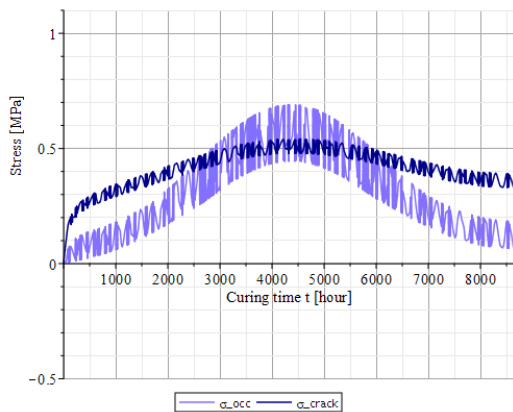
Figure H.129: N4_Aug16_8−3_10 σ_{occ} vs σ_{crack}
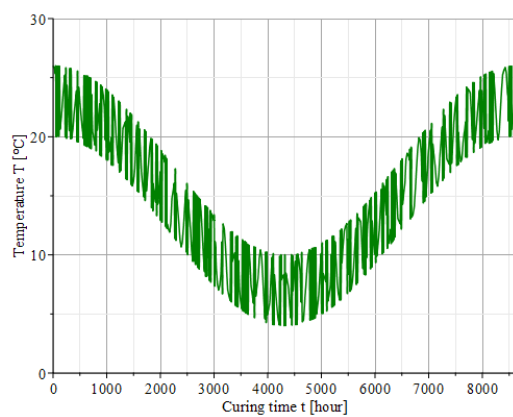
Figure H.130: N4_Aug16_8−3_10 Base temperature
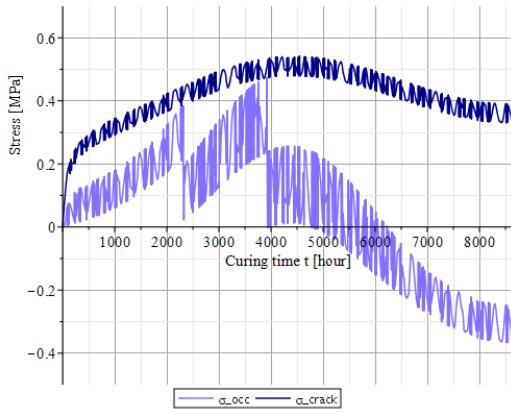
Figure H.131: N4_Aug16_8–3_10 σ_{occ} vs σ_{crack}
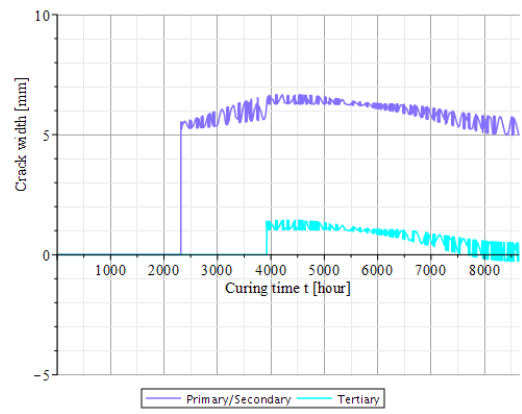
Figure H.132: N4_Aug16_8–3_10 Crack width

H.44. N4_Aug16_8–3_4
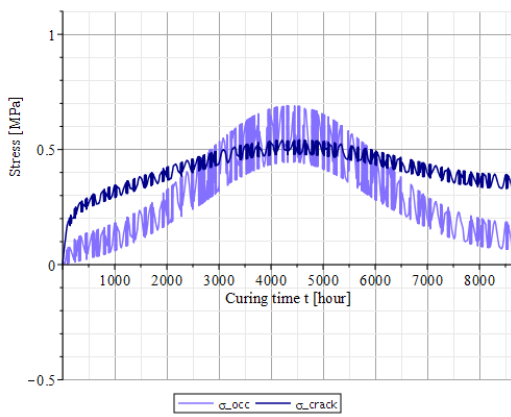
Figure H.133: N4_Aug16_8–3_4 σ_{occ} vs σ_{crack}
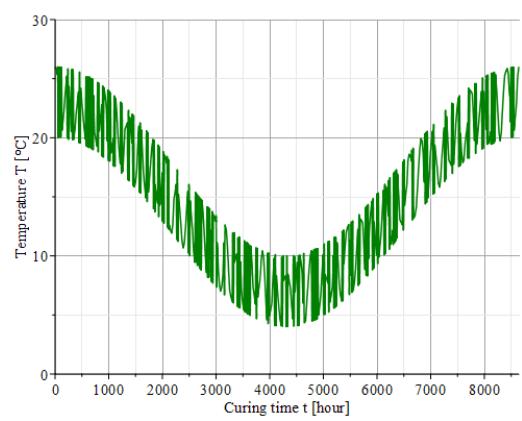
Figure H.134: N4_Aug16_8–3_4 Base temperature
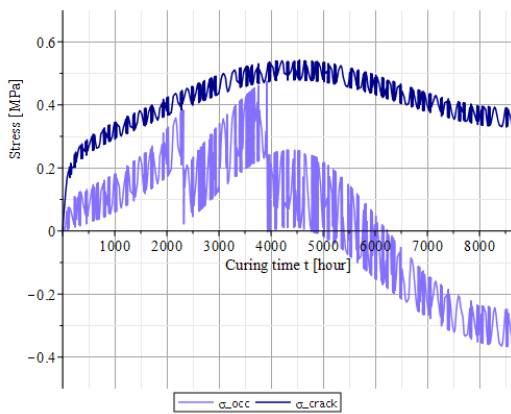
Figure H.135: N4_Aug16_8–3_4 σ_{occ} vs σ_{crack}
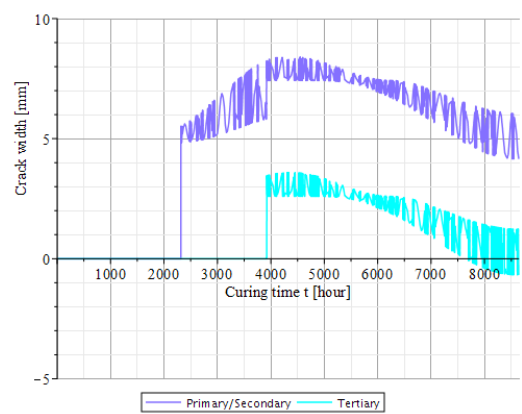
Figure H.136: N4_Aug16_8–3_4 Crack width

H.45. N4_AUG16_6–1
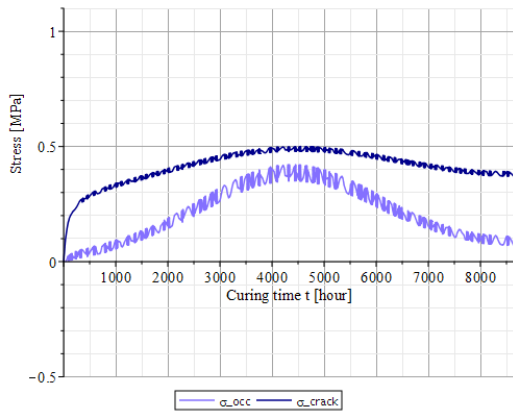
Figure H.137: N4_Aug16_6–1 σ_{occ} vs σ_{crack}
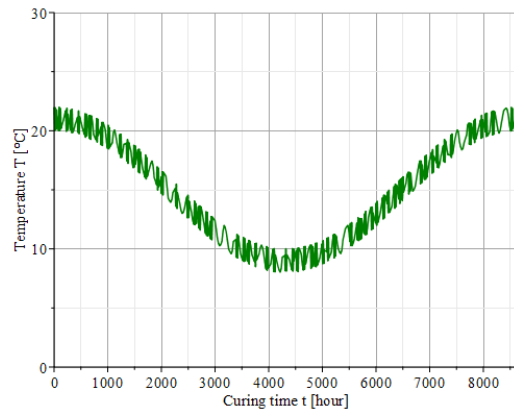
Figure H.138: N4_Aug16_6–1 Base temperature

H.46. N4_AUG22_10–5_10
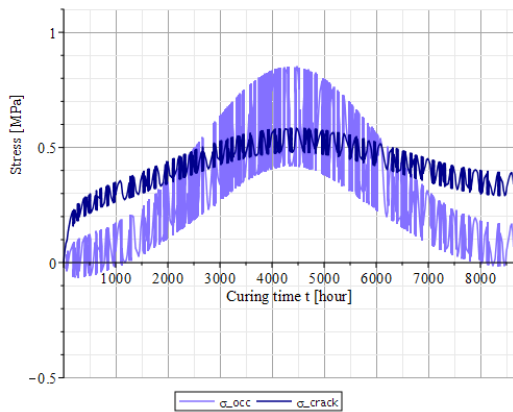
Figure H.139: N4_Aug22_10–5_10 σ_{occ} vs σ_{crack}
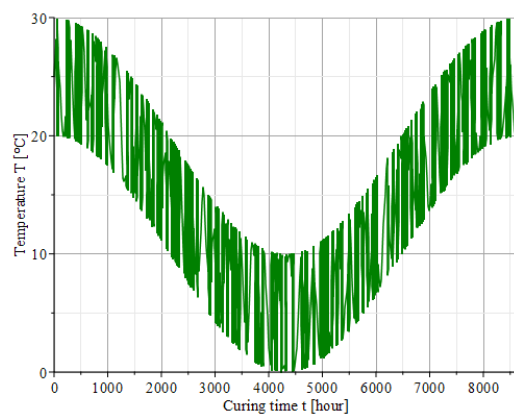
Figure H.140: N4_Aug22_10–5_10 Base temperature
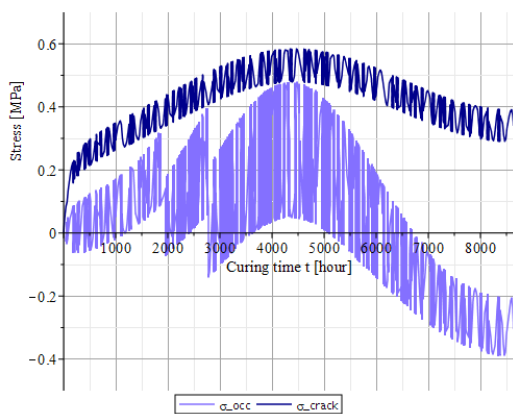
Figure H.141: N4_Aug22_10–5_10 σ_{occ} vs σ_{crack}
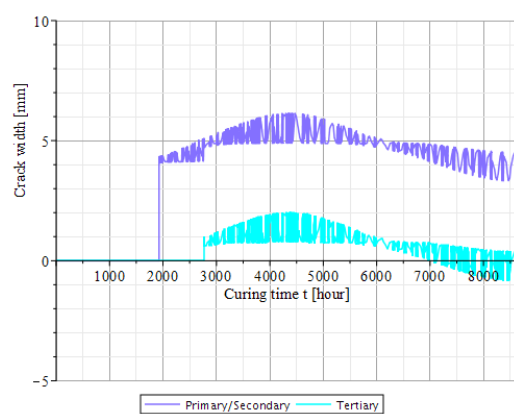
Figure H.142: N4_Aug22_10–5_10 Crack width

H.47. N4_Aug22_10–5_4
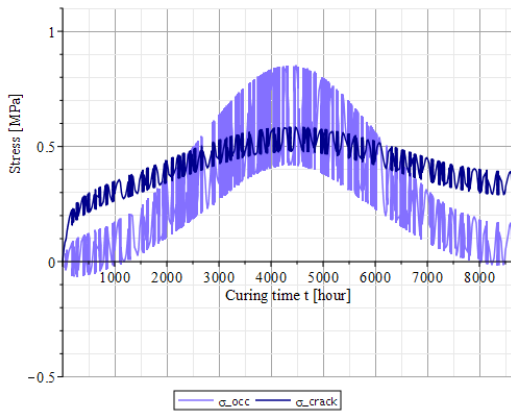
Figure H.143: N4_Aug22_10–5_4 σ_{occ} vs σ_{crack}
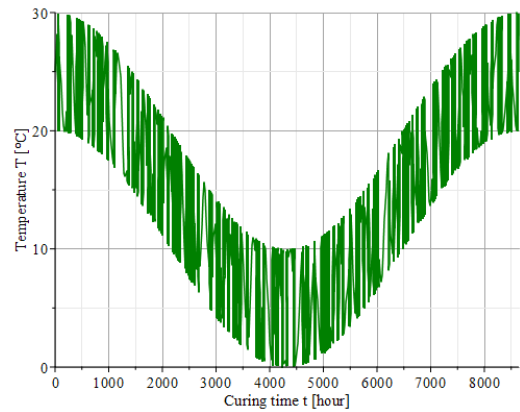
Figure H.144: N4_Aug22_10–5_4 Base temperature
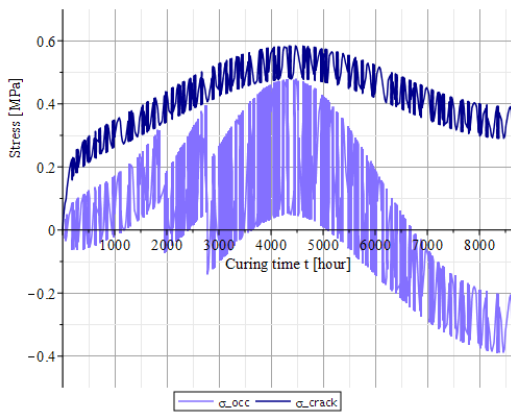
Figure H.145: N4_Aug22_10–5_4 σ_{occ} vs σ_{crack}
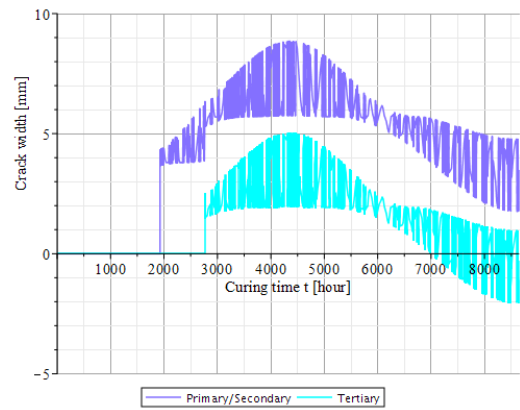
Figure H.146: N4_Aug22_10–5_4 Crack width

H.48. N4_Aug22_8–3_10
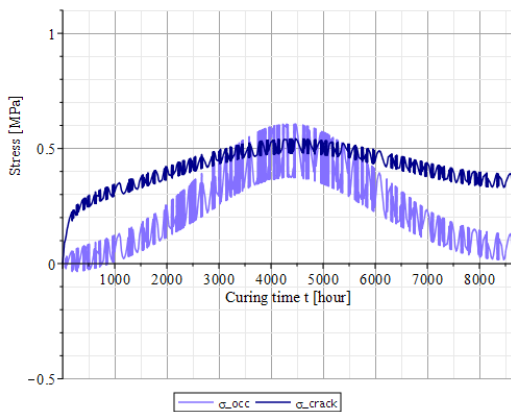
Figure H.147: N4_Aug22_8–3_10 σ_{occ} vs σ_{crack}
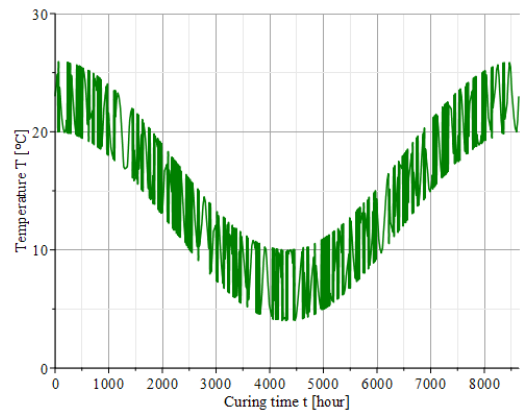
Figure H.148: N4_Aug22_8–3_10 Base temperature
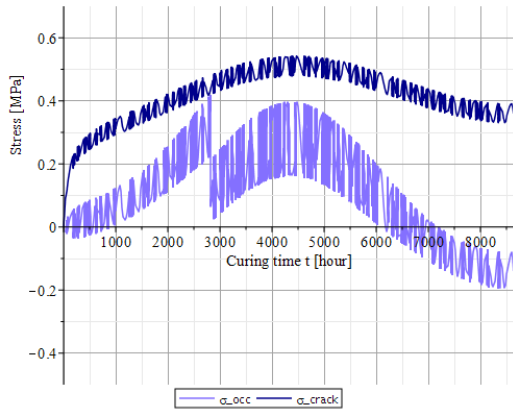
Figure H.149: N4_Aug22_8–3_10 σ_{occ} vs σ_{crack}
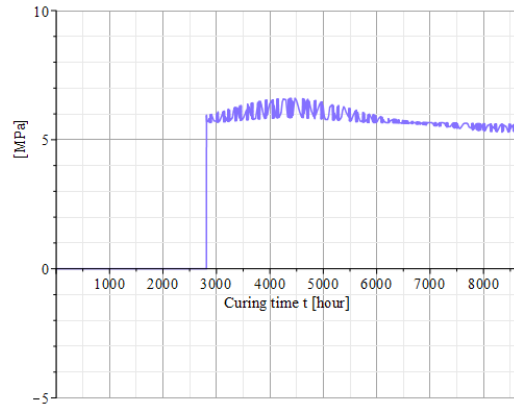
Figure H.150: N4_Aug22_8–3_10 Crack width

H.49. N4_AUG22_8–3_4
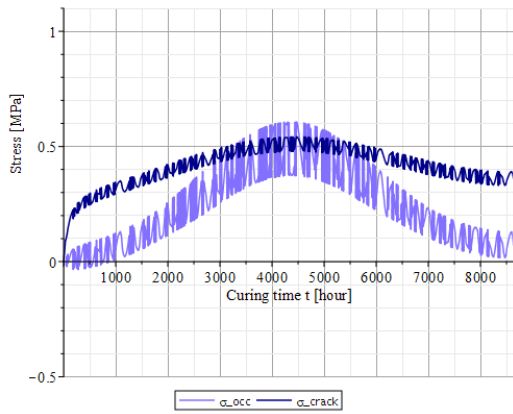
Figure H.151: N4_Aug22_8–3_4 σ_{occ} vs σ_{crack}
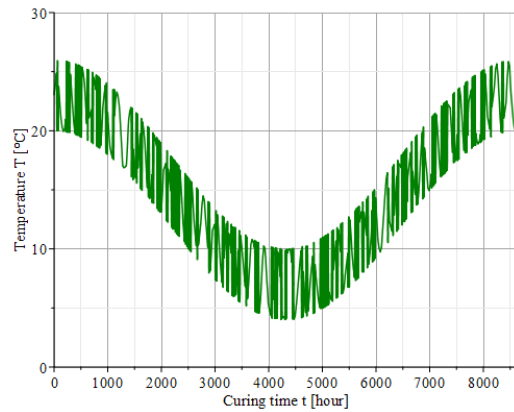
Figure H.152: N4_Aug22_8–3_4 Base temperature
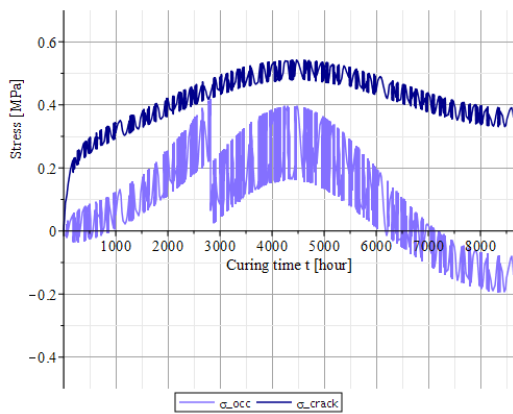
Figure H.153: N4_Aug22_8–3_4 σ_{occ} vs σ_{crack}
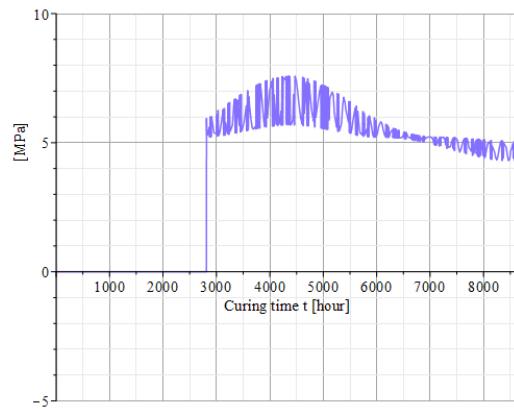
Figure H.154: N4_Aug22_8–3_4 Crack width

H.50. N4_Aug22_6–1
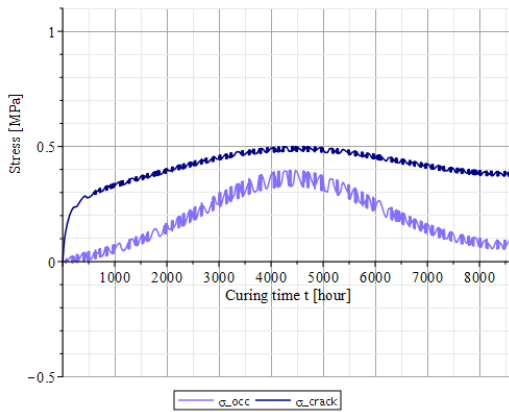
Figure H.155: N4_Aug22_6–1 σ_{occ} vs σ_{crack}
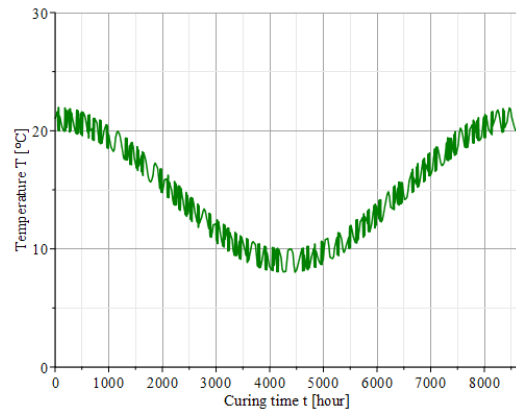
Figure H.156: N4_Aug22_6–1 Base temperature

H.51. N4_Nov10_10–5_10
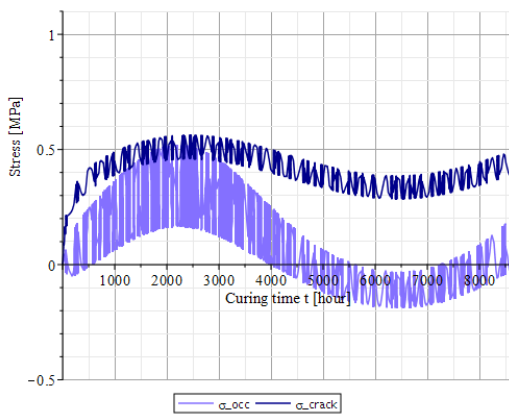
Figure H.157: N4_Nov10_10–5_10 σ_{occ} vs σ_{crack}
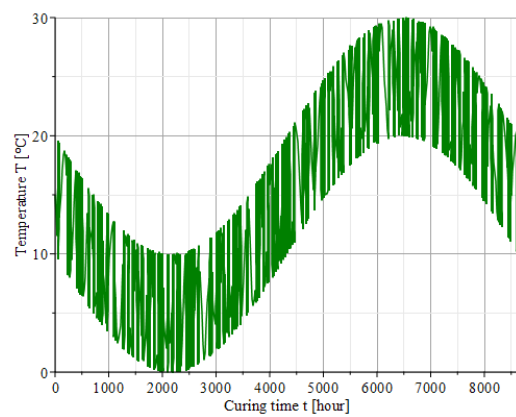
Figure H.158: N4_Nov10_10–5_10 Base temperature
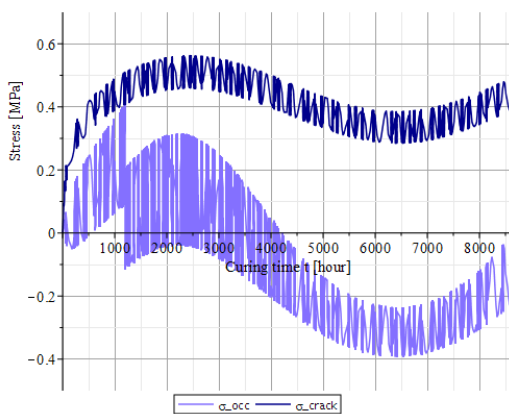
Figure H.159: N4_Nov10_10–5_10 σ_{occ} vs σ_{crack}
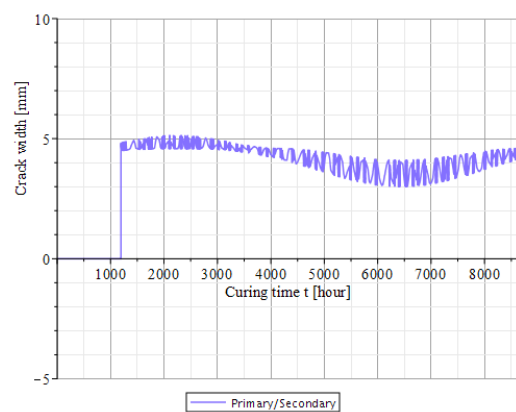
Figure H.160: N4_Nov10_10–5_10 Crack width

H.52. N4_Nov10_10–5_4
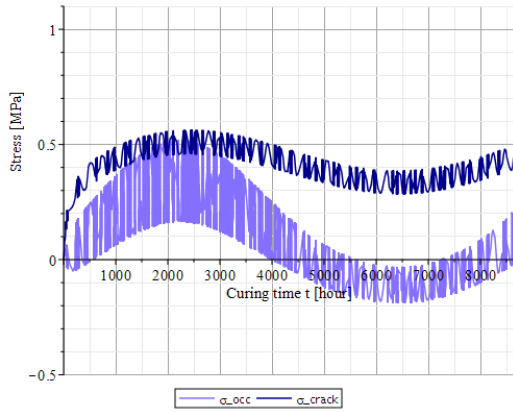
Figure H.161: N4_Nov10_10–5_4 σ_{occ} vs σ_{crack}
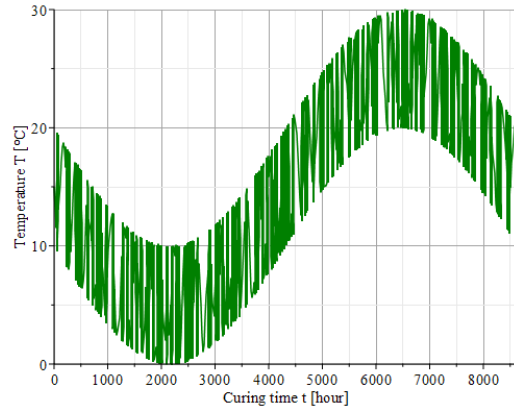
Figure H.162: N4_Nov10_10–5_4 Base temperature
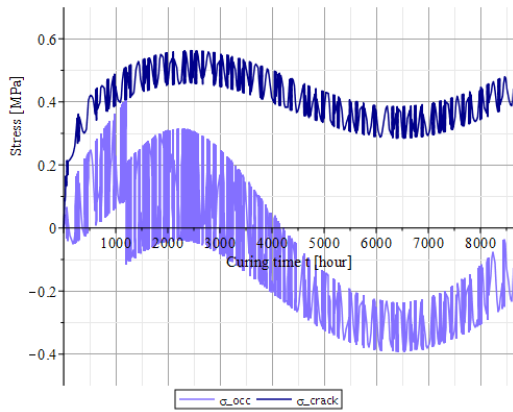
Figure H.163: N4_Nov10_10–5_4 σ_{occ} vs σ_{crack}
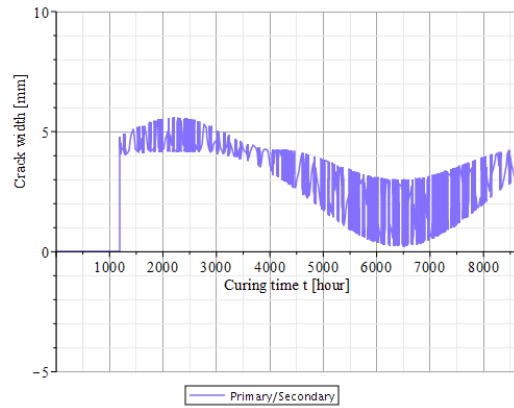
Figure H.164: N4_Nov10_10–5_4 Crack width

H.53. N4_Nov10_8–3
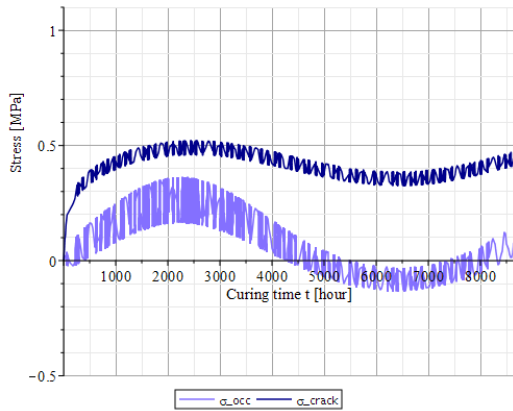
Figure H.165: N4_Nov10_8–3 σ_{occ} vs σ_{crack}
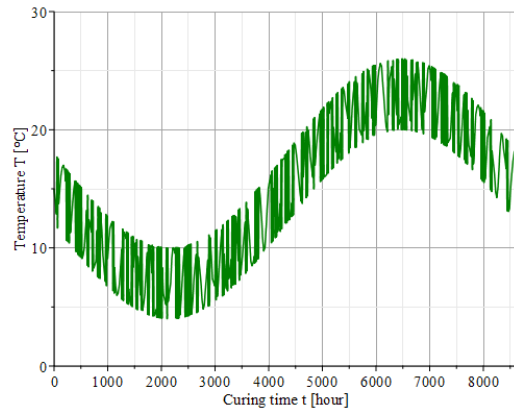
Figure H.166: N4_Nov10_8–3 Base temperature

H.54. N4_Nov10_6–1
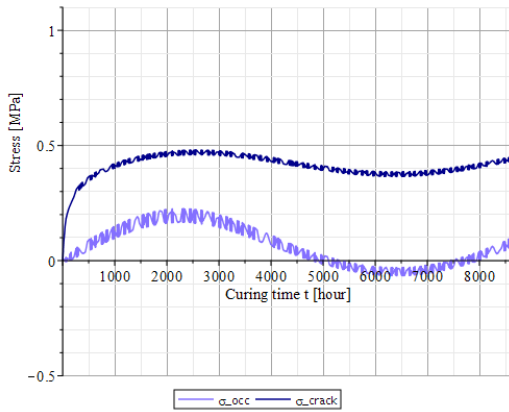
Figure H.167: N4_Nov10_6–1 σ_{occ} vs σ_{crack}
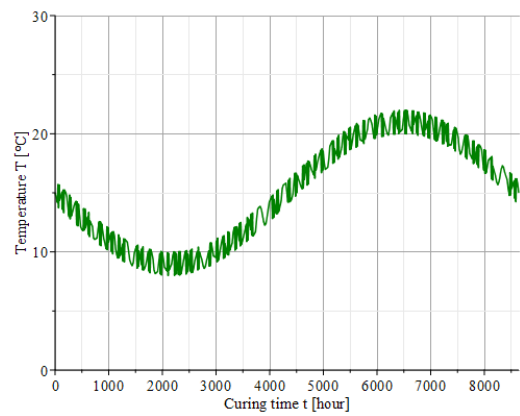
Figure H.168: N4_Nov10_6–1 Base temperature

H.55. N4_Feb04_10–5
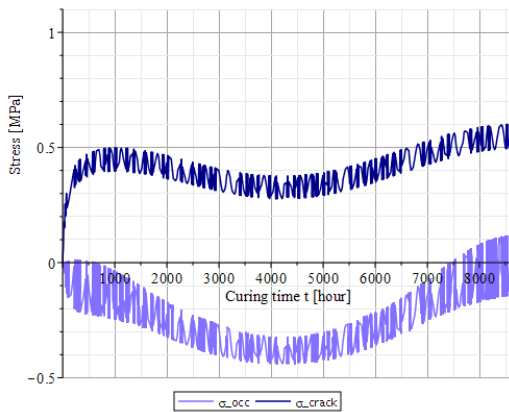
Figure H.169: N4_Feb04_10–5 σ_{occ} vs σ_{crack}
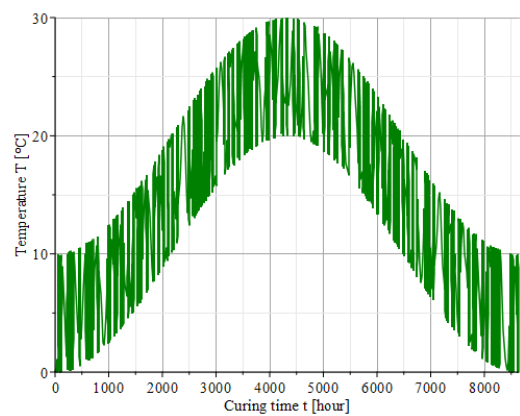
Figure H.170: N4_Feb04_10–5 Base temperature

H.56. N4_Feb04_8–3
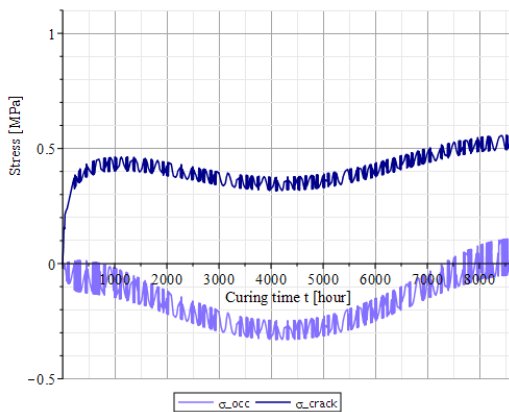
Figure H.171: N4_Feb04_8–3 σ_{occ} vs σ_{crack}
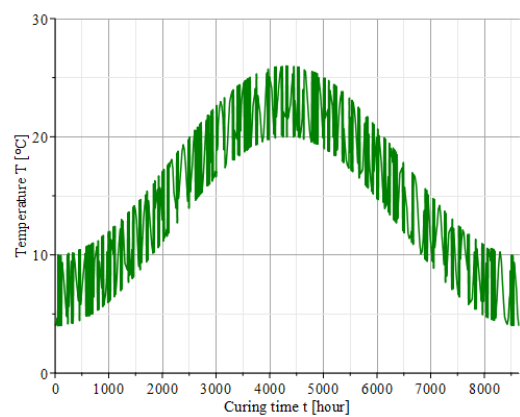
Figure H.172: N4_Feb4_8–3 Base temperature

H.57. N4_Feb04_6−1
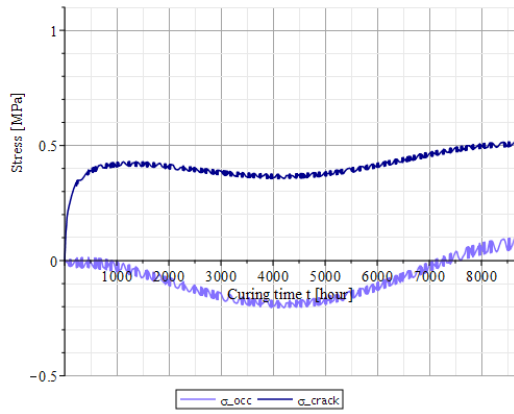
Figure H.173: N4_Feb04_6−1 σ_{occ} vs σ_{crack}
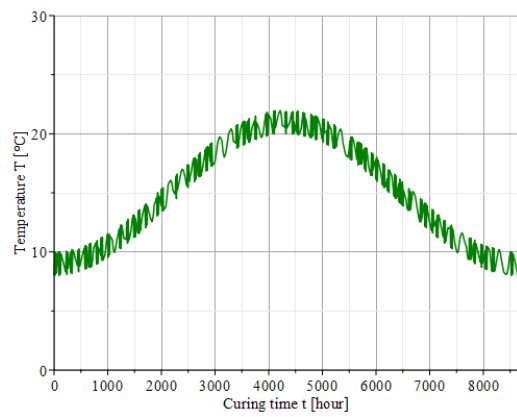
Figure H.174: N4_Feb04_6−1 Base temperature